CoA Note No.72

THE COLLEGE OF AERONAUTICS

CRANFIELD

INVESTIGATION INTO THE USE OF FREON 12 AS A WORKING MEDIUM IN A HIGH-SPEED WIND-TUNNEL

by

O. M. POZNIAK

NOTE NO. 72

NOVEMBER 1957.

THE COLLEGE OF AERONAUTICS

CRANFIELD

"INVESTIGATION INTO THE USE OF FREON 12 AS A WORKING MEDIUM IN A HIGH-SPEED WIND-TUNNEL".

by

O. M. POZNIAK, B.Sc.

SUMMARY

The Freon 12 tunnel project at the College of Aeronautics was started to gain experience in the design of such tunnels and subsequently to investigate their use for aerodynamic measurements and the correlation of these with similar measurements in air.

Reports dealing with the use of heavy gases are listed and the factors affecting the choice of any particular gas are discussed. The most suitable gases are the fluoro-carbons and amongst them C_4F_{10} n-perfluorobutane shows most promise. It can be shown that :

	Mol.wt.	% Power relative to air	% Size at same R,M	B.Pt. °F
F-12 (CCl_2F_2)	121	5.5	33	-30
C_4F_{10}	238	1.8	23	- 2

The application of transonic similarity laws to 2-dimensional flow over wings of infinite aspect ratio to convert pressure measurements obtained in heavy gases to equivalent air values is suggested.

Pressure and wake drag measurement on a 10% thick 2in. chord aerofoil RAE.104 over a Mach number range of 0.4 to 0.85, at a Reynolds number of 1.7×10^6 at M = 0.85 and incidences of 0° and 4°, have been corrected to equivalent air values by means of transonic and area similarity rules, and have been compared with measurements in air on similar aerofoil sections at the National Physical Laboratory. The validity of these rules could not be completely proved, though the small differences were most likely due to the tests not being performed on identical models and in identical tunnels.

The application of transonic similarity to the conversion of wave drag in Freon-12 to equivalent air results gave very good agreement with air measurements. The magnitude of the effects of relaxation times in Freon-12 in the flow about small diameter total head-tubes is shown to be negligible at atmospheric pressure and at a stagnation temperature of $300^\circ K$. The increase of drag about a 2" chord model at similar stagnation conditions is about 0.3% and since smaller models are unlikely to be used this effect is quite negligible.

SUMMARY Cont'd.

The advantages to be gained in flutter testing by using a heavy gas are compared for both the compressible and the incompressible cases. In general the use of a heavy vapour tunnel results in the reduction of flutter velocity, frequency, model stresses and also in the pressure ratio in comparison to a compressed air tunnel.

1. LIST OF CONTENTS.

		Page No.
	Summary.	2
1.	List of contents.	4
2.	Notation.	7
3.	Introduction.	11
4.	Choice of working substance.	12
5.	The effect of γ in Subsonic and Transonic Flow.	14
	5.1. The effect of the ratio of specific heats on isentropic flow relations.	14
	5.2. Compressibility effects on pressure and lift.	16
	5.3. Transonic similarity laws.	17
	5.4. Application of transonic similarity laws to 2-D.flow.	18
	5.5. Application of transnoic similarity laws to finite aspect ratio wings.	19
	5.6. Review of experimental work by Von Doenhoff and Braslow (11).	21
6.	The College of Aeronautics Freon-12 Wind-tunnel	23
	6.1. General design considerations.	23
	6.2. Purification.	25
	6.3. The 5.25 in. x 7.5 in. annular return Freon-12 tunnel at the College of Aeronautics.	25
	6.4. Freon Circuit layout.	27
	6.5. Circulation.	27
	6.6. Detailed description of components.	28
7.	Calibration of Freon-12 Tunnel	30
	7.1. Introduction.	30
	7.2. Tunnel and apparatus.	31
	7.3. Accuracy.	31
	7.4. Experimental measurements.	34
	7.5. Results from total head measurements.	34
	7.6. Transverse variation of static pressure in the working section.	35

List of Contents Cont'd.

		Page No.
	7.7. Variation of static pressure along the working section.	36
	7.8. Working section Mach No.	37
	7.9. Purity of Freon.	37
8.	Two-Dimensional Aerofoil Tests in the Freon-12 Tunnel.	38
	8.1. Model.	38
	8.2. Model mounting and pressure measurements.	38
	8.3. Pitot traverse gear.	39
	8.4. Calculation of results.	39
	8.5. Pressure distributions in Air and Freon-12. $\alpha = 0^{\circ}$	41
	8.6. Drag measurement $\alpha = 0^{\circ}$	42
	8.7. Pressure distributions in Air and Freon-12. $\alpha = 4^{\circ}$	44
	8.8. Drag measurements $\alpha = 4^{\circ}$.	44
9.	Conclusions.	45
	Acknowledgements.	46
	References.	47
	Appendices.	51
1.	Derivation of Transonic Similarity rules.	
2.	Application of Transonic and area similarity rules to two-dimensional flow in Freon-12 and air.	56
3.	Application of Transonic Similarity laws to finite aspect ratio wings in Freon-12 and Air.	58
4.	Application of Area Similarity laws to convert the pressure distribution on wings in Freon-12 to Air results.	59
5.	Power Economy, reduction in size and model stresses in heavy gas tunnels.	60
6.	Mach No. limit for condensation in heavy gases.	62
7.	Reynolds No. in gas mixtures.	63
8.	Reynolds No. in Freon-12 and Freon-12 Air Mixtures.	66
9.	Variation of skin friction between tests in air and Freon-12.	69
10.	The Effect of Relaxation Times.	71

List of Contents Cont'd.

Page No.

11. Determination of gas mixture proportion by means of a sound measuring gauge. 78

12. Comparison of Flutter model testing in compressed air tunnels and tunnels using heavy gases. 81

NOTATION

a = speed of sound

A = area of stream tube

A,B,C = parameters

$\mathbb{R}$ = aspect ratio

b = span of aerofoil; tunnel breadth

c = chord of aerofoil

C' = force and moment coefficient ratio

C_D = drag coefficient

C_f = skin friction coefficient

C_i = vibration heat capacity

C_L = lift coefficient

C_M = moment coefficient

C_N = normal force coefficient

C_p = pressure coefficient $(=\frac{p - p_\infty}{\frac{1}{2}\rho_\infty U^2})$; specific heat at constant pressure

C_{p_a} = heat capacity of active degrees of freedom

C_v = specific heat at constant volume

d = impact tube diameter

$D(K,H)$ = drag function

f = function; frequency

F = integrating factor

g = wing thickness distribution

H = similarity parameter $\mathbb{R}\left[(\gamma+1)M_\infty^2\tau\right]^{\frac{1}{3}}$; total head; Enthalpy

k = viscosity law constant

K = similarity parameter $\dfrac{M_\infty^2 - 1}{\left[(\gamma+1)M_\infty^2\ \bar{\tau}\right]}^{2/3}$; relaxation parameter

l = model reference length

$L(H,K)$ = lift function

m = molecular weight

M = Mach nos.

$M(H,K)$ = moment function

n = no. of atoms in molecule, viscosity scaling factor

p_n = pressure at any of the wall tappings 1, 2, 3, 4.

p = pressure

p' = static pressure at traversing gauge

p_A = atmospheric pressure

p_t = pressure in settling chamber

P = power

$P(H,K;\ \frac{x}{c},\ \frac{y}{b},\ \frac{z}{b})$ = pressure function

$P(K;\ x',\ z')$ = pressure funetion

q = dynamic pressure

q_1 = local velocity around aerofoil

Q,J,G,E = functions

r = density or pressure ratio

R or R_e = Reynolds numbers

$\overline{R}$ = universal gas constant

R_x = $\dfrac{\rho_\infty U_\infty x}{\mu_\infty}$

S,S_i,S' = entropy

t = thickness of aerofoil

ϵ = block age correction

ϵ_s = solid blockage correction

ϵ = wake blockage correction

$\frac{t}{c} = \tau$ = aerofoil thickness chord ratio

T = temperature

u, v, w = velocity components in x, y, z directions

U = free stream velocity

x = mole-fraction of air in gas mixture

(x, y, z) = cartesian coordinates with x in mainstream direction and y in plane of wing perpendicular to mainstream direction

Z = ordinate of aerofoil

α = incidence

γ = ratio of specific heat $\frac{C_p}{C_v}$

ΔC_D = increment in C_D

ϵ = stiffness

ϵ_s = solid blockage correction factor

ϵ_w = wake blockage correction factor

η = power factor; slope

λ = linear scaling factor

μ = viscosity

ρ = density

σ = Prandtl number; wing density

τ = relaxation time; aerofoil thickness chord ratio

τ_w = wall shear stress

ϕ = perturbation velocity potential; function of Mach number

Φ = velocity potential

ω = exponent in viscosity-temperature relation; wave number

β = $\frac{1}{\sqrt{1 - M_\infty^2}}$

SUBSCRIPTS

A	=	Air
c	=	corrected; compressible value
cr	=	critical condition, Mach no. = 1
F	=	Freon - 12
i	=	incompressible value
st	=	stagnation
t	=	settling chamber pressure
u	=	uncorrected
w	=	working section
x	=	differentiation with respect to x direction; mixture properties
y	=	differentiation with respect to y direction
z	=	differentiation with respect to z direction
∞	=	free stream condition

3. Introduction

Heavy vapours have been suggested as possible media for wind-tunnels mainly because of the large power savings that can be obtained in comparison to air (appendix 5).

Other means of obtaining power reduction are by

(a) Pressurisation: this has the disadvantage of increasing model-stresses

(b) Refrigeration: this is generally difficult within a structure like a wind-tunnel

Probably the earliest published report in which attention is drawn to the advantages of using a medium other than air in a wind-tunnel is by Margoulis, 1920, (ref.1). He considers carbon dioxide and shows that in the cases in which (a) Reynolds Number, (b) Mach Numbers(c) both Reynolds number and Mach number are simulated, considerable saving of power is achieved. In a report published at about the same time, M.Munk, 1921 (ref.2), pointed out that a reduction in size and power is avhieved by using compressed air, and also mentions the possibility of using carbon dioxide for the same purpose but dismisses it as impractical because of the additional complications involved. Rubinski 1939 (ref.3) considers a wide range of heavy gases for use in supersonic tunnels and concludes that among other, the Freons, Carbon Tetrachloride and Sulphur-Hexafluoride merit special attention. He also considers the design of a wind-tunnel using CCl_4 to run at a Mach number of 1.3. Smelt, 1945 (ref.4), discusses the relative advantages that result from the use of heavy gases, compressed air and also through refrigeration and lists a large number of possible compounds together with the reduction in power and tunnel size obtainable in each case. The use of heavy vapours were the subject of papers by McKinnon Wood, 1945, (ref.5) who also considers the use of sulphur hexafluoride for powered model tests, and by Bottle, 1948, (ref.6).

The effect of γ, the ratio of specific heats, which for poly atomic gases differs from the value 1.4 for air and other diatomic gases, on supersonic flow was considered by Relf (ref.7), 1952.

The thermodynamic properties and the time lag of vibrational heat-capacity of Freon-12 have been examined by Huber, 1946 (ref.8) to determine its suitability for aerodynamic testing.

The use of a mixture of a monatomic gas, $\gamma = 1.67$, with a heavy polyatomic gas with a low value of γ, such that the resultant γ is equal to 1.4 was suggested by Relf 1952 (ref.9) and Chapman, 1954, (ref.10). The latter report contains a very extensive list of suitable heavy gases.

Von Doenhoff and Braslow, 1953, (ref.11) used Freon-12 in a wind-tunnel, and have evolved a method of correcting the measured force coefficients for the different value of γ to equivalent air values up to the transonic range

In addition gases other than air have been used for ballistic research by Buel, 1948, (ref.12) and Donaldson and Sabol 1951, (ref.13) mainly to achieve very high Mach numbers.

Theodorsen and Regier, 1944 (ref.14) used Freon-12 and Freon-113 to measure the drag of revolving discs, cylinders and streamline rods at high Reynolds and Mach numbers; and Kantrowitz 1953, (ref.15) used Freon 12 to test supersonic compressors.

Gases other than air have been used by Duff 1951 (ref.16) in a shock-tube and Helium was employed by Bogdonoff and Hammitt, 1954 (ref.17) in a hypersonic tunnel as it can be expanded to high Mach numbers without liquification.

4. Choice of working substance

The main requirements for an advantageous medium is a low speed of sound (see appendix 5) together with a low boiling point. It should also be stable and inert chemically, cheap and easily available.

For perfect gases at the same temperatures

$$a \propto \frac{1}{\sqrt{m}}$$

where a = speed of sound

m = molecular weight

and hence the interest lies mainly with heavy vapours, but unfortunately the boiling point of vapours generally increases with increasing molecular weight.

It appears that most of the suitable gases are compounds of fluorine, for a given molecular weight. They have the lowest boiling points and are mostly extremely stable. Among these the Freons require special mention since they are readily available in large quantities and they have already been used experimentally, see ref. (11 and 12). There are however, many compounds which are more stable and efficient than the Freons and yet have a reasonably low boiling point, e.g. $C_4 F_{10}$ one of the series of fluoro-carbons. This can be

seen from the following tables

	Mol.wt.	% power relative to air at same R,M.	% Size	B.Pt. °F
Freon-12 ($CCl_2 F_2$)	121	5.5	33	-30
$C_4 F_{10}$	238	1.8	23	- 2

Many gases of this type have been developed recently and it is believed that their usefulness will largely depend on their cost and availability.

In addition to the above considerations several other factors must be taken into account. These are thermal and caloric imperfections, relaxation time effects and the value γ. Generally $\gamma = \frac{2n+3}{2n+1}$ where n is the number of atoms in the molecule and hence γ for most of the heavy vapours with complex molecules is smaller than $\gamma \sim 1.4$, the value for air and most diatomic gases.

Deviations from perfect gas laws under normal working conditions are found to be usually small and caloric imperfections become considerable only at high temperatures.

Suggestions were made by Relf (ref.9) and independently by Chapman (ref.10) that it would be possible to obtain a mixture of a suitable monatomic gas, e.g. either Argon, Krypton or Xenon, $\gamma = \frac{5}{3}$ and a heavy polyatomic gas with low γ such that the value of γ for the mixture was 1.4 and yet obtain considerable power economy, though not as great as using just a heavy gas by itself. Chapman found that on the whole the values were of the following order to obtain the same Mach and Reynolds number

		% Power relative to air	% Size relative to air
Mixtures of	Argon and heavy vapour	30	70
	Krypton " " "	20	60
	Xenon " " "	10	50
	$CCl_2 F_2$	5.5	33
	$C_4 F_{10}$	1.8	23

but of the monatomic gases Argon is the only one available in large quantities. Chapman also observes that it is possible to obtain mixtures which under low temperature wind tunnel conditions are dynamically similar to air under high temperature flight conditions;

that is dimensionless macroscopic parameters, for instance those involving relaxation time phenomena and temperature variation of specific heat, are equal, whereas air under low temperature wind tunnel condition would behave dissimilarly.

Some of the disadvantages in using a heavy gas are a different value of γ, structural complication because of the necessity of isolating the medium from air and the necessity of additional equipment for purification purposes. The requirements for such a tunnel are somewhat similar to those of a pressurised tunnel, but it is more important to avoid leaks. Additional instrumentation is required to measure the purity of the medium.

5. The effect of γ in subsonic and transonic flow.

5.1. The effect of ratio of specific heat on the isentropic flow relations.

In general γ the ratio of specific heats can be written as

$$\gamma = \frac{2n + 3}{2n + 1} \qquad 5.1.1.$$

where n is the number of atoms in a molecule. γ thus varies from $\frac{5}{3}$ for monatomic gases (e.g. Helium, Argon) to a limiting value approaching unity for heavy gases with complex molecules.

The isentropic flow relations (with suffixes st and cr denoting stagnation and critical values respectively)

(a) Pressure ratio 5.1.2.

$$\frac{p}{p_{st}} = (1 + \frac{\gamma-1}{2} M^2)^{-\frac{\gamma}{\gamma-1}}$$

$$\operatorname{Lt}_{\gamma \to 1} \frac{p}{p_{st}} = e^{\frac{-M^2}{2}}$$

(b) Density ratio 5.1.3.

$$\frac{\rho}{\rho_{st}} = (1 + \frac{\gamma-1}{2} M^2)^{-1/\gamma-1}$$

$$\operatorname{Lt}_{\gamma \to 1} \frac{\rho}{\rho_{st}} = e^{\frac{-M^2}{2}}$$

(c) Area ratio

$$\frac{A}{A_{cr}} = M \left(\frac{2 + (\gamma-1) M^2}{\gamma+1} \right)^{-\frac{\gamma+1}{2(\gamma-1)}} \qquad 5.1.4.$$

$$\lim_{\gamma \to 1} \frac{A}{A_{cr}} = M e^{\frac{1-M^2}{2}}$$

(d) Ratio dynamic pressure to stagnation pressure

$$\frac{q}{p_{st}} = \frac{\gamma M^2}{2} \left(1 + \frac{\gamma-1}{2} M^2 \right)^{-\frac{\gamma}{\gamma-1}} \qquad 5.1.5.$$

$$\lim_{\gamma \to 1} \frac{q}{p_{st}} = \frac{M^2}{2} e^{\frac{-M^2}{2}}$$

(e) Temperature ratio

$$\frac{T}{T_{st}} = \left(1 + \frac{\gamma-1}{2} M^2 \right)^{-1} \qquad 5.1.6.$$

$$\lim_{\gamma \to 1} \frac{T}{T_{st}} = 1.$$

have been plotted in figs. 1, 2, 3, 4, 5, for a Mach number range 0-3 for values of γ equal to $5/3$, $7/5$, $9/8$ and the limiting value of $\gamma=1$.

An examination of these graphs shows that the variation with γ of the area ratio up to $M = 1.4$ is small. The variation of $\frac{p}{p_{st}}$, $\frac{\rho}{\rho_{st}}$ when γ changes from $\gamma = 7/5$ to $9/8$ is about 10%, but when γ varies from $\gamma = 5/3$ to $\gamma = 1.0$ the variation is of the order of 40%.

The temperature ratio $\frac{T}{T_{st}}$ and the ratio of dynamic pressure to stagnation pressure are much more sensitive to a change in γ.

The value of $\gamma = \frac{7}{5}$ corresponds to the value for air and $\gamma = \frac{9}{8} = 1.125$ corresponds to the value for Freon-12.

Fig.5 shows clearly the much larger area ratio required for supersonic ducts if a gas with a low value of γ is used as compared with those using a monatomic gas with $\gamma = 5/3$.

The effect of γ on some supersonic phenomena is discussed in ref.7

5.2. Compressibility effects on pressure and lift.

The ratio of specific heats does not appear in the Prandtl-Glauert rule (ref.19) derived from the linearised compressible flow equations. This rule is limited to small perturbations and hence very thin profiles at small angles of attack at speeds well below the speed of sound. Hence under these conditions the effect of different γ can be expected to be negligible.

Further evidence for the small influence of γ on compressible flow is indicated by the similarity of results obtained in a hydraulic analogy tank, where the effective $\gamma = 2$, and compressible air flow (ref.20) and also from the widely used Karman-Tsien relations (ref.22, 23) which can be derived from the compressible flow equations by putting $\gamma = -1$.

The Prandtl-Glauert rule was modified by Laitone (ref.24) who obtained

$$\frac{C_{pc}}{C_{pi}} = \frac{1}{\sqrt{1-M_\infty^2} + \frac{M_\infty^2 \left(1 + \frac{\gamma-1}{2} M_\infty^2\right) C_{pi}}{2\sqrt{1 - M_\infty^2}}} \qquad 5.2.1$$

where C_{pc}, C_{pi} are the compressible and incompressible values of the pressure coefficient respectively. The Laitone rule gives better experimental agreement and is applicable at somewhat higher subsonic Mach numbers and pressure coefficients than the Prandtl-Glauert rule. This rule is noteworthy for the fact that it includes the factor γ.

Kaplan (ref.25) obtained an expression relating the compressible and incompressible coefficients on an elliptical cylinder and extended it to an arbitrary symmetrical profile.

$$\frac{C_{L_c}}{C_{L_i}} = \beta + \frac{\tau}{1+\tau} \left[\beta(\beta-1) + \frac{1}{4}(\gamma+1)(\beta^2-1)^2\right] \qquad 5.2.2$$

where $\beta = \frac{1}{\sqrt{1-M_\infty^2}}$ and τ = thickness ratio.

This relation is plotted in fig.7 for τ = 0.05, 0.10, 0.15, 0.20 and γ = 1.4.

The lift correction, for the same values of τ and M_∞,

$$\frac{\Delta C_{L_c}}{C_{L_F}} = \frac{\left(C_{L_c}\right)_A - \left(C_{L_c}\right)_F}{\left(C_{L_c}\right)_F}$$

$$= \frac{\frac{1}{4}\,\frac{\tau}{1+\tau}\,(\gamma_A - \gamma_F)(\beta^2-1)^2}{\beta + \frac{\tau}{1+\tau}\left[\beta(\beta-1) + \frac{1}{4}(\gamma_F+1)(\beta^2-1)^2\right]} \qquad 5.2.3.$$

was calculated in the case of Freon and air (γ_A = 1.4 and γ_F = 1.125) and is presented in fig.6 for the cases of τ = 0.20, 0.15, 0.10, 0.05. It is seen that the effect of the difference in specific heats is quite small, e.g. at M_∞ = 0.8, $\frac{\Delta C_L}{C_{L_F}}$ varies from

½% to 1.5% for thickness ratios of 5% to 20%.

5.3. Transonic similarity laws.

The transonic similarity laws indicate useful generalisation concerning the flow behaviour at transonic speeds. Their applicability to relating flows in media with different values of the ratio of specific heats, γ, will be examined.

The transonic similarity laws are derived on the assumption of small perturbation velocities and velocity gradients about either the critical sonic velocity (ref.24, 25) or under the less restrictive conditions of small perturbations about the free-stream velocity (ref.26). A derivation of the transonic rules for two and three dimensional wings is given in appendix I.

The transonic similarity laws are based on potential flow thus excluding from consideration regions having vorticity. They can be applied successfully to subsonic flows with shock waves provided these are weak so that the entropy change across them is small and provided they are only slightly curved so that the variation of entropy from one streamline to another is small and hence the vorticity induced by the shocks can be neglected.

5.4. Application of transonic similarity rules to two-dimensional flow with different value of the ratio of specific heats.

For two-dimensional wings the profile ordinatesare given by

$$\frac{Z}{c} = \tau g\left(\frac{x}{c}\right) \qquad 5.4.1.$$

and the relevant similarity parameter is

$$K = \frac{1 - M_\infty^2}{\left[(\gamma+1)\, M_\infty^2\, \tau\right]^{2/3}} \qquad 5.4.2$$

The transonic similarity rules for pressure and force coefficients (eqn. 21, 22, 23, 24, 25 appendix I.) can then be written

$$C_p = \frac{\tau^{2/3}}{\left[(\gamma+1)M_\infty^2\right]^{1/3}} \quad P\,(K;\, x',\, z')$$

where $x' = \frac{x}{c}$ and $z' = (1-M_\infty^2)^{1/2}\ \frac{z}{c}$

$$\text{and } C_L = \frac{\tau^{2/3}}{\left[(\gamma+1)\, M_\infty^2\right]^{1/3}} \quad L(K)$$

$$C_M = \frac{\tau^{2/3}}{\left[(\gamma+1)\, M_\infty^2\right]^{1/3}} \quad M\,(K) \qquad 5.4.3$$

$$C_D = \frac{\tau^{5/3}}{\left[(\gamma+1)\, M_\infty^2\right]^{1/3}} \quad D(K)$$

In the case of wings of identical profiles and at the same incidence in two flows with different value of the ratio of specific heats γ_1, γ_2, (where suffixes 1, 2, are used to designate the two flows) but at the same value of the similarity parameter K, we have from eqn.5.4.2

$$\frac{(1 - M_{\infty 1}^2)}{\left[(\gamma_1+1)\, M_{\infty 1}^2\right]^{2/3}} = \frac{1 - M_{\infty 2}^2}{\left[(\gamma_2+1)\, M_{\infty 2}^2\right]^{2/3}} \qquad 5.4.4$$

and at points, given by the same dimensionless parameters

$x'_1 = x'_2$, $z'_1 = z'_2$.

We have from equations 5.4.3.

$$\left(\frac{C_{p_1}}{C_{p_2}}\right)_{K, x_1, z_1} = \left[\frac{(\gamma_2+1)\ M^2_{\infty_2}}{(\gamma_1+1)\ M^2_{\infty_1}}\right]^{1/3} \qquad 5.4.5.$$

and

$$C' = \left(\frac{C_{L_1}}{C_{L_2}}\right)_K = \left(\frac{C_{M_1}}{C_{M_2}}\right)_K = \left(\frac{C_{D_1}}{C_{D_2}}\right)_K = \left[\frac{(\gamma_2+1)\ M^2_{\infty_2}}{(\gamma_1+1)\ M^2_{\infty_1}}\right]^{1/3} \qquad 5.4.6.$$

Thus the ratio of the force coefficients for similar two-dimensional flow about identical profiles according to the transonic similarity law is given by equations 5.4.5. and 5.4.6.

5.5. Application of transonic similarity laws to finite aspect ratio wings.

In the case of three-dimensional flow, two similarity parameters H,K, occur in the transonic similarity rules given by equations 21, 23, 24, 25 appendix 1. These similarity rules are

$$C_p = \frac{\tau^{2/3}}{\left[(\gamma+1)\ M^2_\infty\right]^{1/3}} \qquad P\left(H, K, ; \frac{x}{c}, \frac{y}{b}, \frac{z}{b}\right) \qquad 5.5.1.$$

$$C_L = \frac{\tau^{2/3}}{\left[(\gamma+1)\ M^2_\infty\right]^{1/3}} \qquad L\ (H,K) \qquad 5.5.2.$$

$$C_M = \frac{\tau^{2/3}}{\left[(\gamma+1)\ M^2_\infty\right]^{1/3}} \qquad M\ (H,K) \qquad 5.5.3.$$

$$C_D = \frac{\tau^{5/3}}{\left[(\gamma+1)\ M^2_\infty\right]^{1/3}} \qquad D\ (H,K) \qquad 5.5.4.$$

where

$$K = \frac{1 - M^2_\infty}{\left[(\gamma+1)\ M^2_\infty\ \tau\right]^{2/3}} \qquad 5.5.5.$$

$$H = AR\left[(\gamma+1)\ M^2_\infty\ \tau\right]^{1/3} \qquad 5.5.6.$$

To obtain similar flows in fluids of different values of γ, the ratios of the specific heats, both H and K must be kept constant, and two special cases arise:-

(a) $\quad AR_1 = AR_2$

$$M_{\infty_1} = M_{\infty_2} \qquad 5.5.7$$

and $(\gamma_1+1)\tau_1 = (\gamma_2+1)\tau_2$

These satisfy the requirement of H and K being constant.

The similarity rules then give

$$\left(\frac{C_{p_{\gamma_1}}}{C_{p_{\gamma_2}}}\right)_{M_\infty,\ AR,\ (\gamma+1)\tau;\ \frac{x}{c},\ \frac{y}{b},\ \frac{z}{b}} = \left(\frac{C_{L_{\gamma_1}}}{C_{L_{\gamma_2}}}\right)_{M_\infty,\ AR,\ (\gamma+1)\tau}$$

$$= \left(\frac{C_{M\,\gamma_1}}{C_{M\,\gamma_2}}\right)_{M_\infty,\ AR,\ (\gamma+1)\tau} = \frac{\tau_1}{\tau_2} = \frac{\gamma_2+1}{\gamma_1+1} \qquad 5.5.8$$

and $$\left(\frac{C_{D_{\gamma_1}}}{C_{D_{\gamma_2}}}\right)_{M_\infty,\ AR,\ (\gamma+1)\tau} = \left(\frac{\tau_1}{\tau_2}\right)^2 = \left(\frac{\gamma_2+1}{\gamma_1+1}\right)^2 \qquad 5.5.9$$

Thus similarity exists for flows with different γ about three-dimensional wings of the same aspect ratio and at the same Mach number, but for related profiles of different thickness parameter.

(b) $\quad \tau_1 = \tau_2$

For H and K to be constant

$$\left[\frac{1 - M_\infty^2}{(\gamma+1)M_\infty^2}\right]^{2/3} = \text{const.} \qquad 5.5.10$$

and $$AR\left[1 - M_\infty^2\right]^{\frac{1}{2}} = \text{const.}$$

or $$AR\left[(\gamma+1)\,M_\infty^2\right]^{1/3} = \text{const.} \qquad 5.5.11$$

In this case to preserve similarity, the thickness parameter remains the same, but both the corresponding Mach numbers and aspect ratios are different.

The similarity laws give for the force coefficients in this case,

$$\left[\frac{C_{p_{Y_1}}}{C_{p_{Y_2}}}\right]_{H,K,\tau;\ \frac{x}{c},\frac{y}{b},\frac{z}{b}} = \left[\frac{C_{L_{Y_1}}}{C_{L_{Y_2}}}\right]_{H,K,\tau} = \left[\frac{C_{M_{Y_1}}}{C_{M_{Y_2}}}\right]_{H,K,\tau}$$

$$= \frac{C_{D_{Y_1}}}{C_{D_{Y_2}}} = \left[\frac{1 - M_{\infty_2}^2}{1 - M_{\infty_1}^2}\right]^{\frac{1}{2}} \qquad 5.5.12$$

5.6. Review of experimental work by von Doenhoff and Braslow (ref.11)

Von Doenhoff and Braslow (ref.11) used Freon-12 ($\gamma = 1.13$) as a testing medium in the Langley Low Turbulence Tunnel. Measurements of the pressure distributions were made in the Mach number range of 0.4 - 1.2 and at Reynolds numbers (at $M \leq 1$) of about 9.5×10^6 per foot chord on swept and unswept wings of aspect ratios of 4.0 to 9.0. The measurements were then compared with those made in air and methods of converting Freon data to air data were developed based on the streamline similarity concept using the critical area ratio $\frac{A_{cr}}{A}$

where A_{cr} = Area at sonic speed

A = " " any other speed

Stream-line similarity is shown to be consistent with transonic similarity laws if the thickness ratio of the body in Freon is $\left(\frac{1 + \gamma_A}{1 + \gamma_F}\right)^{\frac{1}{4}}$ or 1.030 as great as in air. In practice this difference in thickness was considered to be negligible and bodies of the same thickness were tested in air and in Freon. The results showed that no basic differences in flow phenomena exist at subsonic speeds and on the whole the corrections obtained on the assumption of area similarity seem to deal adequately with the small differences that do exist between Freon and air flow. An uncertainty exists when streamline similarity is applied to swept wings. For wings of small aspect ratio it is sufficient to apply it to the flow in the free-stream direction whereas for infinite AR it should be applied to the flow normal to the leading edge. Pressure distances measured in Freon-12 at various free-stream Mach numbers for a number of aerofoils were converted, by assuming streamline similarity, to equivalent pressure

distributions in air. The conversion factors for normal forces and pitching and hinge moment coefficients were plotted against the free-stream Mach number. Von Doenhoff concludes that the overall conversion coefficient can be considered to depend only on the free-stream Mach number and to be independent of the magnitude of the pressure distribution. Whilst the results quoted for conversion factors of the normal force coefficients seem to justify such a simplication, in the case of pitching moment and hinge moment conversion coefficients this seems doubtful as the scatter of the results is appreciable.

The conversion factors based on streamline similarity are different for the induced part of the drag and the wake drag and both depend mainly on the free-stream Mach number . To convert subsonic Freon drag results an estimate of the induced drag part is made by calculation and the rest is assumed to be wake drag and the separate conversion factors applied. At supersonic speeds the drag is resolved into that due to skin friction, which is assumed to be independent of angle of attack and that due to pressure which for the normal thin supersonic aerofoils with low leading edge suction can be assumed to be $\simeq C_N \alpha$

where C_N = normal force coefficient

α = angle of attack.

Hence to convert drag at supersonic speeds the drag is measured when $C_N = 0$ and the wake drag conversion factor is applied to this part of the drag and at any other incidence the normal-force conversion coefficient is applied to the remainder of the drag.

Since the spanwise normal-force coefficients are all multiplied by the same factor, the normal force conversion factor also applies to the rolling moment.

To convert side-force and yawing moments the nature of the forces involved has to be decided. For instance in the case of the yawing moment due to non-uniform skin-friction the wake drag conversion coefficient is applied but for the yawing moment caused by the deflection of the rudder the application of the normal force conversion coefficient is necessary.

The greatest difference between Freon and air results was considered to be most likely near the trailing edge. In order to obtain a critical check on the method of converting freon data generally and moments in particular in this region the hinge moments on an elevator on a full-span unswept tail plane were measured in Freon-12 and in air. The converted Freon data agreed well with the air data to at least the accuracy of the air data itself.

Critical discussion of von Doenhoff's results and conclusions drawn from it.

Von Doenhoff's results indicate that no basic differences exist between air ($\gamma = 1.4$) and Freon-12 ($\gamma = 1.13$) flows at subsonic and low supersonic Mach numbers. This is so even in the presence of strong shocks and with a large area of the wing stalled. Stream line similarity was successfully employed to transform pressure distributions and overall forces, but the following should be noted:-

(1) Wake-drag. No actual measurements of the loss of total head in the wake in Freon-12 were made by von Doenhoff. Experimental justification of the applicability of stream-line similarity would be desirable.

(2) Swept Wings. An ambiguity exists in the application of streamline similarity to swept wings.

(3) Moments. The accuracy obtained if the conversion factor is assumed to be dependent only on the free-stream Mach number may not be sufficient. This is indicated by the scatter of the conversion factor when plotted against free-stream mach number.

The difference in area ratio at the same Mach number between air and Freon become appreciable at supersonic Mach numbers (e.g. $M > 1.2$) and hence it is doubtful whether stream-line similarity exists at supersonic Mach numbers much in excess of about 1.2. To investigate the usefulness of Freon-12 at Mach numbers greater than 1.2 would require a supersonic tunnel equipped with Schlieren Apparatus. For economic reasons this tunnel could be an intermittent type. Shock-wave boundary layer interaction could be studied in such a tunnel.

Measurements in Freon-12 of wake drag and pressure distributions on swept wing models are necessary in order to obtain the appropriate conversion factors. The first of these has been partially explored in the present series of tests.

6. The College of Aeronautics Freon-12 Wind-tunnel

The general design of wind-tunnels using a medium other than air is discussed, followed by a detailed description of the College of Aeronautics Freon-12 wind tunnel.

6.1. General design considerations

The simplest approach to the use of a medium other than air for aerodynamic testing is a blow-down tunnel in which the gas is allowed to escape directly to atmosphere (ref.17) The savings obtained by dispensing with any additional equipment are offset by

the loss of the gas after each run.

In general the design is not unlike that of a compressed air tunnel except that it is more important to make the tunnel leak-proof to avoid either large losses or the contamination of the gas by air. In addition provision has to be made for:-

(a) Filling the tunnel with the gas

(b) removing the gas

(c) purifying the gas

(d) storage.

Additional problems may arise because of the special properties of the medium, though in general the gases that are considered are substantially non-corrosive, non-toxic, non-inflammable and stable (see section 6.3)

To fill the tunnel with the gas the air can be evacuated, as in the College of Aeronautics tunnel, or if a heavy vapour is used it is possible to introduce it slowly at a low point in the tunnel and to remove the air from the highest point. This latter method is especially useful if the tunnel shell cannot withstand pressure differences as is often the case.

Recovery

If it is desirable to avoid the loss of the gas each time access to the tunnel is required, provision has to be made to remove most of it from the tunnel, to a storing unit. Pressure bulkheads around the working section will be a means of considerable time saving when access only to the model is required. The capacity of the pumping equipment will depend on the volume of the tunnel system and the time interval in which it is required to reach a specified low pressure. It should be pointed out that as the system is invariably never completely leak proof the lowest pressure that can be reached will depend on the capacity of the pump and the rate of leakage.

The storage containers are much more bulky if the medium is stored in the gaseous state rather than as a liquid. Liquid storage is only practical if the critical temperature of the medium is well above the room temperature encountered, otherwise constant refrigeration would be necessary.

6.2. Purification

Some mixing of the gas with air and moisture is unavoidable. If the gas is to be used repeatedly some means of purifying it will be necessary. Moisture can be removed by passing the gas over a suitable drier containing for example silica gel or activated alumina. Both these desiccants are liable to disintegrate into small particles which are then carried away by the gas. The risk of disintegration increases at higher gas velocities. The drying of the medium in the liquid phase when the velocities are much lower and the time of contact correspondingly longer, might prove advantageous.

When the vapour is liquified, non-condensible gas impurities, such as air will collect above the liquid and the pressure will rise as liquification proceeds. The non-condensible vapours will have to be purged when the maximum delivery pressure of the condensing unit is reached. Ideally the proportion of the vapour in the purged gas will be equal to the ratio of the saturation vapour pressure p_s at the temperature of the liquid to the pressure in the liquid container, p.

i.e. to $\frac{p_s}{p}$

The saturation pressure decreases with the liquid temperature and hence for minimum vapour losses it is desirable to have low liquid temperature combined with high pressure in the output stage of the condenser. In practice the proportion of vapour lost will probably be greater than $\frac{p_s}{p}$, as additional vapour tends to remain suspended in the form of fine mist in the purged mixture.

6.3. The 5.25in.x7.5inannular return F-12 Tunnel at the College of Aeronautics

A programme of research into the use of media other than air in wind-tunnels was initiated at the College of Aeronautics in 1951 and Freon-12 was chosen as a working medium.

Properties of Freon-12 (Dichlorodi-fluoro-methane, CCl_2F_2)

The physical and thermodynamic properties are listed in ref.35(at low pressures) and ref.33.

The critical temperature is 111.5°C and critical pressure 39.6 atm. The vapour pressure at 60°F is 72.4 lb/sq.in. Freon-12 in the liquid state is colourless and has a faint ethereal odour. It is stable at ordinary temperaturesbut dissociates when in contact with a red-hot surface or flame. It is also non toxic, non-irritant, non-inflammable and non-explosive.

It does not corrode ordinary metals and alloys used industrially except for magnesium and its alloys.

Most lubricants used for refrigeration purposes are mixible without reaction, though separation can occur at low temperatures.

It is seen from this description that no special difficulties arise in the handling of Freon-12, except that special bearing design is required because of the de-oiling properties.

Tunnel

It was decided to utilise a 1/16th model of the RAE Annular Return High Speed Tunnel (ref.29). A cross-sectional drawing appears in fig.8. The working section is 7.5in.x 5.25in.and 10.25in.long. Access to the working section is via removable covers in the outer-shell and the annulus. The annulus is made of gun metal and supported by streamline struts. Pressure connections to outside manometers enter the annulus inside these struts. The outer shell is of cast iron and can withstand vacuum and two atmospheres absolute. The cast iron shell was found to be extremely porous and had to be painted with special resins to make it leakproof at low pressures. The internal volume of the tunnel is about 18 cu.ft.

Fan & Motor

To seal the fan-shaft effectively which has to revolve at high speed, is very difficult and hence the whole motor was enclosed in a pressure shell which was ventilated to the rest of the tunnel.

Originally the fan was mounted on a fan-shaft which was supported on two special impregnated cage bearings. These were tried because of the de-lubricating properties of Freon-12. The motor drove the fan-shaft through a flexible coupling. Serious ventilation trouble was experienced which was mainly due to insufficiently rigid mounting of the motor, the tunnel housing itself acting as a diaphragm. The original arrangement was abandoned in favour of the present one which has the fan mounted directly on the motor shaft. The motor is now fixed to the tunnel end cover so as to provide least overhang. The motor is a synchronous induction motor giving 100 H.P. at 10000 RPM. A sketch of the associated control equipment is shown in fig.9.

The 13 blade fan is of one stage with fixed guide vanes upstream and downstream.

Freon-12 Circuit Lay-out

A diagrammatic sketch of the Freon-12 tunnel system is presented in fig.9. A general description of the system and the manner of operation is given below, followed by a detailed description of the various units.

The gas exit pipes leave the top of the tunnel at three points and there is also one connection to the top of the gas storage tank. Similar connections exist to the bottom of the tunnel and storage tank for the entry pipes. This ensures that any residual air left over in the tunnel is efficiently displaced by the heavy Freon gas. The exit pipe leads to a Geryk vacuum pump capable of exhausting the whole system to 0.5 mm Hg abs. pressure in about $\frac{1}{2}$ hr.

The Freon-12, which is stored as a liquid in a special container at up to 180 lb/sq.in. abs pressure, is then allowed to evaporate through an orifice plate. The orifice plate prevents a too rapid evaporation and consequent large drop in temperature which would cause any moisture present to freeze and probably block the passages. From there the Freon passes through a "stillite" oil filter which serves to remove any oil mist carried over by the vapour. This may be caused by oil dissolved in the liquid Freon phase. Most of the oil is picked up in either the condenser pumps or the circulation pump, both of which are of the reciprocating type.

The Freon-12 vapour then passes through an activated alumina bed and then a silica gel drier into either the gas storage tank or through a heat exchanger into the tunnel. The activated alumina will also remove any oil mist that may have remained in the Freon. The heat exchanger utilises the hot air from a 1 kw heater which is provided in the silica gel unit for reactivation. In practice it is not used, as the gas after evaporation very quickly reaches room temperature.

6.5. Circulation

Constant stagnation pressure is maintained in the tunnel by means of an automatic valve, controlling the rate of flow through the circulation pump and the suction of the condensing unit. Fresh gas is allowed to enter the tunnel from the gas storage tank. By continually circulating the gas in the tunnel its purity can be maintained over longer periods. It also serves to maintain lower running temperatures especially if the condensing unit is used to circulate the gas. The gas storage tank is used for the dual purpose of increasing the effective volume of the tunnel and also to permit the removal of the gas from the tunnel without reliquifying it.

The condenser can work up to a delivery pressure of 165 lb/sq.in. This is just over double the vapour pressure of Freon-12 at room temperature and hence the composition of the mixture purged during liquification will be almost of equal amount of Freon-12 and non-condensible gases. Thus efficient recovery of the Freon-12 is not possible for mixtures containing relatively large proportion of air.

The minimum inlet pressure to the condensing unit is about $\frac{1}{3}$ atm. and hence for efficient recovery of Freon-12 from the system it would be necessary to use an auxiliary pump.

The capacity of the gas storage tank is 70 cu.ft. and that of the whole system approximately 100 cu.ft.

The total charge of Freon required at 1 atm. pressure and 60° F is about 36 lb.

While the tunnel is running a small amount of Freon controlled by a valve is allowed to pass through the sound measuring gauge, (see section 6.6.) so as to keep a constant check on the purity of the Freon -12.

Care was taken in the design of the system to prevent any liquid Freon being sealed in the pipe circuits as this might cause rupture should the temperature increase.

The tunnel pressure when evacuated can be measured on a vacustat.

Valves are provided in the circuits so that in addition to operational requirements it is possible to seal off each unit from the tunnel to allow quick repairs. It was found necessary at all times to ensure that the valve packing glands were adequately tightened to prevent leakage.

6.6. Detailed Description of Components

Liquid Receiver: The capacity is approximately 3600 cu.in. for a maximum charge of 152 lb of Freon-12. Provision is made for the transfer of liquid Freon-12 directly from the manufacturers containers. The whole receiver is suspended from a balance to enable the mass of gas to be determined.

Freon Condensing Unit

The "Pulsometer" compressor is a twin cylinder reciprocating type delivering 385 cu.ft. per hr., at 700 r.p.m. It is capable of delivering approximately 0.75 cu.ft./min. at atmospheric inlet pressure

and an exit pressure of about 120 lb/sq.in. The water circulation through the cooler is about 150 g.p.h. at 60° F.

Stillite filter

Stillite is a form of slag wool of which the fibres are of very small diameter, the general theory of fibre filters has been the subject of papers by Stairmand (ref.36).

The required packing density is 17 lb/ft^3, at a face velocity of 1 ft/sec. This gives a pressure drop of 0.3 lb/sq.in/foot depth of packing. The filters operate in the Stokes' flow regime and hence the pressure drop is proportional to the face velocity.

The filter on the freon-tunnel consists of a horizontal disc of 14" diameter and 3" thick. The gas flows upwards through the disc and at face velocities less than 0.5 ft/sec. the oil should be able to drain against the flow of the gas.

Activated Alumina Drier

The drier consists of a cylinder of 8" diameter and 3'6" long filled with granules of activated alumina. During operation cold Freon-12 gas from the liquid condenser is passed through coils embedded in the activated alumina to remove the heat liberated by the absorption of moisture from the vapour that is passed through the alumina itself.

Silica Gel Drier

The plant is designed to dry 2 c.f.m of Freon-12 at pressures ranging from 14.7 lb/sq.in to 30 lb.sq.in. with inlet temperatures of about 60° F down to a moisture content of less than 0.0002 lbs per lb. of dry Freon. The plant can perform this duty for a period of about 8 hrs. It has then to be regenerated by heating and drying by means of the fan and heater unit supplied with it.

Automatic stagnation pressure control valve

This is a Short & Mason pneumatically operated control valve operating over the pressure range zero to two atmospheres using atmospheric pressure as the reference pressure.

Pulsometer type 'Geryk' Rotary Vacuum Pump

The swept volume of the pump is 20 cu.ft/min at 360 r.p.m. and it is capable of achieving 0.005 mm. Hg. The lowest pressure it was possible to achieve in the tunnel was 0.05 mm.Hg.

Circulating Pump (Polsometer)

This is a reciprocating type of pump having a swept volume of 7 c.f.m. The minimum inlet pressure was 1 in.Hg. absolute when the delivery pressure was about 30 lb/sq.in. Some difficulties were experienced with the use of this pump due to the gas picking up oil in its passage through the pump.

Description of the sound measuring gauge

A special gauge to measure the speed of sound in Freon-12 was designed by the Electrical Department of the College of Aeronautics. A schematic diagram of the gauge appears in fig.10.

The principle employed in this gauge is to measure the time required for a signal to travel a given distance.

A high intensity sharp fronted signal is fed into one of the transducers and is also used to open a gate allowing pulses from a quartz oscillator to pass to a microsecond counter. The arrival of the signal at the receiving transducer is used to shut the gate. In order to obtain the speed of sound from the measurements the temperature of the gas has to be known and is measured by a thermometer in the outlet pipe of the tube. The sampling rate of the gauge can be adjusted to give 1 sec, 2 sec, 5 sec, and 15 sec. sampling intervals.

The transducers consist of thin aluminium foil stretched between a magnet. This gives maximum responsiveness to sharp edged signals and also acts as a good positional location.

The distance between the two transducers is three feet and the diameter of the pipe is 4in.

The proportion of air in the freon is found by the method discussed in appendix 11.

7. Calibration of Freon Tunnel

7.1. Introduction

The 1/16th scale model of the R.A.E. High Speed Tunnel was calibrated with Freon-12 over the entire speed range. The uniformity of flow in the working section was determined by measuring the pressure at wall tappings and by means of a traversing pitot-static tube.

7.2. Tunnel and Apparatus

The tunnel was calibrated in terms of the pressure differences between the settling chamber and the first tapping which is $3\frac{7}{8}$" ahead of the working section. The pressure at this tapping should not be affected by the presence of the model. This pressure difference was measured on a "master manometer", which is a null reading instrument, and can be read to within 0.002" of mercury. A diagram of the arrangement appears in fig.11. The pressures at the four tappings in the working section and at the tapping ahead of it are denoted by p_1, p_2, p_3, p_4, p_5 respectively and the pressure recorded by the static tube is denoted by p'. The difference between these pressures was measured on a bank of manometers filled with Butyl Phthlate. In addition the stagnation pressure, and the total head and static pressure of the traversing pitot tube were recorded against an atmospheric datum. A thermo-couple mounted on a strut projecting into the centre of the settling chamber allowed the stagnation temperature to be read.

Figures 12 and 13 show the pitot-static tube and its traversing mechanism. The gauge is designed to fit into the limited space in the annulus and is driven by a remotely controlled selsyn motor through an arrangement of gears and a screw jack.

7.3. Accuracy

Notation

p_A = atmospheric pressure

p_t = pressure at wall tapping in settling chamber

p_1 = pressure at wall tapping 1.7 in. downstream of beginning of working section

p_2 = pressure at wall tapping 4 in. " " " " " "

p_3 = pressure at wall tapping 6.3 in. " " " " " "

p_4 = pressure at wall tapping 8.45 in. " " " " " "

p_5 = pressure at wall tapping $3\frac{7}{8}$ in. " " " " " "

p_n = pressure at any of the wall tappings 1, 2, 3, 4.

H = total head pressure in working section

(a) Instruments

The manometers can be read to within 0.05in.with the exception of the master manometer and the barometer used to measure atmospheric pressure. These can be read to within 0.002in.Hg. The specific gravity of Butyl Phthlate is 1.053 and hence 0.05in.Butyl Phthlate $\approx$ 0.005 in.Hg

With p_A = 30inHg and p_t = 400inButyl Phthlate

$\Delta p_A = \pm$ 0.001 in. Hg.

$\therefore \Delta(p_A - p_t) = \pm$ 0.1inButyl Phthlate

Thus $\Delta p_t = \Delta p_A + \Delta(p_A - p_t) = \pm$ 0.1 in. Butyl Phthlate

and the accuracy of the settling chamber pressure is

$$\frac{\Delta p_t}{p_t} = \pm 0.0003$$

The accuracy of the difference between any of the pressures

p_1, p_2, p_3, p_4, p_5, p' is $\pm$ 0.2inButyl Phthlate

or $$\frac{\Delta p_n}{p_t} = \pm 0.0005$$

(b) Accuracy of Measurements

The pressure difference $p_t - p_5$ measured on the master manometer was found to be sufficiently steady at low speed, $M_\infty = 0.4$, to be read within $\pm$ 0.010inHg and at $M_\infty = 0.8$ to only about $\pm$ 0.1inHg.

At $M_\infty = 0.8$, the difference between the pressures p_1, $p_2 \cdots p_5$ could be read with an estimated accuracy of $\pm$ 0.2inButyl Phthlate.

Hence (at atmospheric stagnation pressure) and $M_\infty = 0.4$,

$$\frac{\Delta p_t}{p_t} = \pm \frac{0.01}{30} \approx \pm 0.0003 = \frac{\Delta H}{H}$$

Since $\Delta(p_t - p_5) = \pm$ 0.01inHg.

we have $$\frac{\Delta(p_t - p_5)}{p_t - p_5} = \pm 0.003 \text{ if } p_t - p_5 = 3 \text{ in.Hg.}$$

Hence $$\frac{\Delta\left(\frac{H - p}{H}\right)}{\frac{H - p}{H}} \approx \pm 0.003$$

and with $\left(\frac{H - p}{H}\right)_{M_\infty = 0.4} = 0.1$

we have $\Delta\left(\frac{H - p}{H}\right) = \pm 0.0003$

Therefore $\Delta M_\infty = \pm 0.001$ and $\frac{\Delta M_\infty}{M_\infty} = \pm 0.2\%$

At $M_\infty = 0.8$

Since $\Delta (p_t - p_5) = \pm 0.1$ in.Hg. and $(p_t - p_5) = 10$ in.Hg.

we have $\frac{\Delta(p_t - p_5)}{p_t - p_5} = \pm 0.01$

Therefore $\Delta\left(\frac{H - p}{H}\right) = 0.01 \times 0.3 = \pm 0.003$

and $\Delta M_\infty = \pm 0.005$ or $\frac{\Delta M_\infty}{M_\infty} = \pm 0.5\%$.

Accuracy of the Mach number variation along the working section

At $M_\infty = 0.4$

$\Delta(p_5 - p_n) \approx \Delta p = \pm 0.1$ in Butyl Phthlate

giving $\frac{\Delta p}{p} = \frac{0.1}{400} \simeq \pm 0.0003$.

and $\frac{\Delta M_\infty}{M_\infty} = \pm 0.002$ or $\Delta M_\infty = \pm 0.001$

At $M_\infty = 0.8$

$\Delta(p_5 - p_n) = \Delta p = \pm 0.4$ Butyl Phthlate

giving $\frac{\Delta p}{p} = \frac{0.4}{300} = 0.001$.

and $\frac{\Delta M_\infty}{M_\infty} = \pm 0.001$ or $\underline{\Delta M_\infty = \pm 0.001}$

7.4. Experimental Measurements

All the manometers, shown in fig.11 and the stagnation temperature were read while the fan speed was kept constant. The operator controlling the motor speed was unable to observe the master manometer and hence no attempt was made to run the tunnel at any specific Mach number or to keep it accurately constant during a run. In the higher speed range the readings were taken before the tunnel reached its terminal temperature which continued to increase over a considerable period in spite of continuous cooling of the tunnel. However the change in temperature was small during the interval required to take readings. Sets of readings were taken while the fan r.p.m. was increased in steps of 300 from about 3600 to 7200 rpm equivalent to a Mach number range of 0.4 to 0.9.

Readings were taken with the total head tube at 0.75", 1.25", 1.75", 2.25", 2.75", 3.25", 3.75", 4.25" and 4.5" from the wall from which the gauge was mounted.

Readings were also taken at 1.7" (opposite pressure hole no.1) 5.4" and 8.45" (opposite pressure hole no.4) downstream of the beginning of the working section along the centre-line of the tunnel.

7.5 Results from total head measurements

The error in assuming that the pitot tube pressure is the actual total head pressure should be negligible even if the pitot tube is yawed slightly, which might be the case at high speeds.

$\frac{H - p_t}{p_t}$ was plotted over the whole speed range and the various transverse positions for each of the three downstream positions (see fig. 14, 15, 16), 'x' denotes the downstream distance of the plane of measurement and 'y' the distance of the total head tube from the wall on which it is mounted.
The variation of $\frac{H - p_t}{p_t}$ for the various transverse positions of the gauge was then found.

From the above figures

$$\frac{\Delta H}{H} \simeq \frac{\Delta H - p_t}{p_t} \simeq \pm 0.001 \text{ at } M_\infty = 0.4$$

giving $$\frac{\Delta M_\infty}{M_\infty} = \pm 0.005$$

and $$\Delta M_\infty = \pm 0.002.$$

At $M_\infty = 0.8$

$$\frac{\Delta H}{H} = \Delta\left(\frac{H - p_t}{p_t}\right) = \pm 0.003.$$

giving $$\frac{\Delta M_\infty}{M_\infty} = \pm 0.003$$

or $$\Delta M_\infty = \pm 0.003$$

The average values of $\frac{H - p_t}{p_t}$ at the various transverse positions, are plotted in fig.17 for the three downstream positions. They agree with one another to within 0.0005 and also are close to the tunnel centre-line values.

They also agree well with the calculated value of $\frac{H - p_t}{p_t}$ based on the Area ratio

$$\frac{A_s}{A_w} = 6.55$$

where A_s = settling chamber area

and A_w = working section area

7.6. Transverse Variation of static pressure in the working section

The variation of static pressure across the working section is more difficult to measure, as corrections due to variable blockage and yaw which might arise through bending of the tube under load may be large.

$\frac{p_1 - p'}{p_t}$ and $\frac{p_4 - p'}{p_t}$ were plotted in fig.18 and 19 in the case where the plane of measurement coincided with pressure holes 1 and 4 respectively.

$\frac{p' - p_1}{p_t}$ and $\frac{p' - p_4}{p_t} \approx \pm 0.0005$

giving $\frac{\Delta M_\infty}{M_\infty} \simeq 0.003$ or $\underline{\Delta M_\infty = \pm 0.001}$ at $M_\infty = 0.4$

At higher speeds the scatter of results becomes greater but is probably not representative of the actual static pressure variation in the absence of the pitot tube.

From the variation of static and total head pressure in the working section the flow is estimated to be uniform at least to within $\underline{\Delta M_\infty \approx \pm 0.005}$

7.7. Variation of static pressure along the working section

Measurement of the pressure at the four wall tappings in the working section (p_1, p_2, p_3, p_4) and at the tapping ahead of the working section (p_5) were made with an empty working section.

The values of $\frac{p_5 - p_1}{p_t}$

$\frac{p_2 - p_1}{p_t}$, $\frac{p_3 - p_1}{p_t}$, $\frac{p_4 - p_1}{p_t}$ with the tunnel empty agreed with those made when the pitot static tube was mounted opposite pressure hole 4 (e.g. 8.45in.downstream of beginning of w.s.)
They are plotted in figs. 20, 21, 22, 23 respectively as a function of the tunnel pressure ratio $\frac{p_t - p_5}{p_t}$.

$\frac{p_5 - p_1}{p_t}$ is plotted in fig.23 using measurements made with the tunnel completely empty.

The variation of Mach number from the value at station 2 was calculated from

$$\Delta M = \frac{\partial M}{\partial (p/H)} \cdot \Delta\left(\frac{p}{H}\right) = \frac{\partial M}{\partial (p/H}, \cdot \frac{\Delta p}{H} \quad \text{with } \gamma = 1.125$$

assuming no variation of total head.

Using the values of $\frac{p_5 - p_1}{p_t}$, $\frac{p_1 - p_2}{p_t}$ ..... $\frac{p_4 - p_1}{p_t}$ obtained from figs. 20 - 23 as $\frac{\Delta p}{H}$ in the above equation the value of the

Mach number variation along the working section was calculated and is plotted in fig.24 for $M_2 = 0.4,\ 0.5,\ 0.6,\ 0.7,\ 0.8,\ 0.85$.

The maximum deviation of Mach number in the working section from the value at station 2 on the basis of these measurements is $\Delta M = 0.003$ at $M_2 = 0.4$ and $\Delta M = 0.005$ at $M_2 = 0.85$.

7.8. Working section Mach number

The working section Mach number was based on the static pressure measured at No.2 tapping in the working section. Thus, if

$$\frac{H - p_t}{p_t} = h \quad \text{then} \quad H = p_t\,(h + 1)$$

and

$$\frac{p_t - p_2}{p_t} = \pi \quad \text{or} \quad p_2 = p_t\,(1 - \pi)$$

giving

$$\frac{p_2}{H} = \frac{1 - \pi}{1 + h}$$

h is found from fig.15 and π from figs. 13, 20.

The Mach number was then calculated from the isentropic flow relation

$$\frac{p}{H} = \left[1 + \frac{\gamma - 1}{2} M^2\right]^{-\frac{\gamma}{\gamma + 1}}$$

with $\gamma = 1.125$

The accuracy of the calibration is estimated to be $\Delta M = \pm 0.005$.

7.9. Purity of Freon

The amount of air present in the Freon was usually from 2% to 6% (by mole fraction) this was frequently checked by means of the sound gauge measurements.

8. Two-dimensional aerofoil tests in the Freon-12 tunnel

8.1. Model

A 2in.chord model of an RAE 104 10% Symmetrical aerofoil section was obtained through the courtesy of the N.P.L. The ordinate of the RAE 104 section are given in (ref.31) and the position of the pressure holes on the model are shown in fig.25.

A large number of tests have been made at the N.P.L. on the two-dimensional models of RAE 104 symmetrical aerofoils including some on a 5in.chord model in the 18in.x 14in.tunnel.

Comparison of measurements were made between those on the 2in.chord model in the Freon-12 tunnel at atmospheric stagnation pressure, and similar measurements in the N.P.L. 18in.x 14in.air tunnel on the 5 in. chord model at atmospheric stagnation pressure.

In this comparison we have

(a) The Reynolds number is almost identical

(b) The ratio of tunnel height to tunnel width in the two cases is very similar, e.g:-

$$\frac{h}{b} = \left(\frac{18}{14}\right)_{\text{Air}} = 1.3 \quad \text{and} \quad \left(\frac{7.5}{5.75}\right)_{\text{Freon-12}} = 1.4.$$

and

(c) The ratio of model maximum thickness to tunnel height in the case of air and Freon-12 tunnel is

$$\frac{0.5}{18} = 0.028 \quad \text{and} \quad \frac{0.2}{7.5} = 0.027$$

respectively. Hence the magnitude of the solid blockage correction will be of the same order. This allows for a comparison on the basis of results uncorrected for blockage.

8.2. Model Mounting and pressure measurements

New side walls with turn-tables to take the 2in.chord model were made. The turn-tables were equipped with a vernier allowing the model incidence to be positioned with an accuracy of approximately $\pm$ 5 minutes.

The position of the model in the working section is shown in fig.26.

Pressure Measurements

The pressure difference between the working section reference pressure and the settling chamber pressure was measured on a master manometer. The pressures on the wing were measured on a butyl phthlate manometer at low speeds and on a mercury manometer at high speeds. The difference between atmospheric pressure and the settling chamber pressure was also recorded. The total head pressure can then be obtained from fig.17 or directly from readings of a 1 mm outside diam. total head tube mounted 1in.downstream of the trailing edge and 1.5in.from the walls and floor (see fig.26).

8.3. Pitot traverse gear

A remotely controlled traverse gauge was designed for pitot traverse measurement from which the wake drag was determined. As there was not sufficient room in the annular space adjacent to the walls parallel with the wing, the gauge had to be mounted of the same walls as the wing itself (fig.12). A nearly vertical traverse of the pitot tube was made by swinging it about a hinge mounted in the tunnel wall. The radius of the pitot head arm was 3.3in.so that the traverse of the wake was not at mid-span. The head was driven by a selsyn motor through a reducing gear box. The total head tube was mounted about a hinge in the working section wall and was driven by a wheel working on a quadrant affixed to it.

The whole driving mechanism was contained in a gas proof box to prevent leaks into the working section. One turn of the motor moved the head through 0.001 in.

The motor was driven electrically and the number of turns with respect to the central position were noted. At the start of these tests the pitot head consisted of a $\frac{3}{8}$in. length of 0.020in. outside diam. tubing telescoped into a tube of larger diameter, but this was found unsatisfactory due to a too large time lag. Finally a head of 0.040in.outside diam. tubing was used. This head proved satisfactory except that it read low when the tunnel warmed up after running at high speeds for prolonged periods. This was eventually traced to some plastic tubes which developed leaks at the higher temperature encountered in the tunnel. Modification to the tube connections provided adequate sealing.

8.4. Calculation of Results

The uncorrected Mach number M_u was obtained from the calibration chart. The pressure coefficient C_p was calculated from

$$C_p = C_{p_u} - \left(\Delta C_p\right)_{\text{blockage}} = \left(\frac{p_n - p_\infty}{\frac{1}{2}\rho_\infty U^2} - \frac{p_c - p_\infty}{\frac{1}{2}\rho_\infty U^2}\right) = \left\{\frac{(p_n - p_5) + (p_5 - p_2) + (p_2 - p_c)}{\frac{1}{2}\rho_\infty U^2}\right\}$$

where p_n = pressure at n^{th} tapping on wing

$p_\infty = p_2$ = free stream static pressure based on "no.2" wall tapping 3.95in.down stream of the working section.

p_5 = reference static pressure based on the tapping 2.15in.ahead of working section.

$$p_2 - p_c = \Delta p = p \cdot \gamma \cdot M^2 \epsilon$$

$$\epsilon = \epsilon_s + \epsilon_w$$

ϵ_s = solid blockage factor

$$= 0.52 \left(1 + 1.2 \frac{t}{c}\right) \frac{A}{h^2} \frac{1}{\beta^3}$$

A = aerofoil cross-sectional area = 0.266 sq.in.

h = tunnel height = 7.5 in.

$$\beta = \sqrt{1 - M^2}$$

ϵ_w = wake blockage factor = $0.0667 \frac{C_D}{\beta^2}$.

and $$\delta M = M_c - M_u = M_u \left(1 + 0.0625 M_u^2\right) \epsilon$$

Calculation of ratio of static pressure to total head

The ratio of static pressure to total head is given by

$$\frac{p_n}{H} = \frac{\left(p_n - p_5\right) - \left(p_t - p_5\right) + p_t}{\left(H - p_t\right) + p_t}$$

where $\frac{H - p_t}{p_t}$ can be obtained from the calibration graph or alternatively $H - p_t$ can be obtained by direct measurement from the reference total head tube.

Results - fixed transition at leading edge

The transition was fixed near the leading edge of the wing by painting on a layer of grade F carborundum powder mixed with Durofix for 7% of the chord. The thickness of the layer was about 0.005 in. The experience of the National Physical Laboratory has shown that, with this transition band, the drag of the aeroifoil was not appreciably increased over that expected with the transition at the leading edge.

The pressure distribution over the wing was measured at

M corr = 0.402, 0.447, 0.499, 0.555,
0.601, 0.653, 0.683, 0.703,
0.728, 0.762, 0.787, 0.806, 0.851

8.5. Pressure distributions in Air and Freon-12. $\alpha = 0^{\circ}$

The pressure coefficients and the ratio $\frac{p}{H}$ were calculated and are presented in tables 1, 2 and 3. $C_p(0)$ is the reduced value of the pressure coefficients at M = 0 using the Prandtl-Glauert law. The calculated chordwise pressure distribution at M = 0 and $\alpha = 0^{\circ}$ is plotted in fig.27 (ref.31). The measured pressure distributions in Freon are given in fig.28. The pressure distributions obtained by N.P.L. in the 14 x 18in. tunnel for the 5 in. chord aerofoil are plotted in fig.29. Comparison between these two sets of results show that in general the pressure distribution in Freon and air are very similar. It can also be seen that at M = 0.85 the shock wave position is approximately the same in the two cases.

To compare the pressure coefficients in Freon-12 and air, the Freon-12 results for the various chordwise stations on the aerofoil have been plotted as a function of the Mach number in figs. 30 to 38. The results of the N.P.L. tests in air on the 2in. model in the 8 x 20 in. tunnel and on the 5in. chord model in the 14 x 18in. have also been plotted in figs. 30 to 38. The Freon-12 results have been converted by means of the area similarity and the transonic similarity rules and are tabulated in table 4. The converted results have also been plotted in figs. 30 to 38. Except at higher Mach numbers the application of the area similarity law to the front portion of the aerofoil gives a pressure coefficient correction and a corresponding small difference in the freestream Mach number. The converted results fall approximately on the same C_p v M_∞ curve. The difference between the converted pressure coefficients obtained from the application of either the area similarity law or the transonic similarity law to convert the Freon-12 to air results is very small. Application of the transonic similarity law is simpler as the correction term is expressed only as a percentage of a function of the free-stream mach number. No definite conclusion as to the advantages of either method could be drawn as the difference between the Freon and air results was in all probability not only due to a difference in the ratio of specific heat. This is borne out by the difference between the pressure distributions in air on the 2in. and the 5in. chord models.

The chord wise pressure distributions in terms of $\frac{p}{H}$ are plotted in figs. 39 and 40.

The air results are the N.P.L. measurements on the 5in. chord model.

The pressure ratio $\frac{p}{H}$ is plotted as a function of the free-stream Mach number in figs. 41 to 50 together with the air values and the converted values based (a) on the assumption of area similarity (b) equal Mach number distribution.*

The agreement of the results is good except at the higher Mach numbers.

Owing to the small number of pressure holes on the 2in.chord model the pressure distributions were not integrated to determine the overall force coefficients.

8.6. Drag Measurement $\alpha = 0^{\circ}$

The wake drag of the RAE 104 aerofoil was measured by use of the pitot traverse method. The total head loss was measured on a U-tube filled with butyl phthalate with the settling chamber pressure as reference. The plane of measurement was one chord behind the trailing edge.

A simple method of calculating the drag from the wake traverse after R & M. No.2914 was used, assuming that the static pressure is equal to the free-stream static everywhere in the wake. The integrating factor

$$F = 2\left(\frac{H_1}{H_\infty}\right)^{\frac{\gamma-1}{\gamma}} \left\{ \frac{1-\left(\frac{P_\infty}{H_1}\right)^{\frac{\gamma-1}{\gamma}}}{1-\left(\frac{P_\infty}{H_\infty}\right)^{\frac{\gamma-1}{\gamma}}} \right\} \left[1 - \left\{ \frac{1-\left(\frac{P_\infty}{H_1}\right)^{\frac{\gamma-1}{\gamma}}}{1-\left(\frac{P_\infty}{H_\infty}\right)^{\frac{\gamma-1}{\gamma}}} \right\} \right] \frac{H_\infty - P_\infty}{H_\infty - H_1}$$

where $H_1 = 0.25\, H_\infty + 0.75\, H_m$

H_m = minimum total head pressure

H_∞ = total head in free-stream

P_∞ = static pressure in free-stream

---

* Footnote

In this case it is assumed that the Mach number is the same at corresponding points in the two flows for the same free-stream Mach number.

$$C_D = F \int \frac{H_\infty - H}{H_\infty - P_\infty} \, d\left(\frac{y}{c}\right)$$

was calculated (see fig.51) for the case of $\gamma = 1.125$ for a number of values of $\frac{H_m}{H_\infty}$ corresponding to $(H_\infty - H_m) = 5, 10, 20, 30, 40, 50$ ins. of Butyl Phthalate at H_∞ = atmospheric pressure for a range of Mach numbers.

The wake measurements are presented in fig.52 and 53 and the N.P.L. and Freon-12 drag results are listed in table 3 and are plotted in fig.54 as a function of free-stream Mach number. The wake drag measurement on the RAE 104 aerofoil at the N.P.L. were made on the 5 in. chord model so that the Reynolds number of the tests was very nearly the same.

e.g. N.P.L. Reynolds number 1.8×10^6 at $M = 0.85$

C.o.A. Reynolds number 1.7×10^6 at $M = 0.85$

It was found that the drag coefficients at $M = 0.6$ in Freon-12 were transition free 0.0093, transition fixed 0.0107 and in Air transition fixed 0.0087.

Transition was fixed in the N.P.L. 14 x 18in tunnel tests on the 5in. chord RAE 104 aerofoil by ejecting air at 10% chord, and occurred at approximately 20% chord.

On the basis of theoretical estimates the N.P.L. results would be expected to give a drag coefficient 0.0015 lower than the Freon-12 measurements with transition fixed at the leading edge. This accounts sufficiently well for the measured difference of 0.0020.

The drag rise in Freon-12 appears to occur at a Mach number of 0.03 lower than in air. This however, is based on only one measurement which is not reliable since at the higher Mach numbers the unmodified pitot head gave spurious readings because of the continuously rising temperature during the experiment. This is confirmed by examining the pressure distributions, where it is seen that the drag rise occurs well after supersonic velocities on the aerofoil have been reached. On the other hand the Freon-12 drag measurements with transition free which were made with the modified pitot head agree closely with the air results. In this case the measured drag rise occurred at a lower Mach number in Freon-12, the difference being 0.01. However, this does not agree with either the area similarity rule or the transonic similarity rule which predict that the Freon-12 drag rise Mach number should be greater than the corresponding air Mach number by 0.01.

8.7. Pressure Distributions in Air and Freon-12 at $\alpha = 4^{\circ}$

The incidence of the wing was adjusted to 4°, the accuracy being approximately $\pm 5'$ on the vernier setting. The "upper" surface had four pressure holes at 0.80, 0.35, 0.20, 0.10 of the chord. On the lower surface there were six pressure holes at 0.05, 0.10, 0.50, 0.60, 0.70, 0.90 of the chord. Transition was fixed at the leading edge, as in the case of the 0° measurements, by means of a carborundum layer extending to 7% of chord.

The pressure distributions in terms of $\frac{p}{H}$ on the N.P.L. wing are plotted in figs. 55 and 56. On the upper surface supersonic flow is apparent at $M = 0.603$ and the shock moves back to 50% of the chord at $M = 0.740$. The maximum Mach number on the upper surface is of the order of 1.4.

In figs57 to 66 the pressure coefficient measured in air (N.P.L. tests) (5in.chord model) and Freon-12 (2in.chord model) are plotted as a function of the free-stream Mach number. These results have also been converted by means of the area and transonic similarity rules. Fairly good agreement was obtained. Several interesting conclusions can be drawn from these results.

(a) The shock-wave on the upper surface in Freon and air occur at the same chordwise position for equal free-stream Mach numbers.

(b) Conversion of the pressure coefficients by means of the transonic and area similarity rules gives very similar results. It would appear that the transonic similarity rules can be used even if the free-stream Mach number is fairly low.

(c) No definite conclusion as to the validity of either rule could be drawn as the difference between the Freon and air results might be partly due to slight differences in the flow uniformity between the two tunnels, the use of different models etc.

The variation of the pressure ratio $\frac{p}{H}$ with Mach number at each hole is plotted in figs. 67 to 75 together with the converted results by means of the area similarity rule.

8.8. Drag measurements $\alpha = 4^{\circ}$

Pitot traverse measurements in the wake (figs. 77 to 81) were made at $M_{\infty} = 0.403$, 0.607, 0.712, 0.761 and 0.796 and from these the drag coefficients were evaluated. The results are tabulated in table 5 together with the N.P.L. measurements. The results are plotted in fig.54. The drag begins to rise above its low speed value at $M = 0.6$ corresponding to the setting up of supersonic flow on the upper surface.

The value of the drag coefficients before the drag rise is found to be higher in Freon-12 by 0.0045. This is probably due to the different transition positions on the two aerofoils.

A correlation between the wave drag in Freon-12 and air was made following the method suggested in ref.32. The wave drag was taken as the difference between the drag coefficients at any Mach number and its low speed value taken at $M_\infty = 0.402$ and is plotted in fig.76. The values in Freon-12 of $C_D - C_{D_{C\ M=0.4}}$ were converted by means of the transonic similarity laws. It is seen that very good agreement was obtained except for a single point at $M = 0.6$. The drag was also converted to the equivalent air value by means of the area similarity law. The agreement in this case with the air values was not as good.

9. Conclusions

The Freon-12 tunnel project at The College of Aeronautics was started to gain experience in the design of such tunnels and subsequently to investigate their use for aerodynamic measurements and the correlation of these with similar measurements in air.

Pressure distributions on a RAE 104 10% thick aerofoil were made in Freon-12 and the results compared with measurements made in air at incidence of 0° and 4°. A novel method of converting Freon-12 measurements to air was attempted by means of the transonic similarity rules and was compared with results converted by means of the area or streamline similarity rule. The difference between the converted results by either method was found to be small.

No definite conclusion as to the correctness of either method could be drawn from the above comparison but in general the distribution in terms of pressure coefficients in Freon-12 and air were very similar, the position of shocks in both gases was very similar at equal Mach numbers.

The application of transonic similarity rules to convert the measured wave drag in Freon-12 to its equivalent air value produced good agreement with the measured wave drag in air.

Freon-12 proved to be a satisfactory wind-tunnel medium and it is shown that in the high subsonic speed range the application of transonic similarity rules to convert results to equivalent air values was satisfactory.

10. Acknowledgments

The author wishes to thank Mr. G.M. Lilley for supervising this work; Messrs. E.W.E.Rogers and C.S.Sinnott of the High Speed Aerodynamics Division of the N.P.L. for the loan of the model and results and helpful discussions, Mr. G.W.Holloway for the design of some of the apparatus and Mr. S.H. Lilley for the supervision of the tunnel. Thanks are also due to I.C.I. Research Department for their assistance in oil filtration and other problems relating to the use of Freon-12.

Professor A.D.Young, now of Queen Mary College, initiated this research.

This work was performed under the Ministry of Supply Contract No. 7/EXPTL/528/PR3.

References

1. Margoulis, W. — Nouvelle methode d'essai de modeles en soufflerus aerodynamiques. Comptes Rendus de L'Academie des Sciences, CL XXl. (1920), 997-999.

2. Munk, M.M. — On a new type of wind tunnel . NACA TN.60 (1921).

3 Bubinsky, Ivan.A. — The use of heavy gases or vapours for high speed wind-tunnels. Aero.Sci. vol.6., 1939, p.446.

4. Smelt, R. — Power economy in high-speed wind tunnels by choice of working fluid and temperature. R.A.E. Rep. Aero 2081, 1945.

5. McKinnon Wood — The use of a special fluid for attaining a high Reynolds number in a variable density tunnel. ARC Report 9153, 1945.

6. Bottle, D.W. — Note on the use of flourine compounds as working fluids for wind tunnels. R.A.E. TN.Aero 1948. 1948.

7. Relf, Ernest F. — Note on the effect of variation of on some supersonic phenomena. ARC. Rep. 14686, 1952.

8. Huber, Paul W. — Use of Freon-12 as a fluid for aerodynamic testing. NACA. TN.1024, 1946.

9. Relf, Ernest F. — Note on the use of rare gases in high speed wind tunnels. ARC. Rep. 14732, 1952.

10. Chapman, Dean R. — Some possibilities of using gas mixtures other than air in aerodynamic research. NACA. TN.3226, 1954.

11. von Doenhoff, A.E. and Braslow, A.L. — Studies of the use of Freon-12 as a wind-tunnel testing medium. NACA TN.3000, 1953.

12. Buell, C.E. — Spark photography of projectile flight in special gases. Part I. The Freons. New Mexico School of Mines, Res. & Dev.Division. Tech.Rep. 453, 1948.

13. Donaldson, Coleman Du P., & Sabol, A.P. — Experiments on aerodynamic phenomena at Mach numbers in the range from 10 to 20. Proc. of First U.S. Nat. Congress Appl. Mech., 1951, pp.757-762.

14. Theodorson, R. & Regier, A. — Experiments on drag of revolving discs, cylinders and streamline rods at high speeds. NACA Rep.793, 1944.

15. Kantrowitz, A. — The supersonic axial-flow compressor. NACA Rep.974, 1946.

16a. Duff, Russel E. — The use of real gases in a shock-tube. Univ. of Mich, Engr. Res. Inst. Proj.M720-4, Rep. 51-3, 1951.

16b. Griffith, Wayland. — Vibrational relaxation times in gases. J.Appl.Phys., vol.21, 1950, pp.1319-1325.

17a Bogdonoff, S.M. & Hammitt, A.G. — The Princeton. Helium Hypersonic Tunnel and preliminary results above M=11. Princeton Univ., Dept. Aero.Eng. Rep. No.260, 1954.

17b. Bethe, H.A. & Teller, E. — Deviations from thermal equilibrium in shock waves. Aberdeen Proving Ground, Aberdeen, Ballistic Research Laboratory, Rep.X-117, 1945.

18. Mueller, J.N. — Conversion of inviscid normal force coefficients in helium to equivalent coefficients in air for simple shapes at hypersonic speeds. NACA TN.3807, 1956.

19. Glauert, H. — The effect of compressibility on the lift of an aerofoil. A.R.C. R & M. 1135.

20. Orlin, W.J., Lindenor, N.J. & Bitterley, J.G. — Application of the analogy between water flow with a free surface and two-dimensional compressible gas flow. NACA Rep.875, 1947.

22. von Karman, Th. — Compressibility effects in aerodynamics. J.Aero.Sci. vol.8, 1941, pp.337-356.

23. Tsien, H.S. — Two-dimensional subsonic flow of compressible fluids. J.Aero.Sci., vol.6, 1939. p.399.

24. Laitone, E.V. — New compressibility corrections for two-dimensional subsonic flow. J.Aero.Sci. Vol.18, 1951, p.350.

25. Kaplan, C. — Effect of compressibility at high subsonic velocities on the lifting force acting on an elliptic cylinder. NACA TN.1118, 1946.

26. von Karman, T. — Similarity laws of transonic flow. J.Maths. and Phys. vol.26, 1947, p.182-190.

27. Spreiter, J.R. — Similarity laws for transonic flow about wings of finite span. NACA TN.2273, 1951.

28. McDevitt, John B. — A correlation by means of transonic similarity law of the experimentally determined characteristics of 18 cambered wings of rectangular planforms. NACA R.M.A53G31. 1953.

29. Thom, A. & Penning, W.C.A. — The design and work of the Farnborough High Speed Tunnel. Royal Aero.Soc.Jnl. vol 52, 1948 pp.205-250.

30. Rogers, E.W.E. & others — Tests at high subsonic speeds on a 10% thick pressure plotting aerofoil of RAE.104 section. A.R.C. R & M. No. 2863.

31. Pankhurst, R.C. & Squire, H.B. — Calculated pressure distributions for the RAE 100-104 aerofoil sections. A.R.C. CP.80, 1950.

32. McDevitt, John.B. — A correlation by means of the transonic similarity rules of the experimentally determined characteristics of 22 rectangular wings of symmetrical profile. NACA R.M.A51 L176, 1952.

33. I.C.I.Ltd., — Data on Arcton Refrigerants,

34. Young, A.D. — Skin friction in the laminar boundary layer in compressible flow. College of Aeronautics Report 20, 1948.

35. Kinetic Chemicals Inc. Washington. Delaware. — Thermodynamic properties of Freon-12 at low pressures.

36. Stairmand — Dust Collection by inpingement and diffusion. Trans.Inst.Eng.Chem. vol.28, 1950.

37. Kantrowitz, A. — Heat capacity lag in gas dynamics. J.Chem.Phys. vol.14, 1946, p.150.

38. Gunn, J.C. — Relaxation time effect in gas dynamics. ARC. R & M.2338.

39. Bethe & Teller — Deviations from thermal equilibrium in shock-waves. Rep. No. X-117, Ballistic Res.Lab. Aberdeen Proving Ground, 1942.

40. Griffith — Vibrational relaxation times in gases. Appl.Phys. vol.21, 1950. pp.1319-1325.

41. Huber, Paul W. & Kantrowitz, A. — Heat capacity lag measurements in various gases. J.Chem.Phys. vol.15, 1947, pp.275-284.

42. Rossing, T.D. & others — Heat capacity lag of gaseous mixtures. NACA TN.3558, 1954.

43. Duncan, W.J. — Models for the determination of critical flutter speeds. ARC. R & M. 1425.

APPENDIX I.

Derivation of transonic similarity rules

The equation for irrotational flow of an inviscid compressible fluid is

$$\left(1 - \frac{u^2}{a^2}\right)\Phi_{xx} + \left(1 - \frac{v^2}{a^2}\right)\Phi_{yy} + \left(1 - \frac{w^2}{a^2}\right)\Phi_{zz}$$

$$- \frac{2uv}{a^2}\Phi_{xy} - \frac{2uw}{a^2}\Phi_{xz} - \frac{2vw}{a^2}\Phi_{yz} = 0 \qquad 1.1.$$

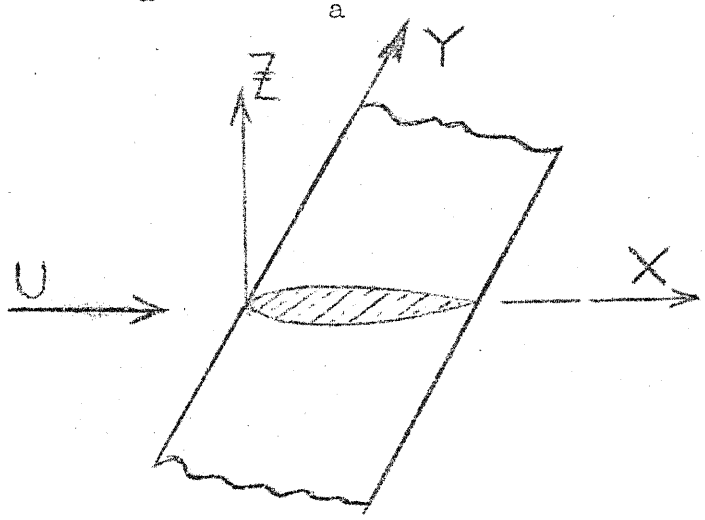

where $u = \Phi_x$, $v = \Phi_y$, $w = \Phi_z$. 1.2.

The speed of sound is given by

$$\frac{a^2}{a_\infty^2} = 1 - \frac{\gamma-1}{2}\left(\frac{u^2 + v^2 + w^2}{a_\infty^2} - M_\infty^2\right) \qquad 1.3.$$

On substituting a perturbation potential ϕ defined by

$$\Phi = U\ (x + \phi) \qquad 1.4.$$

we have $u = U\ (1 + \phi_x)$, $v = U\ \phi_y$, $w = U\ \phi_z$ 1.5.

into (1.1.) we obtain

$$\phi_{xx}\left[1 - M_\infty^2 - (\gamma+1)\, M_\infty^2\ \phi_x - \frac{\gamma+1}{2} M_\infty^2\ \phi_x^2 - \frac{\gamma-1}{2} M_\infty^2\ (\phi_y^2 + \phi_x^2)\right]$$

$$+\ \phi_{yy}\left[1 - \frac{\gamma+1}{2} M_\infty^2\ \phi_y^2 - \frac{\gamma-1}{2} M_\infty^2\ (2\phi_x + \phi_x^2 + \phi_z^2)\right]$$

$$+\ \phi_{zz}\left[1 - \frac{\gamma+1}{2} M_\infty^2\ \phi_z^2 - \frac{\gamma-1}{2} M_\infty^2\ (2\phi_x + \phi_y^2 + \phi_x^2)\right]$$

$$- 2 M_\infty^2\ \phi_{xy}(\phi_y + \phi_x \phi_y) - 2 M_\infty^2\ \phi_{xz}(\phi_z + \phi_x \phi_z)$$

$$- 2 M_\infty^2\ \phi_{yz}\ \phi_y\ \phi_z = 0 \qquad 1.6.$$

Since in general ϕ_{xx} is greater than ϕ_{xy}, ϕ_{xz}, ϕ_{yz}, ϕ_{yy} and ϕ_{zz} for transonic flows we may neglect all the second order terms in (1.3.) except that involving $\phi_x\ \phi_{xx}$ and obtain

$$\left[1 - M_\infty^2 - (\gamma+1)\, M_\infty^2\ \phi_x\right]\phi_{xx} + \phi_{yy} + \phi_{zz} = 0 \qquad 1.7.$$

Boundary conditions

(a) The flow at infinity is uniform

$$(\Phi_x)_\infty = U \quad \text{and} \quad (\Phi_y) = (\Phi_z) = 0$$

or in terms of the perturbation potential

$$(\phi_x)_\infty = (\phi\ y)_\infty = (\phi_z)_\infty = 0.$$

(b) The flow is tangential to the wing surface

$$\frac{1}{U}\ (\Phi_z)_w = \frac{\partial Z}{\partial x} \quad \text{or} \quad (\phi_z)_w = \frac{\partial Z}{\partial x} \qquad 1.8.$$

where Z the wing profile function is given by

$$\frac{Z}{c} = \tau\ g\left(\frac{x}{c}, \frac{y}{b}\right) \qquad 1.9.$$

In equation 1.9. $g\left(\frac{x}{c}, \frac{y}{b}\right)$ is a dimensionless profile shape function and must be identical for related wings.
In general a variation of τ represents simultaneous changes of the thickness ratio, camber and angle of attack. In the special case of a non-lifting wing with symmetrical section τ is proportional to the thickness ratio; for an inclined flat plate τ is proportional to the angle of attack.

Substituting eqn.1.9. into 1.8. and assuming that the boundary conditions on the wing surface are replaceable by boundary conditions on the $Z = 0$ plane, we have

$$(\phi_z)_{z=0} = \frac{\partial Z}{\partial x} = \tau \frac{\partial}{\partial x/c}\ .\ g\left(\frac{x}{c}, \frac{y}{b}\right)\ . \qquad 1.10.$$

Derivation of similarity parameters

We now write the perturbation potential in the form

$$\phi = A\, f\left(\frac{x}{c}, B\,y, Cz\right) = A\, f\left(x_1, y_1, z_1\right) \qquad 1.11$$

where only A, B, C are functions of τ, M_∞, b and c.

Substituting 1.11 into 1.7.

$$\left[1 - M_\infty^2 - (\gamma+1)\, M_\infty^2 \frac{A}{c} f_{x^1}\right] \frac{A}{c^2} f_{x^1x^1} + A\,B^2 f_{y^1y^1} + A\,C^2 f_{z^1z^1} = 0 \qquad 1.12$$

For f to be a function of the dimensionless space parameters x^1, y^1, z^1 only we have

$$\left.\begin{aligned} A &= \frac{c\,(1 - M_\infty^2)}{(\gamma+1)\, M_\infty^2} \\ B = C &= \frac{\sqrt{1 - M_\infty^2}}{c} \end{aligned}\right\} \qquad 1.13$$

The differential equation then takes the form

$$(1 - f_{x^1})\, f_{x^1x^1} + f_{y^1y^1} + f_{z^1z^1} = 0 \qquad 1.14$$

and hence does not depend explicitly on A, B and C.

The boundary conditions at the surface yield from eqn. 1.8

$$A\,C\, f_{z^1}(x^1, y^1, 0) = \tau \frac{\partial\, g\left(\frac{x}{c}, \frac{y}{b}\right)}{\partial\, \frac{x}{c}} \qquad 1.15$$

If equation 1.15 is not to depend explicitly on A, B and C

$$y^1 \simeq \frac{y}{b} \quad \text{and} \quad A\,C \simeq \tau \qquad 1.16$$

Note: If function g is to be the same for swept wings ÆR tan Λ must be constant and the taper ratio must be same.

ÆR = aspect ratio

Λ = sweep angle

From A C = const. and equation 1.13 we get

$$\frac{(1 - M_\infty^2)^{3/2}}{(\gamma+1)\, M_\infty^2} = \text{const.}\ \tau$$

$$\text{or} \qquad K = \frac{1 - M_\infty^2}{\left[(\gamma+1)\, M_\infty^2\, \tau\right]^{2/3}} = \text{const.} \qquad 1.17.$$

and from $B = C = \frac{\text{const}}{b}$

since AR = aspect ratio $\frac{b}{c}$

hence $\frac{b}{c}\,(1 - M_\infty^2)^{\frac{1}{2}} = \text{const.} = AR\,(1 - M_\infty^2)^{\frac{1}{2}}$

or using equation 1.16

$$AR\left[(\gamma+1)\ M_\infty^2\ \tau\right]^{\frac{1}{3}} = \text{const.} = H \qquad 1.18.$$

The parameter $AR\left[(\gamma+1)\, M_\infty^2\, \tau\right]^{\frac{1}{3}}$ is preferable to $AR\,(1 - M_\infty^2)^{\frac{1}{2}}$ as ambiguity is avoided at $M_\infty = 1$, when $K = 0$ and then the only parameter appearing in the equations is $H = AR\left[(\gamma+1)\ \tau\right]^{\frac{1}{3}}$

The boundary conditions of equation (14) becomes

$$K^{3/2}\ f_{z^1}\ (x_1, y_1, 0) = \frac{\partial}{\partial x}\ g\,(x_1, \frac{y}{b}) \qquad 1.19.$$

and hence f the solution of the differential equation 1.14 satisfying the boundary conditions 1.19 is identical in terms of the coordinates x^1, y^1, z^1 for related wings (i.e. having same profile ordinate function $g_1(\frac{x}{c}, \frac{y}{b})$ if the parameters K and H are kept constant since $y^1 = H\,K^{\frac{1}{2}}\,\frac{y}{b}$ and $z_1 = H\,K^{\frac{1}{2}}\,\frac{z}{b}$

The perturbation velocity potential for related flows can then be written

$$\phi = \frac{c\ \tau^{2/3}}{(\gamma+1)\, M_\infty^2}\ \frac{1}{3}\ F\,(H, K, \frac{x}{c}, \frac{y}{b}, \frac{z}{b}). \qquad 1.20.$$

Force coefficients

The approximate form of the pressure coefficients is

$$Cp\ \alpha\ \phi_x$$

$$\text{i.e.} \quad Cp = \frac{\tau^{\frac{2}{3}}}{\left[(\gamma+1)\, M_\infty^2\right]^{\frac{1}{3}}}\ P\,(H, K, \frac{x}{c}, \frac{y}{b}, \frac{z}{b}) \qquad 1.21.$$

Lift

The expression for the lift coefficient is found by integrating the vertical component of the pressure coefficient round the contour assuming the profile to be very thin.

e.g. $$C_L = \frac{1}{S} \oint \left(Cp\right)_{z=o} \, dx \, dy \qquad 1.22.$$

For related wings Area = S = const. b x c

i.e. $$C_L = \frac{1}{\text{const.}} \left(Cp\right)_{z=o} d\frac{x}{c} \cdot d\frac{y}{b}$$

$$= \frac{\tau^{2/3}}{\left[(\gamma+1) M_\infty^2\right]^{1/3}} L(H\,K) \qquad 1.23.$$

Moment Coefficient C_M

Similarly $$C_M = \frac{1}{Sc} \oint Cp \; x \, dx \, dy = \frac{1}{\text{const.}} \oint Cp \; \frac{x}{c} \, d\left(\frac{x}{c}\right) d\left(\frac{y}{b}\right)$$

$$= \frac{\tau^{2/3}}{\left[(\gamma+1) M_\infty^2\right]^{1/3}} M(H,K) \qquad 1.24$$

Drag Coefficient C_D

$$C_D = \frac{1}{S} \oint Cp \left(\frac{dz}{dx}\right)_w dx. \, dy$$

$$= \frac{\tau^{5/3}}{\left[(\gamma+1) M_\infty^2\right]^{1/3}} D(H,K) \qquad 1.25$$

Since $$K^{\frac{1}{2}} = \frac{\sqrt{1 - M_\infty^2}}{\left[(\gamma+1)\tau \; M_\infty^2\right]^{1/3}}$$

we can derive the following alternative relations

$$Cp = \frac{\tau}{\sqrt{1 - M_\infty^2}} \; Q\left(H, K, \frac{x}{c}, \frac{y}{b}, \frac{z}{b}\right) \qquad 1.26.$$

$$C_L = \frac{\tau}{\sqrt{1 - M_\infty^2}} \; J(H,K) \qquad 1.27.$$

$$Cm = \frac{\tau}{\sqrt{1 - M_\infty^2}} \; G(H,K) \qquad 1.28.$$

$$C_D = \frac{\tau^2}{\sqrt{1 - M_\infty^2}} \quad E\,(H,K) \qquad 1.29.$$

These results are equivalent to those of Prandtl-Glauert in subsonic flows. They can also be used in supersonic flows if $\sqrt{1 - M_\infty^2}$ is replaced by $\sqrt{M_\infty^2 - 1}$

APPENDIX II

Application of Transonic and area similarity laws to two-dimensional flow in Freon-12 and Air

From equations 5.4.5. and 5.4.6.

$$\left(\frac{Cp_1}{Cp_2}\right)_{K,x',z'} = \left[\frac{(\gamma_2+1)}{(\gamma_1+1)} \quad \frac{M_{\infty 2}^2}{M_{\infty 1}^2}\right]^{1/3} \qquad 2.1.$$

and

$$C' = \left(\frac{C_{L_1}}{C_{L_2}}\right)_K = \left(\frac{C_{M_1}}{C_{M_2}}\right)_K = \left(\frac{C_{D_1}}{C_{D_2}}\right)_K = \left[\frac{(\gamma_2+1)\, M_{\infty_2}^2}{(\gamma_1+1)\, M_{\infty_1}^2}\right]^{1/3} \qquad 2.2.$$

The Mach numbers at which these results are to be compared have to satisfy the following equation:

$$\frac{1 - M_{\infty_1}^2}{\left[(\gamma_1+1)\, M_{\infty_1}^2\, \tau\right]^{2/3}} = \frac{1 - M_{\infty_2}^2}{\left[(\gamma_2+1)\, M_{\infty_2}^2\, \tau\right]^{2/3}} = K$$

The difference between the Mach numbers $\Delta M = M_2 - M_1$ is small and can be sufficiently accurately calculated from the following formula

$$\Delta M = \left(\frac{dM}{d\gamma}\right)_{K,\tau} \cdot \Delta\gamma = (\gamma_2 - \gamma_1) \left(\frac{dM}{d\gamma}\right)_{K,\tau} \qquad 2.3.$$

$$= -\frac{(\gamma_2 - \gamma_1)\, M_{\infty_1}\, (1 - M_{\infty_1}^2)}{(\gamma_1+1)\, (M_{\infty_1}^2 + 2)}$$

In the case of Freon and Air the ratios of specific heats are $\gamma = 1.125$ and 1.4 respectively

$$\text{e.g.} \quad M_F - M_A = \frac{+ 0.1146\, M_{\infty A}\,(1 - M^2_{\infty A})}{(M^2_{\infty A} + 2)} \qquad 2.4.$$

Eqn. 2.4. is plotted in fig.82.

The expression for the critical area ratio is

$$\frac{A_{cr}}{A} = M \left[\frac{1 + \frac{\gamma-1}{2} M^2}{\frac{\gamma+1}{2}} \right]^{-\frac{\gamma+1}{2(\gamma-1)}} \qquad 2.5.$$

and it can be shown that the difference in Mach number at which these pressure coefficients are to be compared according to the area similarity rule is

$$M_F - M_A = 0.34375\, M_A \left[1 + \frac{5 + M_A^2}{1 - M_A^2} \ln \left(\frac{5 + M_A^2}{6} \right) \right] \qquad 2.6.$$

in the case of Freon-12 and air, Equation 2.6 is plotted in fig.82.

The Mach number increment in the case of Freon-12 and air derived in a similar way from

$$\frac{M_\infty^2 - 1}{\left[\tau\,(\gamma+1) \right]^{2/3}} = \text{const.}$$

is given for comparison in fig.82. It is seen that the latter relation gives a divergent Mach increment when approaching $M = 0$.

The ratio of force coefficients for the two-dimensional case

$$C' = \left(\frac{C_{p_1}}{C_{p_2}} \right)_{K,x',z'} = \left(\frac{C_{L_1}}{C_{L_2}} \right)_K = \left(\frac{C_{M_1}}{C_{M_2}} \right)_K = \left(\frac{C_{D_1}}{C_{D_2}} \right)_K = \left[\frac{(\gamma_2+1)\, M^2_{\infty_2}}{(\gamma_1+1)\, M^2_{\infty_1}} \right]^{1/3}$$

giving $$C' = \left(\frac{C_A}{C_F} \right)_K = \left[\frac{(\gamma_F + 1)\, M^2_{\infty F}}{(\gamma_A+1)\, M^2_{\infty A}} \right]^{1/3} = \left[0.886\, \frac{M^2_{\infty F}}{M^2_{\infty A}} \right]^{1/3} \qquad 2.7.$$

for Freon-12 and air is plotted in fig.83.

APPENDIX III

Application of transonic similarity laws to finite aspect ratio wings in Freon-12 and Air

In the case of wings of the same aspect ratio and at the same Mach numbers we have from equation 5.5.8. in the case of force coefficients C_p, C_L, C_M.

$$\left.\begin{aligned} \frac{C_A}{C_F} &= \frac{\tau_A}{\tau_F} = \frac{\gamma_F+1}{\gamma_A+1} = 0.886 \\ \text{or} \quad \frac{C_F - C_A}{C_F} &= 1 - \frac{C_A}{C_F} = 0.114 \end{aligned}\right\} \qquad 3.1.$$

In the case of drag coefficients from 5.5.9.

$$\left(\frac{C_{D\gamma_1}}{C_{D\gamma_2}}\right)_{M_\infty, R, (\gamma+1)\tau} = \left(\frac{\tau_1}{\tau_2}\right)^2 = \left(\frac{\gamma_2+1}{\gamma_1+1}\right)^2$$

For similar flows in Freon and air

$$\frac{C_{D_A}}{C_{D_F}} = 0.785$$

or

$$\frac{C_{D_F} - C_{D_A}}{C_{D_F}} = 0.215$$

Thus the increase in drag coefficients is 21.5%. This of course applies to wave drag only. (ref.32).

In the case in which wings of the same thickness are compared the ratio of the pressure, lift, moment and drag coefficients is

$$C' = \frac{C_A}{C_F} = \left[\frac{1 - M_{\infty F}^2}{1 - M_{\infty A}^2}\right]^{1/2}_{\tau, K} = \left[\frac{(\gamma_F+1)\, M_{\infty F}^2}{(\gamma_A+1)\, M_{\infty A}^2}\right]^{1/3}$$

These relations are plotted in fig.84 provided that the aspect ratios of the wings are varied according to

$$\frac{(AR)_A}{(AR)_F} = \left[\frac{1 - M^2_{\infty F}}{1 - M^2_{\infty A}}\right]^{\frac{1}{2}}$$

The aspect ratio variation amounts only to 4.5% and for normal aspect ratios can be neglected.

APPENDIX IV.

Application of area similarity law to convert the pressure distributions on wings in Freon-12 to air results

The ratio of the stream-tube area at any point in the flow to that at a point when M = 1.0 is given by

$$\frac{A_{cr}}{A} = M\left[\frac{1 + \frac{\gamma-1}{2} M^2}{\frac{\gamma+1}{2}}\right]^{-\frac{\gamma+1}{2(\gamma-1)}}$$

Von Doenhoff assumed that at corresponding free stream Mach numbers the area ratio in the flows with different values of γ is identical.

In other words it is assumed that the geometry of the streamlines around a given body is independent of the gas in which the body is immersed provided that the comparison is made at corresponding freestream Mach numbers according to the Mach number-area ratio relation.

The correction to the pressure coefficient will depend on the value of both the freestream and the local Mach number. To simplify the application of the area similarity rule the difference between the pressure coefficient in Freon-12 and the corresponding pressure coefficient in air is plotted in fig.85 with the Freon-12 pressure coefficients as the abscissa for various values of the free-stream Mach number.

The difference in the static pressure ratio between Freon-12 (γ = 1.125) and air (γ = 1.4) is plotted in fig.86 as a function of the free-stream Freon-12 Mach number (also $\frac{p}{H}$ in Freon) calculated both on the basis of equal Mach number distributions and on stream-tube area similarity. There is less justification for the assumption of equal Mach number distributions than stream tube area similarity although both rules lead to similar correction factors in subsonic flow.

APPENDIX V

Power economy reduction in size and model stresses in heavy gas tunnels

The power required to drive a tunnel is usually written

$$P = \frac{1}{2} \rho V_w^3 A_w . \eta . \qquad 5.1.$$

where η = tunnel power factor

A = cross-sectional area of working section

c = chord of model

μ = viscosity

a = speed of sound (working section)

γ = ratio of specific heats

p = pressure (working section)

R = Reynolds number

M = Mach number

If the variation of the tunnel power factor η with Reynolds number and Mach number is neglected, then for any particular tunnel the power required can be written as

$$P = \frac{1}{2} \eta . \frac{A}{c^2} . R^2 . M . \frac{\mu^2 a^3}{\gamma p} \qquad 5.2.$$

Thus for the same R, M, η and blockage factor $\frac{A}{c^2}$.

$$P \propto \frac{\mu^2 a^3}{\gamma p} \qquad 5.3.$$

(b) Size of tunnel

$$\text{We have } c = \frac{R\mu}{\rho v} = \frac{R}{M} . \frac{\mu a^3}{\gamma p} \qquad 5.4.$$

Thus for the same Reynolds number, Mach number and pressure in the working section

$$c \propto \frac{\mu a^3}{\gamma} \qquad 5.5.$$

(c) Model Stresses

At a fixed Reynolds number and Mach number the forces on a wing depend on $\frac{1}{2}\rho V^2$ which can be rewritten as $\frac{1}{2}\gamma p M^2$, i.e., for minimum stresses at constant M

$$\gamma . p \qquad 5.6.$$

must be minimum.

(d) Pressurisation:

The viscosity (μ), velocity of sound (a) and the ratio of specific heat (γ) can be considered independent of pressure for most states of a gas.

From relations 5.3, 5.4, and 5.6., we see that increasing the tunnel pressure will:- (1) decrease power consumption at const. Reynolds and Mach numbers.
(2) increase model stresses directly.
(3) reduce the tunnel size for fixed R and M.

(e) Refrigeration:

If T is the absolute temperature of a gas we can write for most gases

$$\text{velocity of sound } a \ \alpha \ T^{1/2}$$

$$\text{viscosity } \mu \ \alpha \ \frac{T^{3/2}}{(T+C)}$$

where C = Sutherlands constant which varies from gas to gas.

The power and size of a tunnel at constant Reynolds number, Mach number and tunnel pressure for any one gas can then be written as

$$P \ \alpha \ \frac{T^{9/2}}{(T+C)^2} \qquad 5.7.$$

$$C \ \alpha \ \frac{T^3}{(T+C)} \qquad 5.8.$$

It is obvious that both the power and the size are decreased if the temperature is lowered without affecting the model stresses (which are proportional to γp.)

(f) Choice of working medium

Gases having lower speeds of sound (i.e. large molecular weight) have mostly lower viscosities, since these gases have generally more complex molecules than the constituents of air. They will also have a lower ratio of specific heats. Hence from expressions 5.3, 5.5, and 5.6, we see that for heavy gases both size and power requirements are reduced and that there also is a small reduction of model stresses in comparison to tests in air at the same Reynolds number and Mach number.

APPENDIX VI.

Mach number limit in heavy gases for condensation

If the variation of specific heats and imperfect gas effects are negligible the limiting reservoir conditions for an expansion to any Mach number can be found from the isentropic flow relation.

$$\frac{p}{p_{st}} = \left(1 + \frac{\gamma-1}{2} M^2\right)^{-\frac{\gamma}{\gamma-1}} = \left(\frac{T}{T_{st}}\right)^{\frac{\gamma}{\gamma-1}}$$

and a knowledge of the saturation vapour pressure and temperature p_s and T_s.

Smelt (ref.4) derives a relation based on the following argument; local Mach numbers greater than 1.4 do not occur in general if the free-stream Mach Number M_∞ is subsonic. Thus an extreme case occurs if $M = \sqrt{2}$ and $M_\infty = 0$.

$$\text{i.e. } \frac{T}{T_\infty} = \frac{\left(\frac{\gamma-1}{2} M_\infty^2 + 1\right)}{\left(\frac{\gamma-1}{2} M^2 + 1\right)} = \frac{1}{\gamma}$$

i.e., the free-stream temperature must be greater than γ times the boiling point of the gas at a pressure p where

$$p = \gamma^{-\frac{\gamma}{\gamma-1}} \cdot p_\infty .$$

p_∞ = free-stream pressure.

In most cases the variation of specific heat with temperature cannot be neglected, as the rate at which the temperature varies in an expansion $T \propto p^{\frac{\gamma}{\gamma-1}}$ is quite sensitive to γ (ref.10). The minimum temperature T_m permissible

in an isentropic expansion can be found graphically by plotting the isentrope defined by the reservoir tunnel conditions p_{st}, T_{st} against log p and log T and finding its intersection with the saturation vapour pressure curve. The maximum Mach number M is then found from the relation

$$M^2 = \frac{2}{\gamma_{Tm}} \frac{1}{\bar{R} T_m} (H_{st} - H)$$

where H_{st} = enthalpy at reservoir cond^{n}.

H = enthalpy at temperature T_m.

and can be calculated from spectroscopic data.

APPENDIX VII

The Reynolds number in gas mixtures

The Reynolds number, R_e, can be written

$$R_e = \frac{1}{\mu_w} U_w \rho_w = \frac{1}{\mu_{st}} \rho_{st} a_{st} \frac{M_w}{\left[1 + \frac{\gamma-1}{2} M_w^2\right]^{\frac{7-\gamma}{6(\gamma-1)}}} \qquad 7.1.$$

where suffixes w and st denote working-section and stagnation conditions respectively, and it is assumed that the variation of viscosity over a limited range of temperature can be represented by

$$\mu = k T^{2/3} \qquad 7.2.$$

Alternatively we can write

$$R_e = \frac{1}{k T_{st}} p_{st}^{7/6} \sqrt{\frac{\gamma m}{\bar{R}}} \frac{M_w}{\left[1 + \frac{\gamma-1}{2} M_w^2\right]^{\frac{7-\gamma}{6(\gamma-1)}}} \qquad 7.3.$$

where $\bar{R}$ is the universal gas constant

and m is the molecular weight

Equation 7.3 shows that the Reynolds number for any given gas is proportional to p_{st} and $T_{st}^{-7/6}$ approximately.

If x is the mole fraction of the component denoted by suffix (1) and suffix (x) is used to denote properties of the mixture, from equation 7.3. we have

$$\left[\frac{R_e}{p_{st}^{1}}\right]_x = \frac{1}{\left(\mu_{st}\right)_x}\sqrt{\frac{\gamma_x m_x}{\bar{R} T_{st}}} \cdot M\left(1+\frac{\gamma_x-1}{2}M^2\right)^{\frac{\gamma_x-7}{6(\gamma_x-1)}} \qquad 7.4.$$

Where (see ref.10)

$$\gamma_x = \frac{x(\gamma_1-\gamma_2)+\gamma_2(1-\gamma_1)}{\left[x(\gamma_1-\gamma_2)+1-\gamma_1\right]} \qquad 7.5.$$

and

$$\mu_x = \frac{\mu_1}{1+\frac{\frac{1-x}{x}\left[1+\sqrt{\frac{\mu_1}{\mu_2}}\left(\frac{m_2}{m_1}\right)^{\frac{1}{4}}\right]^2}{2\sqrt{2}\left(1+\frac{m_1}{m_2}\right)^{\frac{1}{2}}}} + \frac{\mu_2}{1+\frac{\frac{x}{1-x}\left[1+\sqrt{\frac{\mu_2}{\mu_1}}\left(\frac{m_1}{m_2}\right)^{\frac{1}{4}}\right]^2}{2\sqrt{2}\left(1+\frac{m_2}{m_1}\right)^{\frac{1}{2}}}} \qquad 7.6.$$

and

$$m_x = x\,m_1 + (1-x)\,m_2 \qquad 7.7.$$

Substituting x in equations 7.5, 7.6, 7.7., the Reynolds number can then be calculated from equation 7.4.

For small x, e.g. a small proportion of component (1) in the mixture, we can write to a first approximation

$$\left[\frac{R_e}{p_{st}^{1}}\right]_x \sim \left[\frac{R_e}{p_{st}^{1}}\right]_{x=0} + \left[\frac{\partial\left(\frac{R_e}{p_{st}^{1}}\right)}{\partial x}\right]_{x=0} x \qquad 7.8.$$

From equation 7.3.

$$\frac{1}{\left(\frac{R_e}{p_{st}}\right)}\frac{\partial\left(\frac{R_e}{p_{st}^{1}}\right)}{\partial x} = \left[\frac{1}{2m_x}\frac{\partial m}{\partial x} - \frac{1}{\mu_x}\cdot\frac{\partial \mu_x}{\partial x} + \left\{\frac{\ln\left(1+\frac{\gamma_x-1}{2}M^2\right)}{\left[\gamma_x-1\right]^2} + \frac{1}{2\gamma_x} + \frac{\gamma_x-7}{6(\gamma_x-1)}\cdot\frac{M^2}{2}\cdot\frac{1}{1+\left(\frac{\gamma_x-1}{2}M^2\right)}\right\}\frac{\partial \gamma_x}{\partial x}\right] \qquad 7.9.$$

From equation 7.5

$$\frac{\partial \gamma_x}{\partial x} = \frac{(\gamma_1-\gamma_2)\ (1-\gamma_1)\ (1-\gamma_2)}{\left[x\ (\gamma_1-\gamma_2) + (1-\gamma_1)\right]^2} \qquad 7.10$$

giving $\left(\frac{\partial \gamma_x}{\partial x}\right)_{x=o} = \frac{(\gamma_1-\gamma_2)\ (1-\gamma_2)}{(1-\gamma_1)}$

From 7.6 $\left(\frac{\partial \mu_x}{\partial x}\right)_{x=o} = \frac{\mu_1\, 2\sqrt{2}\left(1+\frac{m_1}{m_2}\right)^{\frac{1}{2}}}{\left[1+\sqrt{\frac{\mu_1}{\mu_2}}\left(\frac{m_2}{m_1}\right)^{\frac{1}{4}}\right]^2} - \frac{\mu_2\left[1+\sqrt{\frac{\mu_2}{\mu_1}}\left(\frac{m_1}{m_2}\right)^{1/4}\right]^2}{2\sqrt{2}\left(1+\frac{m_2}{m_1}\right)^{1/2}}$ 7.11.

From 7.7. $\frac{\partial m_x}{\partial x} = m_1 - m_2$ 7.12.

Thus equation 7.9 together with 7.10, 7.11 and 7.12 becomes

$$\left[\frac{1}{\left(\frac{R_e}{p_{st}1}\right)}\cdot\frac{\partial\left(\frac{R_e}{p_{st}1}\right)}{\partial x}\right]_{x=o} = \frac{m_1-m_2}{2\,m_2} - \frac{1}{\mu_2}\,\frac{\mu_1\,2\sqrt{2}\left(1+\frac{m_1}{m_2}\right)^{1/2}}{\left[1+\sqrt{\frac{\mu_1}{\mu_2}}\left(\frac{m_2}{m_1}\right)^{1/4}\right]^2} - \frac{\mu_2\left[1+\sqrt{\frac{\mu_2}{\mu_1}}\left(\frac{m_1}{m_2}\right)^{\frac{1}{4}}\right]^2}{2\sqrt{2}\left(1+\frac{m_2}{m_1}\right)^{1/2}}$$

$$+\left\{\frac{\log e\left(1+\frac{\gamma_2-1}{2}M^2\right)}{\left[\gamma_2-1\right]^2} + \frac{1}{2\gamma_2} + \frac{\gamma_2-7}{6(\gamma_2-1)}\cdot\frac{M^2}{2}\,\frac{1}{\left(1+\frac{\gamma_2-1}{2}M^2\right)}\right\}(\gamma_1-\gamma_2)\ \frac{(1-\gamma_2)}{(1-\gamma_1)} \qquad 7.13.$$

Equation 7.8 is of the form

$$\left(\frac{R_e}{p_{st}1}\right)_x \simeq \left(\frac{R_e}{p_{st}1}\right)_{x=o}\left[1+\left\{\text{const.} + f(M)\right\}x\right] \qquad 7.14.$$

for any two gases.

In the speed range M 0 to 1.0, f(M) is small compared to the constant and for the very approximate estimation of the Re No. it can be neglected.

The effect of a changing γ on $\phi = \left(1 + \frac{\gamma-1}{2} M^2\right)^{\frac{\gamma-7}{6(\gamma-1)}}$ is small and hence if an estimate of Reynolds number over a larger range of x is required we can write from 7.4.

$$\left(\frac{R_e}{p_{st}\ell}\right)_x = \frac{1}{\mu_{st}x}\sqrt{\frac{\gamma_x m_x}{\bar{R}}} \cdot M. \quad \phi x$$

$$= \frac{1}{\mu_{st}x}\sqrt{\frac{\gamma_x m_x}{\bar{R}}}\ M. \ \phi_{x=o}\left[1 + \left\{\frac{1}{\phi}\frac{\partial\phi}{\partial x}\right\}_{x=o} x\right] \qquad 7.15.$$

where $\left[\frac{1}{\phi}\frac{\partial\phi}{\partial x}\right]_{x=o} = \left\{\frac{\log_e\left(1+\frac{\gamma_2-1}{2}M^2\right)}{\left[\gamma_2-1\right]^2} + \frac{\gamma_2-7}{6(\gamma_2-1)} \cdot \frac{M^2}{2}\frac{1}{\left(\frac{\gamma_2-1}{2}M^2\right)}\right\}(\gamma_1-\gamma_2)\frac{(1-\gamma_2)}{(1-\gamma_1)}$ 7.16.

For selected values of γ_1 and γ_2 $\phi_{x=o}$ and $\left(\frac{1}{\phi}\frac{\partial\phi}{\partial x}\right)_{x=o}$ are functions of M only. The Reynolds number of gas mixture can easily be obtained from equation 7.15 when $(\mu_{st}\gamma)_x$, γ_x and m_x are given. With the assumed dependence of viscosity on temperature the Reynolds number is proportional to $T_{st}^{-7/6}$.

APPENDIX VIII

Reynolds number in Freon-12 and Freon-12-Air mixtures

The equation for the Reynolds number in Freon-12 was obtained using the following values

γ = 1.125 (ref.8)

vel. of sound = 485 ft/sec. at T = 228°K and 1 atm pr. (ref.4)

density ρ = 0.01011 slugs/cu.ft. at T = 288°K and 1 atm pr. (ref.33)

viscosity $\mu = 2.58 \quad 10^{-7} \ \frac{\text{slugs}}{\text{ft.sec.}}$ at T = 288°K. (ref.4).

Thus for a stagnation temperature of 288°K.

$$\frac{R_e}{\ell p_{st}} = 1.90 \times 10^7 \ M \ (1 + 0.0625 \ M^2)^{-\frac{47}{6}} \qquad 8.1.$$

where ℓ is in ft and p_{st} in atmospheres.

Equation 8.1. is plotted together with the corresponding Reynolds number ratio for air at a stagnation temperature of 288°K.

The ratio of $\left(\frac{R_e}{\ell p_{st}}\right)_F \Big/ \left(\frac{R_e}{\ell p_{st}}\right)_A$

for the same stagnation temperature is plotted in fig.87. It is seen that this ratio varies from 2.7 to 2.6 as the Mach number increases from 0 to 1.0.

Freon-12 and Air Mixture

The values of viscosity μ_x, ratio of specific heats γ_x, and moelcular wt. m_x calculated from equations 7.6, 7.5 and 7.7 respectively for Freon-12 and air mixtures are plotted against x the mole fraction of air in the mixture in fig.88.

The following values of viscosity, ratio of specific heat and γ were used

	γ	m molec.wt	μ viscosity (slugs/ft.sec. at 288°K.)
Freon-12	1.125	120.9	$2.58 \quad 10^{-7}$
Air	1.4	28.97	$3.78 \quad 10^{-7}$

The relations derived in Appendix XII have been evaluated using the above gas properties.

Thus $\frac{m_1 - m_2}{2 m_2} = -0.3801$

$$\frac{1}{2\gamma_2} \cdot \left[\frac{\partial \gamma_x}{\partial x}\right]_{x=0} = \frac{\gamma_1 - \gamma_2}{2 \gamma_2} \cdot \frac{1-\gamma_2}{1-\gamma_1} = 0.0382.$$

$$\frac{1}{\mu_2}\left[\frac{\partial \mu_x}{\partial x}\right]_{x=0} = \frac{1}{\mu_2}\left[\frac{\mu_1 \cdot 2\sqrt{2}\cdot\left(1+\frac{m_1}{m_2}\right)^{1/2}}{\left[1+\sqrt{\frac{\mu_1}{\mu_2}}\left(\frac{m_2}{m_1}\right)^{1/4}\right]^2} = \frac{\mu_2\left[1+\sqrt{\frac{\mu_2}{\mu_1}}\left(\frac{m_2}{m_1}\right)^{1/4}\right]^2}{2\sqrt{2}\left(1+\frac{m_2}{m_1}\right)^{1/2}}\right]$$

$$= 0.2651$$

$$\phi_{x=0} = (1+0.0625\,M^2)^{\frac{47}{6}}$$

The relation $\left[\frac{1}{\phi}\frac{\partial \phi}{\partial x}\right]_{x=0} = \left[\frac{\partial}{\partial x}\left(1+\frac{\gamma_x-1}{2}M^2\right)^{\frac{\gamma_x-7}{6(\gamma_x-1)}}\right]_{x=0}$ (see eqn.7.16)

is plotted as a function of M for the range 0 to 1 in Fig.89.

Since $\frac{1}{\phi}\left(\frac{\partial \phi}{\partial x}\right)_{x=0}$ is small compared with unity the Reynolds number in Freon-12 containing a small proportion of air can be found readily from

$$\left(\frac{R_e}{p_{st}\ell}\right)_x \sim \left(\frac{R_e}{p_{st}\ell}\right)_{x=0}\left[1+\left\{\left(\frac{1}{\phi}\frac{\partial \phi}{\partial x}\right)_{x=0} - 0.607\right\}x\right] \qquad 8.2.$$

$$\sim \left(\frac{R_e}{p_{st}\ell}\right)_{x=0}\left[1-0.607\,x\right] \quad M=0$$

$$\sim \left(\frac{R_e}{p_{st}\ell}\right)_{x=0}\left[1-.590\,x\right] \quad M=1$$

For most purposes it is sufficiently accurate to use

$$\left(\frac{R_e}{p_{st}\ell}\right)_x = \left(\frac{R_e}{p_{st}\ell}\right)_{x=0}\left[1-0.6\,x\right]$$ over the Mach number range 0 to 1.

APPENDIX IX

Variation of skin friction between tests in air and Freon-12

It is usual when considering the flow round a body to neglect the effects of viscosity except in the thin boundary layer near the surface. Compressible boundary layer theory is complicated by the interdependence of the equations of motion and energy due to the variation of density, viscosity and thermal conductivity with temperature. Possible differences in the form of the boundary layer in different media would add to the uncertainties when comparing flows in different media (e.g. by such means as the area similarity rule or transonic similarity laws) and these effects would be aggravated by the interactions of shock waves with boundary layers.

Comparison of Skin-friction coefficients in air and Freon in a steady laminar boundary layer on a flat plate at zero incidence and no heat transfer

A formula for the skin-friction coefficient in a steady laminar boundary layer on a flat plate at zero incidence and no heat transfer was described by Young (ref. 34) assuming the temperature variation of viscosity to be $\mu = \text{const. } T^{\omega}$ The relation is

$$C_f \sqrt{R_x} = 0.664\left[1 + 0.365\,(\gamma-1)\,M^2\,\sigma^{1/2}\right]^{-\frac{(1-\omega)}{2}} \qquad 9.1.$$

where $C_f = \dfrac{2\tau_w}{\rho_\infty U_\infty^2}$ = skin friction coefficient

τ_w = intensity of skin friction at wall

σ = Prandtl number

ρ_∞, U_∞, μ_∞ = free-stream density, velocity and viscosity respectively.

$R_x = \dfrac{U_\infty \rho_\infty x}{\mu_\infty}$ = Reynolds Number.

x = coordinate in the flow direction measured from the leading edge of the plate.

M = Mach Number

γ = ratio of specific heats

suffices F and A denote quantities in Freon-12 and Air respectively.

$C_f \sqrt{R_x}$ was calculated for air and Freon-12 at free stream Mach Numbers in the range 0 to 3. The values for ω in $\mu = \text{const } T^{\omega}$ and σ for Freon were calculated from (ref.8). $C_f \sqrt{R_x}$ is plotted against the free-stream Mach number in fig.90. The difference between the Freon-12 and air values is about $\frac{1}{2}\%$ at M = 1 and increases to about 4% at M = 3.

The percentage conversion factor

$$\left[\frac{(C_f)_F - (C_f)_A}{(C_f)_F}\right] \times 100 \times 100$$

was calculated from equation 9.1 and is also plotted in fig.90 assuming of course the same free stream Reynolds number where $(C_f)_A$ is the value of the air skin friction coefficient at the corresponding free stream air Mach number M_A from the area similarity rule (ref.11) The values of the conversion factor thus derived are plotted against the free-stream Freon Mach number and are compared with the wake-drag conversion factor obtained by Von Doenhoff in(ref.11). It is seen that the latter increases with Mach number much more rapidly.
In the derivations of the above results the following gas properties were used.

Freon-12

For temperature range 492-582° Fabs.

$\mu = \text{const } T^{\omega}$ where $\omega = 0.69$

$\sigma = 0.788$ $\gamma = 1.13$

Air $\sigma = 0.709$ $\gamma = 1.4$ $\omega = 0.776$

APPENDIX X.

The effect of relaxation times

Summary

The effect of heat capacity lag in gas dynamics are summarised with emphasis on the differences that might exist between Freon-12 and Air. A list of measurements of the relaxation time in Freon-12 is given. The magnitude of the relaxation effects about a 10% thick 2 in. chord wing and the pressure losses in Freon-12 ahead of a small impact tube are calculated.

10.2. Introduction

When a gas undergoes rapid compression such as occur in compressible flow, the vibrational energy of the molecules does not adjust itself instantaneously to the equilibrium value. The magnitude of the departure depends on the relaxation time of the gas and the rate of change of temperature in the flow. The relaxation time is defined as the time required for the excess of vibrational energy above equilibrium position to be reduced to $\frac{1}{e}$ of its original value. The return of the energy partition within the gas to equilibrium conditions is an irreversible process and results in an increase of entropy. This entropy increase in gases will give rise to additional losses, and hence care must be exercised in substituting media other than air in wind-tunnels and other test facilities. Heat lag may give rise to drag even in the case of non-viscous subsonic flow.

The effects of heat capacity lag in gas flow can be summarised as follows

(a) Entropy increases in flows in which rapid compressions occur.

(b) Diffuse shock waves may occur.

(c) Dispersion and absorption of sound occur.

The effects of Heat capacity lag in gas dynamics was considered by A.Kantrowitz (ref.37) and J.C. Gunn (ref.38), and its effect on plane shock waves was treated by Bethe and Teller (ref.39), Chapman (ref.10) and Huber (ref.8) consider these effects in Freon-12.

10.3. Measurement of relaxation times

Relaxation times in gases are calculated either from dispersion and absorption of sound waves or from impact tube measurements. The latter method was developed by A.Kantrowitz (ref.37).

The various relaxation times of Freon-12 are listed below:

Ref.	T°K	τ secs.
8		
40	292	$8\ 10^{-8}$
41	297	$2\ 10^{-8}$
42	300	$7.8 \pm 0.6\ \ 10^{-8}$

The relaxation times increase with decreasing temperature (ref.38) and are inversely proportional to pressure. The addition of up to 10% of air did not produce any change in the relaxation times. The relaxation time of mixtures 18% Freon-12 in Argon and Helium was found to be $2.5 10^{-7}$ and $0.9\ \ 10^{-7}$ sec., respectively.

The relaxation times of a gas can be affected quite appreciably by the addition of some impurities e.g collisions between CO_2 and water molecules are 500 times as effective as collisions between CO_2 in exciting vibration in CO_2 molecules (ref.37)

10.4. Vibrational heat capacity of Freon-12

Monatomic gases like A, K, Xe, have no vibration heat capacities and hence do not exhibit relaxation time effects.

The thermodynamic properties of polyatomic gases can be accurately computed from infra-red or Raman spectroscopic equations developed by methods of statistical mechanics.

The vibrational heat capacities are given by the following formulae.

For diatomic and linear molecules we have

$$\frac{C_i}{R} = \sum_{i=1}^{3n-5} \left(\frac{\frac{hc\omega_i}{2kT}}{\sinh \frac{hc\omega_i}{2kT}} \right)^2 \qquad 10.4.1.$$

and for non-linear molecules not subject to internal rotation

$$\frac{C_i}{R} = \sum_{i=1}^{3n-6} \left(\frac{\frac{hc\omega_i}{2kT}}{\sinh \frac{hc\omega_i}{2kT}} \right)^2 \qquad 10.4.2.$$

where C_i = vibrational heat capacity

$\overline{R}$ = gas constant

$\frac{hc}{k}$ = 1.4385 °K cm.

T = temp. °K

n = number of atoms in molecule

w_i = wave number for each gas

The wave numbers w_i for a number of heavy gases are listed in ref.(10). It is seen that the more complex molecules have higher vibrational heat capacities.

The wave numbers w_i (cm^{-1}) of Freon-12(CCl_2F_2) are given as

261, 318, 437, 455, 473, 667, 906, 1101, 1159

The translational and rotational heat capacity of a polyatomic molecule is $3\overline{R}$.

Thus
$$\frac{C_p}{\overline{R}} = 4 + \sum_{i=1}^{3n-6} \left(\frac{\frac{hcw_i}{2kT}}{\sinh \frac{hcw_i}{2kT}} \right)^2 \qquad 10.4.3.$$

$\frac{C_p}{\overline{R}}$ was calculated from formula 10.4.3. and is presented in fig.91 for the temperature range 200° - 600°K.

10.5. Energy dissipations in gases with heat capacity lag

The theoretical treatment of the problem of heat capacity lag in a general flow case is greatly simplified if the effect on velocity distribution is neglected and also if the temperature changes in the flow are sufficiently small so that both the relaxation time and specific heat capacities can be taken to be constant. Thus the flow pattern obtained in an incompressible fluid can be used as a first approximation. Making assumptions as above Kantrowitz shows that for similar flow patterns the non-dimensional entropy losses depend only on a single parameter

$$K = \frac{d}{\tau U} \qquad 10.5.1.$$

where d = typical length (say tube diameter)

U = typical velocity

τ = relaxation time

The non-dimensional entropy change $\Delta S'$ is defined

$$\Delta S' = \frac{\Delta S}{\Delta S_i} \qquad 10.5.2.$$

ΔS = actual entropy change.

ΔS_i = entropy increase following instantaneous compression to rest.

The non-dimensional entropy losses about a source shaped impact tube using these assumptions were calculated (ref.37) as a function of K and are reproduced in fig.92 (K is based on tube diameter).

The following approximate equations apply

$$\Delta S' = \frac{1.743}{K} \qquad \text{K large} \qquad 10.5.3.$$

and $\Delta S' = 1.452K + (1-1.008K)^2$ when K is small. 10.5.4.

The range of applicability can be seen from fig.92.

10.6. Calculation of the change in stagnation pressure, due to relaxation effects, as measured by a total head tube in Freon-12.

If the compression time is long compared with the relaxation time the pressure and temperature in the freestream ahead of a total head tube will rise isentropically from their values p_∞ and T_∞ to their stagnation value p_{st} and T_{st}.

When however the compression time is small compared with the relaxation time the vibrational energy lags behind the temperature rise. The result is that the equilibrium pressure and temperature p_2 and T_2 are smaller than p_{st} and T_{st} respectively.

It can be shown (ref.37) that for an instantaneous compression, neglecting the variation of the specific heats with temperature,

$$\left(\frac{p_{st}}{p_2}\right)_i = \left[\frac{\frac{C_p}{C_i} - 1}{\frac{C_p}{C_i} - \frac{T_\infty}{T_{st}}}\right]^{\frac{Cp_a}{R}} \left(\frac{T_{st}}{T_1}\right)^{\frac{C_i}{R}} \qquad 10.6.1.$$

where Cp_a is the heat capacity of the active degreesof freedom

and C_i is the vibrational heat capacity

and the corresponding gain in entropy is found from

$$\frac{\Delta S_i}{R} = M \left(\frac{p_{st}}{p_2} \right)_i \qquad 10.6.2.$$

But the entropy rise during compression at an impact tube is

$$\Delta S = \Delta S' \quad \Delta S_i \qquad 10.6.3.$$

where ΔS_i is found from equation 10.6.2. and $\Delta S'$ is a function of $K = \frac{d}{\tau U}$ (see equations 10.5.3. and 10.5.4).

and $$\frac{\Delta S}{R} = M \left(\frac{p_{st}}{p_2} \right)^{\Delta S'} \qquad 10.6.4.$$

Hence $$\frac{p_{st}}{p_2} = \left(\frac{p_{st}}{p_2} \right)_i$$

$$\doteq 1 + \Delta S' \left[\left(\frac{p_{st}}{p_2} \right)_i - 1 \right] \qquad 10.6.5.$$

if $\left(\frac{p_{st}}{p_2} \right)_i - 1$ is small.

The variation of the relaxation time with temperature is neglected and although it is inversely proportional to pressure, its value is taken corresponding to the stagnation pressure.

The following values of the pressure ratio for instantaneous compression, with $T_{st} = 300^{\circ}K$, were calculated for Freon-12

M	0	0.2	0.4	0.6	0.8	1.0
$\left[\left(\frac{p_{st}}{p_2} \right)_i - 1 \right]$	0	0	0.0005	0.006	0.007	0.039

The relaxation parameter K can be written

$$K = \frac{d}{\tau U} = \frac{d}{\tau M a} = \frac{d}{\tau M a_{st}} \frac{a_{st}}{a} = \frac{d}{\tau M a_{st}} \left(1 + \frac{\gamma-1}{2} M^2\right)^{1/2} \qquad 10.6.6.$$

If $d = 0.00083$ ft.

$T_{st} = 300^{\circ}K$

$a_{st} = 495$ ft/sec.

$\tau = 8 \quad 10^{-8}$ sec.

and since for subsonic flow

$$\left(1 + \frac{\gamma-1}{2} M^2\right)^{1/2} \doteq 1$$

We have $K = \frac{21}{M}$ 10.6.7.

Now from equation 10.5.3.

$$\Delta S' = \frac{1.743}{K} \quad \text{when K large.}$$

Thus for a 0.01 in. diameter impact tube we have

M	0	0.2	0.4	0.6	0.8	1.0
$\Delta S'$	0	0.0016	0.0033	0.005	0.0066	0.0083
$\left[\frac{p_{st}}{p_2} - 1\right]$	0	0	0	0 .000030	0.000044	0.00032

From the above values it can be seen that the use of a 0.010 in. diameter total-head tube in Freon-12 is quite permissible at the stagnation pressures and temperatures considered. The very low pressure losses arise mainly because of the fairly short relaxation time and also because the low value of γ does not give rise to large temperature differences. A worse case would arise if the flow were considered at a lower stagnation pressure, where the relaxation time is somewhat larger, and at a higher speed.

10.7. Estimation of drag changes due to relaxation effects

Using a perturbation method, the change in drag coefficient due to relaxation effects on an aerofoil can be shown to be (ref.38)

$$\Delta C_D = M_\infty^2 \frac{2 C_i \overline{R}}{C_{p_a} C_v} \frac{1}{K} \frac{t}{c} \int \left(\frac{q_1}{U_\infty}\right)^4 \cdot \frac{\partial}{\partial s}\left(\frac{q_1}{U_\infty}\right) \sin \eta \; ds. \qquad 10.7.1.$$

where η = slope of aerofoil boundary

$K = \frac{t}{\tau U}$

t = aerofoil thickness

c = aerofoil chord

M_∞ = incident Mach number

(q_1) = local velocity

s = distance along boundary

Gunn has evaluated the value of the integral for some symmetrical Joukowski aerofoil sections at zero incidence.

$$\frac{t}{c} \int \left(\frac{q_1}{U_\infty}\right)^4 \sin\eta \, \frac{\partial}{\partial s} \left(\frac{q_1}{U_\infty}\right) . \, ds \, .$$

0.104	1.1
0.151	1.9
0.207	2.6

10.7.2.

The above results are based on incompressible flow and their use is justified by convenience.

The factor K can be written

$$K = \frac{t}{\tau U_\infty} = \frac{t}{\tau M_\infty a} = \frac{t}{\tau M_\infty a_{st}} \cdot \frac{a_{st}}{a} = \frac{t}{\tau M_\infty a_{st}} \left(1 + \frac{\gamma-1}{2} M_\infty^2\right)^{1/2}$$

10.7.3.

The most unfavourable case arises at high Mach number and high temperature about small wings, that is for small values of K, and large thickness chord ratios.

Estimation of drag coefficient change due to relaxation time effects in Freon-12 about a 2in. chord 10% thick aerofoil section at $M_\infty = 0.8$

We will take a stagnation temperature of $300^\circ K$ and assume that the relaxation time at this temperature is $8 \quad 10^{-8}$ sec.

The speed of sound in Freon-12 at $300^\circ K$ = 495 ft/sec.

and $\left(1 + \frac{\gamma-1}{2} M_\infty^2\right)^{1/2} \doteq 1.$ at $M_\infty = 0.8$.

Hence from equation 10.7.3. we have $K = \frac{0.2}{8 \times 10^{-8} \times 495 \times 12 \times M_\infty} = \frac{420}{M_\infty}$

10.7.4.

If we substitute 10.7.2 for a 10% thick aerofoil and 10.7.4. together with the value of $\frac{C_i \bar{R}}{C_{p_a} C_v}$ obtained from fig.91 into equation 10.7.1 we find that

$$\Delta C_D = M_\infty^3 \cdot 2 \frac{C_i \bar{R}}{C_{p_a} C_v} \cdot \frac{t}{KC} \int \left(\frac{q_1}{U}\right)^4 \frac{\partial}{\partial s} \left(\frac{q_1}{U}\right)^6 \sin \eta \, d s$$

$$= M_\infty^3 \cdot \frac{2.4.75}{4.0.\times 7.75} \cdot \frac{0.1}{420} \cdot 1.1 = 0.00008 M_\infty^3 \qquad 10.7.5.$$

Hence with $M_\infty = 0.8$ we have $\Delta C_D = 0.00004$
Comparing this with the measured drag coefficient $C_D \sim 0.01$ it can be seen that the change is only 0.4%.

It is unusual to make measurements on wings smaller than 2in chord and hence in most cases it would seem that on relaxation time effects in the flow about wings in Freon-12 are negligible. It should be noted that viscous effects are neglected in deriving equation 10.7.1.

APPENDIX XI

The determination of gas mixture proportions by means of a sound Measuring Gauge

11.1. Speed of sound in a gas mixture

For a binary mixture of two thermally perfect gases denoted by subscripts 1 and 2, we can derive the following equations where x is the mole fraction of component (1) and as a subscript denotes the properties of the mixture itself.

Speed of sound of mixture $a_x = \sqrt{\frac{\gamma_x \bar{R} T}{m_x}}$ 11.1.1.

Molecular weight of mixture $m_x = x m_1 + (1-x) m_2$ 11.1.2.

and $$\frac{1}{1-\gamma} = \frac{x}{1-\gamma_1} + \frac{1-x}{1-\gamma_2} \qquad 11.1.3.$$

Thus in terms of the properties of the components the speed of sound in the mixture is

$$a_x = \sqrt{\frac{\gamma_x \bar{R} T}{m_x}} = \sqrt{\frac{\left[x(\gamma_1-\gamma_2)+\gamma_2(1-\gamma_1)\right]\bar{R}T}{\left[x(\gamma_1-\gamma_2)+1-\gamma_1\right](x m_1+(1-x)m_2)}} \qquad 11.1.4.$$

$$= a_2 \sqrt{\frac{x\left(\frac{\gamma_1}{\gamma_2}-1\right)+(1-\gamma_1)}{\left[1+x\left(\frac{m_1}{m_2}-1\right)\right]\left[x(\gamma_1-\gamma_2)+1-\gamma_1\right]}}$$

Equation 11.1.4. indicates that the proportion of the constituents can be found by measuring the speed of sound of the mixture provided the properties of the components are known.

11.2. Constants for the sound measuring gauge for a Freon-12 and air mixture.

In the temperature and pressure ranges in which Freon-12 measurements will be made, Freon-12 can be considered an ideal gas. For instance the deviation of $\frac{pV}{RT}$ from unity is only about 2% at atmospheric pressure and in the temperature range 470°-550°F and is considerably less at lower pressures. (ref.8).

Since in most cases air will only be present as an impurity in Freon it will be preferable to use an actual value of the speed of sound of Freon in equation 11.1.4 rather than the ideal gas value obtained from $\sqrt{\frac{\gamma_2 \bar{R}T}{m_2}}$. The speed of sound in Freon-12 at atmospheric pressure and 288°K is given as 485 ft/sec (ref.8,4,6) and square root variation with temperature is assumed.

A representative value of 1.125 for the specific heat ratio in Freon-12 is then used in the expression in square root brackets in 11.1.4, which can be regarded as a correction term due to the small amount of air present.

The following values for the properties of air and Freon-12 were used.

Speed of sound in Freon-12 at atmospheric pressure and 288°K
= 485 ft/sec.

or speed of sound in Freon-12, $a_F = 28.6\sqrt{T°K}$

Molecular wt Freon-12 $m_F = 120.92$

" " Air $m_A = 28.97$

Ratio of specific heats Air $\gamma_A = 1.4$

" " " " Freon-12 $\gamma_F = 1.125$

If x denotes the mole fraction of air in the mixture at $T^{\circ}K$ equation 11.1.4 becomes

$$a_x = 28.6 \sqrt{T} \sqrt{\frac{1 - 0.6111x}{(1 - 0.7604x)(1 - 0.6875x)}} \qquad 11.2.1.$$

11.3. Determination of the proportion of air (by volume) in Freon-12 and air mixtures

The sound gauge measures the time τ (secs) for sound to travel a distance of 3 feet.

Thus $$\tau = \frac{3}{a_x} \qquad 11.3.1.$$

where a_x = speed of sound of mixture containing the mole fraction x of air (ft/sec)

which together with equation 11.2.1 gives

$$\tau \sqrt{T} = 0.1050 \sqrt{\frac{(1-0.7604\ x)(1-0.6875\ x)}{(1 - 0.6111\ x)}} \qquad 11.3.2.$$

The ratio of the specific heat of the mixture γ_x and the proportion of air present as a mole fraction x is plotted in terms of $\tau \sqrt{T^{\circ}K}$ in fig.93. Thus if the reading of the counter and the temperature at which the sound measurements are made is known, γ_x and x can be found from fig.93.

It should be noted that the speed of sound of the mixture is not a linear function of the speed of sound of the components.

APPENDIX XII

Comparison of flutter model testing in compressed air tunnels and tunnels using heavy gases

1. Summary: Model requirements for flutter tests in compressed air tunnels and heavy gas tunnels have been compared. It is shown that:-

(1) Incompressible tests. In the same sized tunnels and at the same pressure ratio the flutter velocity is reduced.

(2) Compressible tests. At moderately high subsonic Mach numbers the changes in flow due to the difference in the ratio of the specific heats are negligible and considerable advantage can be obtained by the use of a heavy gas. In particular the flutter velocity and flutter frequency are reduced. There are also large reductions in tunnel power and pressure ratio (see Appendix V).

At high subsonic and transonic Mach numbers the flow changes due to the difference in specific heats are not negligible but under certain conditions the pressures, forces and moments can be related to the corresponding air values by using the area similarity or transonic similarity assumptions. It is not possible to construct a model of altered density and stiffness ratio which will accurately compensate for the effect of change in γ over the whole Mach number range, though the effects of different γ are very small.

The reductions in flutter velocity, flutter frequency and the tunnel pressure ratio obtainable with Freon-12 are tabulated.

2. Flutter Models

To reproduce flutter conditions in model tests, the model must be designed so that

(a) aerodynamic shape
(b) elastic stiffness distribution
(c) location of elastic axis and centre of gravity
(d) ratio of flexural to torsional stiffness
(e) mass distribution

are similar.

In addition the following dimensionless parameters must remain constant.

$$\frac{c_1 f_1}{U_1} = \frac{c_2 f_2}{U_2} = \text{ratio of time scales} \qquad 2.1.$$

$$\frac{\rho_1 c_1^3 U_1^2}{\epsilon_1} = \frac{\rho_2 c_2^3 U_2^2}{\epsilon_2} = \text{ratio of aerodynamic to elastic forces} \qquad 2.2.$$

$$\frac{\rho_1}{\sigma_1} = \frac{\rho_2}{\sigma_2} = \text{relative densities} \qquad 2.3.$$

$$\frac{\rho_1 c_1 U_1}{\mu_1} = \frac{\rho_2 c_2 U_2}{\mu_2} = \text{Reynolds number} \qquad 2.4.$$

$$\frac{U_1}{a_1} = \frac{U_2}{a_2} = \text{Mach number} \qquad 2.5.$$

$$\gamma_1 = \gamma_2 = \text{Ratio of specific heats} \qquad 2.6.$$

Where c = representative length

f = frequency

U = velocity free-stream

ρ = density of medium

σ = conventional density of wing

ϵ = stiffness (representative restoring moment per radian deflection)

μ = viscosity

a = velocity of sound

The number of variables occurring in the appropriate dimensionless parameters, whose scale can be chosen arbitrarily is equal to the number of primary quantities in which these variables can be expressed. These are three in number, e.g. mass, length and time.

3. Incompressible case

The appropriate dimensionless parameters in this case are those listed in equation 2.1 to 2.4 above. If model tests are carried out at the same temperature, the viscosity scale is fixed, and hence the scale of two more variables can be decided arbitrarily.

3.1. Compressed air tunnel

We have (ref.43)

$$\frac{c_1 f_1}{U_1} = \frac{c_2 f_2}{U_2}$$

$$\frac{\rho_1 c_1^3 U_1^2}{\epsilon_1} = \frac{\rho_2 c_2^3 U_2^2}{\epsilon_2} \qquad 3.1.1.$$

$$\frac{\rho_1}{\sigma_1} = \frac{\rho_2}{\sigma_2}$$

$$\frac{\rho_1 c_1 U_1}{\mu_1} = \frac{\rho_2 c_2 U_2}{\mu_2}$$

where suffix (1) refers to full-scale

and suffix (2) model scale

If these are to be performed at the maximum Reynold number in a given tunnel so that $\frac{\rho_2}{\rho_1} = r$ = maximum compression ratio and $\frac{c_2}{c_1} = \lambda$ maximum scale of model permissible, we have since $\mu_1 = \mu_2$

$$\frac{\sigma_2}{\sigma_1} = r$$

$$\frac{U_2}{U_1} = \frac{1}{\lambda r} < 1 \quad \text{if} \quad r > \frac{1}{\lambda}$$

$$\frac{\epsilon_2}{\epsilon_1} = \frac{\lambda}{r} < 1 \quad \text{if} \quad \lambda < 1 \quad r > 1 \qquad 3.1.2.$$

and $$\frac{f_2}{f_1} = \frac{1}{\lambda^2 r} > 1 \quad \text{if} \quad r > \frac{1}{\lambda}$$

We see therefore that the model flutter velocity and frequency and the model stiffness depend on the choice of the model scale and the tunnel pressure. If the latter is greater than the reciprocal of the model scale the model flutter velocity and its stiffness will be reduced but the model flutter frequency

will increase compared with full scale values.

3.2. Heavy gas tunnel

If we now consider a model of the same size as for the compressed air tunnel but tested at the same pressure ratio in a tunnel using a heavy gas at the same temperature we have

$$\frac{p_3}{p_1} = \frac{p_2}{p_1} = r,$$

where suffixes 1, 2, 3 denote full scale, model air tunnel and model heavy gas tunnel respectively

Therefore $$\frac{\rho_3}{\rho_1} = \frac{m_3 p_3}{m_1 p_1} = \frac{m_3}{m_1} \quad r.$$

where m = Molecular wt.

Now the viscosity of a heavy gas generally decrease with molecular weight.

Let $$n = \frac{\mu_3}{\mu_1} = \frac{\mu_3}{\mu_2}$$

From equation 2.1 to 2.4

$$\frac{U_3}{U_1} = n \frac{m_1}{m_3} \cdot \frac{1}{\lambda r}$$

$$\frac{f_3}{f_1} = n \frac{m_1}{m_3} \cdot \frac{1}{\lambda^2 r} \qquad 3.2.1.$$

$$\frac{\epsilon_3}{\epsilon_1} = n^2 \frac{m_1}{m_3} \cdot \frac{\lambda}{r}$$

Hence comparing equations 3.2.1. with 3.1.2 we find

$$\frac{U_3}{U_2} = n \frac{m_1}{m_3}, \quad \frac{\epsilon_3}{\epsilon_2} = n^2 \frac{m_1}{m_3}, \quad \frac{f_3}{f_2} = n \frac{m_1}{m_3}$$

Thus the flutter velocity, frequency and model stiffness required in the heavy gas tunnel are in general reduced compared with the compressed air tunnel. The power required to drive the heavy gas tunnel is also considerably reduced.

4. Compressible case

The appropriate non-dimensional parameters are equations 2.1. to 2.6. The ratio of specific heats γ has very little effect at moderately high subsonic Mach number. This can be seen from its absence in the linear Prandtl-Glauert relations. Hence the only additional variable that needs to be considered is the Mach number.

The viscosity and speed of sound of a perfect gas are only a function of temperature and hence if tests at the same temperature are considered, the scale of two variables is fixed and only one more scale for model tests can be chosen arbitrarily. This could be the maximum linear dimension of the model.

4.1. Compressed air tunnel

Let the model scale $\frac{c_2}{c_1} = \lambda < 1$, and put $\frac{a_2}{a_1} = 1$

and $\frac{\mu_2}{\mu_1} = 1.$

Hence from equations 2.1 to 2.5

$$\frac{U_2}{U_1} = 1$$

$$\frac{f_2}{f_1} = \frac{\sigma_2}{\sigma_1} = \frac{\rho_2}{\rho_1} = \frac{1}{\lambda} > 1 \qquad 4.1.1.$$

$$\frac{\epsilon_2}{\epsilon_1} = \lambda^2 < 1.$$

In this case the model flutter velocity equals to full scale value whereas the model flutter frequency is increased and the model stiffness is reduced.

4.2. Heavy gas tunnel

Consider a model of the same dimensions as in the compressed air tunnel, but tested in a heavy gas at the same temperature or

$$\frac{c_3}{c_1} = \lambda < 1.$$

We have m_3 = mol. wt. of heavy gas

m_1 = mol. wt. of air.

In general $\frac{\mu_3}{\mu_1} = n < 1$

and $\frac{\gamma_3}{\gamma_1} < 1$

The ratio of the speeds of sound is given by

$$\frac{a_3}{a_1} = \sqrt{\frac{\gamma_3}{\gamma_1} \cdot \frac{m_1}{m_3}}$$

and from equation 2.1. to 2.5.

$$\frac{u_3}{u_1} = \sqrt{\frac{\gamma_3}{\gamma_1} \cdot \frac{m_1}{m_3}} < 1$$

$$\frac{f_3}{f_1} = \frac{1}{\lambda} \cdot \sqrt{\frac{\gamma_3}{\gamma_1} \cdot \frac{m_1}{m_3}} > 1 \quad \text{if} \quad \lambda < \frac{a_3}{a_1} \qquad 4.2.1.$$

$$\frac{\rho_3}{\rho_1} = \frac{\sigma_3}{\sigma_1} = n \sqrt{\frac{\gamma_1 m_3}{\gamma_3 m_1}} \cdot \frac{1}{\lambda} > 1$$

$$\frac{\epsilon_3}{\epsilon_1} = n \left(\frac{\gamma_3}{\gamma_1} \cdot \frac{m_1}{m_3} \right)^{1/2} \cdot \lambda^2 < 1$$

Thus the model flutter speed and stiffness are reduced but the model flutter frequency and density are increased.

4.3. Comparison of compressed air and heavy gas tunnel tests

Comparing equations listed in 4.1.1. and 4.2.1. we see that

$$\frac{U_3}{U_2} = \sqrt{\frac{\gamma_3}{\gamma_1} \frac{m_1}{m_3}} < 1 \qquad 4.3.1.$$

$$\frac{\rho_3}{\rho_2} = \frac{\sigma_3}{\sigma_2} = n \sqrt{\frac{\gamma_1}{\gamma_3} \cdot \frac{m_3}{m_1}}$$

$$\frac{\epsilon_3}{\epsilon_2} = n \left(\frac{\gamma_3}{\gamma_1} \cdot \frac{m_1}{m_3} \right)^{1/2} < 1 \qquad 4.3.1.$$

$$\frac{f_3}{f_2} = \sqrt{\frac{\gamma_3}{\gamma_1} \cdot \frac{m_1}{m_3}} < 1$$

Hence by use of a heavy gas tunnel the speed and frequency of the model tests are reduced and, most important, the model stiffness is also reduced.

The ratio of the pressures in the two tunnels is given by

$$\frac{p_3}{p_2} = n \sqrt{\frac{\gamma_1}{\gamma_3}} \cdot \left(\frac{m_1}{m_2} \right)^{1/2}$$

4.4. <u>The effect of different ratio of specific heat on model flutter tests.</u>

At high subsonic and transonic Mach numbers the changes in flow due to differences in γ cannot be neglected entirely. Measurements of force coefficients can be corrected to corresponding values in air by means of area similarity or transonic similarity assumptions. The difference in the force coefficients are found to be mainly dependent on the free stream Mach number. The conversion coefficients for normal forces and moment coefficients are found to be essentially the same indicating that the changes in the aerodynamic centre position are negligible at least for straight wings.

If $\gamma_1 \neq \gamma_3$

the dimensionless parameters can be written thus

$$\frac{c_2 f_2}{U_2} = \frac{c_3 f_3}{U_3}$$

$$\frac{\rho_2 c_2^3 U_2^2}{\epsilon_2} = \frac{\rho_3 c_3^3 U_3^2}{\epsilon_3} \left[1 + F(M) \right]$$

$$\frac{\rho_2}{\sigma_2} = \frac{\rho_3}{\sigma_3} \cdot \left[1 + F(M) \right] \qquad 4.4.1.$$

$$\frac{\rho_2 U_2 c_2}{\mu_2} = \frac{\rho_3 U_3 c_3}{\mu_3}$$

$$\frac{U_2}{a_2} = \frac{U_3}{a_3} \left[1 + G(M) \right]$$

where $F(M)$ and $G(M)$ are some functions of Mach number.

Also $$\frac{U_3}{U_1} = \frac{a_3}{a_1} \Big/ \left[1 + G(M)\right]$$

$$\frac{\rho_3}{\rho_1} = \frac{a_1}{a_3} \cdot \frac{n}{\lambda} \left[1 + G(M)\right]$$

$$\frac{\epsilon_3}{\epsilon_1} = n \frac{a_3}{a_1} \left[\frac{1 + F(M)}{1 + G(M)}\right] \cdot \lambda^2 \qquad 4.4.2.$$

and $$\frac{\sigma_3}{\sigma_1} = \frac{a_1}{a_3} \cdot \frac{n}{\lambda} \cdot \left[1 + F(M)\right] \left[1 + G(M)\right]$$

From these equations it can be seen that it is impossible to construct a model of different stiffness and density which will completely compensate for the effects of change in γ over the whole Mach number range, though these effects are relatively small.

4.5. Comparison between the parameters for flutter tests in Freon-12 and Air

Gas Properties	m	γ	μslugs/ft.sec.	a ft/sec.
Freon-12	121	1.125	$2.58\ 10^{-7}$	485
Air	29	1.4	$3.79\ 10^{-7}$	1117

The ratios of the viscosities and molecular weights in F-12 (3) and air (2) are respectively

m	$\frac{W_3}{W_2}$
.68	4.2

The flutter velocity ratio $$\frac{U_3}{U_2} = \sqrt{\frac{\gamma_3 m_2}{\gamma_2 m_3}} = 0.43$$

The model density ratio $$\frac{\sigma_3}{\sigma_2} = n \sqrt{\frac{\gamma_2 m_3}{\gamma_3 m_2}} = 1.56$$

The model stiffness ratio $\frac{\epsilon_3}{\epsilon_2} = n\sqrt{\frac{\gamma_3 m_2}{\gamma_2 m_3}} = 0.29$

The model frequency ratio $\frac{f_3}{f_2} = \sqrt{\frac{\gamma_3 m_2}{\gamma_2 m_3}} = 0.43$

The ratio of the pressures $\frac{p_3}{p_2} = m\sqrt{\frac{\gamma_2 m_2}{\gamma_3 m_3}} = 0.37$

TABLE 1

Pressure Distribution on RAE 104/10% Aerofoil in Freon-12.

$\alpha = 0^{\circ}$ Transition at Leading Edge

	Pressure Hole No.	$\frac{x}{c}$	C_p uncorrected	C_p	$C_{p(0)}$	$\frac{p}{H}$
$M_u = 0.398$	1	0.8	-.055	-.045	-.041	.911
	2	0.35	-.295	-.285	-.261	.893
$M_c = 0.402$	3	0.20	-.280	-.270	-.247	.892
	4	0.10	-.261	-.241	-.221	.894
$\epsilon = 0.004$	5	0.90	+.013	+.023	+.021	.917
	6	0.70	-.174	-.164	-.150	.902
$\Delta C_p = 0.010$	7	0.50	-.277	-.267	-.244	.892
	8	0.60	-.264	-.254	-.233	.893
	9	0.35	-.255	-.245	-.225	.894
	10	0.20	-.289	-.279	-.255	.891
$M_u = 0.442$	1	0.8	-.058	-.047	-.042	.891
	2	0.35	-.295	-.284	-.254	.867
$M_c = 0.447$	3	0.20	-.285	-.274	-.245	.868
	4	0.10	-.263	-.252	-.226	.868
$\epsilon = 0.005$	5	0.90	+.013	+.024	+.021	.899
	6	0.70	-.168	-.157	-.141	.880
$\Delta C_p = 0.011$	7	0.50	-.280	-.269	-.241	.868
	8	0.60	-.268	-.257	-.230	.970
	9	0.35	-.255	-.244	-.218	.870
	10	0.20	-.292	-.281	-.251	.867
$M_u = 0.494$	1	0.8	-.095	-.083	-.072	.865
	2	0.35	-.317	-.305	-.264	.835
$M_c = 0.499$	3	0.20	-.310	-.298	-.258	.836
	4	0.10	-.284	-.272	-.236	.839
$\epsilon = 0.005$	5	0.90	+.012	+.025	+.021	.875
	6	0.70	-.177	-.165	-.143	.852
$\Delta C_p = 0.012$	7	0.50	-.298	-.286	-.248	.837
	8	0.60	-.286	-.274	-.237	.838
	9	0.35	-.273	-.261	-.226	.840
	10	0.20	-.315	-.303	-.262	.835

Note: Pressure Hole Nos. 1 - 4 Lower Surface, 5 - 10 Upper Surface.

TABLE 1 Contd.

	Pressure Hole No.	$\frac{x}{c}$	C_p uncorrected	C_p	$C_{p(0)}$	$\frac{p}{H}$
M_u = 0.549	1	0.8	-.044	-.037	.837	
	2	0.35	-.319	-.266	.797	
M_c = 0.555	3	0.20	-.306	-.254	.799	
	4	0.10	-.283	-.236	.802	
ϵ = 0.006	5	0.90	+.023	+.019	.847	
	6	0.70	-.204	-.170	.814	
ΔC_p = 0.014	7	0.50	-.297	-.247	.800	
	8	0.60	-.285	-.237	.802	
	9	0.35	-.264	-.220	.802	
	10	0.20	-.323	-.269	.798	
M_u = 0.595	1	0.8	-.048	-.038	.811	
	2	0.35	-.339	-.272	.763	
M_c = 0.601	3	0.20	-.322	-.258	.766	
	4	0.10	-.298	-.238		
ϵ = 0.006	5	0.90	+.024	+.019	.823	
	6	0.70	-.178	-.143	.790	
ΔC_p = 0.018	7	0.50	-.318	-.254	.766	
	8	0.60	-.303	-.242	.769	
	9	0.35	-.275	-.220	.774	
	10	0.20	-.324	-.259	.765	
M_u = 0.645	1	0.8	-.042	-.032	.784	
	2	0.35	-.361	-.273	.723	
M_c = 0.653	3	0.20	-.342	-.258	.727	
	4	0.10	-.307	-.232	.733	
ϵ = 0.007	5	0.90	+.026	+.020	.797	
	6	0.70	-.187	-.142	.756	
ΔC_p = 0.021	7	0.50	-.370	-.280	.721	
	8	0.60	-.298	-.225	.735	
	9	0.35	-.287	-.217	.737	
	10	0.20	-.365	-.276	.722	

Note: Pressure Hole Nos. 1 - 4 Lower Surface, 5 - 10 Upper Surface.

TABLE 1 Contd.

	Pressure Hole No.	$\frac{x}{c}$	C_p uncorrected	C_p	$C_{p(0)}$	$\frac{p}{H}$
$M_u = 0.675$	1	0.8		-.050	-.036	.765
	2	0.35		-.381	-.278	.698
$M_c = 0.683$	3	0.20		-.357	-.261	.703
	4	0.10		-.317	-.231	.711
$\Delta C_p = 0.025$	5	0.90		+.031	+.023	.781
	6	0.70		-.194	-.142	.736
$\epsilon = 0.008$	7	0.50		-.388	-.283	.697
	8	0.60		-.339	-.248	.706
	9	0.35		-.298	-.217	.714
	10	0.20		-.360	-.263	
$M_u = 0.695$	1	0.8		-.056	-.039	.751
	2	0.35		-.395	-.281	.679
$M_c = 0.703$	3	0.20		-.344	-.245	.689
	4	0.10		-.324	-.230	.694
$\epsilon = 0.009$	5	0.90		+.031	+.022	.769
	6	0.70		-.200	-.142	.721
$\Delta C_p = 0.027$	7	0.50		-.378	-.268	.683
	8	0.60		-.353	-.251	.688
	9	0.35		-.301	-.214	.700
	10	0.20		-.375	-.266	.684
$M_u = 0.719$	1	0.8		-.053	-.036	.736
	2	0.35		-.417	-.286	.656
$M_c = 0.728$	3	0.20		-.360	-.247	.668
	4	0.10		-.332	-.228	.674
$\epsilon = 0.009$	5	0.90		+.032	+.022	.755
	6	0.70		-.208	-.143	.701
$\Delta C_p = 0.031$	7	0.50		-.403	-.276	.658
	8	0.60		-.375	-.257	.664
	9	0.35		-.305	-.210	.680
	10	0.20		-.394	-.270	.660

Note: Pressure Hole Nos. 1 - 4 Lower Surface, 5 - 10 Upper Surface.

TABLE 1 Contd.

	Pressure Hole No.	$\frac{x}{c}$	C_p uncorrected	C_p	$C_{p(0)}$	$\frac{p}{H}$
M_u = 0.751	1	0.8		-.054	-.035	.716
	2	0.35		-.457	-.296	.621
M_c = 0.762	3	0.20		-.387	-.251	.656
	4	0.10		-.338	-.219	.667
ϵ = 0.011	5	0.90		+.038	+.025	.756
	6	0.70		-.217	-.141	.696
ΔC_p = 0.038	7	0.50		-.458	-.297	.642
	8	0.60		-.416	-.270	.649
	9	0.35		-.430	-.278	.646
	10	0.20		-.433	-.281	.645
M_u = 0.776	1	0.8		-.056	-.035	.696
	2	0.35		-.496	-.308	.588
M_c = 0.787	3	0.20		-.414	-.257	.608
	4	0.10		-.342	-.212	.626
ϵ = 0.012	5	0.90		+.043	+.026	.721
	6	0.70		-.224	-.139	.655
ΔC_p = 0.052	7	0.50		-.496	-.308	.588
	8	0.60		-.432	-.268	.604
	9	0.35		-.302	-.188	.636
	10	0.20		-.448	-.279	.599
M_u = 0.792	1	0.8		-.045	-.027	.687
	2	0.35		-.534	-.316	.561
M_c = 0.806	3	0.20		-.426	-.252	.589
	4	0.10		-.334	-.198	.613
ϵ = 0.014	5	0.90		+.049	+.029	.711
	6	0.70		-.217	-.128	.643
ΔC_p = 0.058	7	0.50		-.570	-.337	.549
	8	0.60		-.451	-.267	.582
	9	0.35		-.289	-.171	.624
	10	0.20		-.452	-.268	.582
M_u = 0.827	1	0.8		-.144		.632
	2	0.35		-.528		.528
M_c = 0.851	3	0.20		-.398		.562
	4	0.10				.585
ΔC_p = 0.091	5	0.90		.035		.661
	6	0.70		.473		.543
ϵ = 0.027	7	0.50		.621		.502
	8	0.60		.799		.457
	9	0.35		.219		.612
	10	0.20		.404		.562

Note: Pressure Hole Nos. 1 - 4 Lower Surface, 5 - 10 Upper Surface.

TABLE 2

Pressure coefficient on RAE 104 measured in F-12 and converted to equivalent air values

$\alpha = 0^{\circ}$

	No. Hole	F.12 C_p	Air C_p (TS)	Air C_p (AS)
	1	-.045	-.045	-.045
$M_F = 0.402$	2	-.285	-.281	-.278
	3	-.270	-.273	-.262
$M_A(TS) = 0.383$	4	-.241	-.239	-.233
	5	+.023	+.023	+.023
$M_A(AS) = 0.394$	6	-.164	-.162	-.160
	7	-.266	-.263	-.258
	8	-.254	-.251	-.246
	9	-.245	-.243	-.237
	10	-.279	-.276	-.271
	1	-.047	-.047	-.047
$M_F = 0.447$	2	-.284	-.281	-.276
	3	-.274	-.271	0.266
$M_A(TS) = 0.428$	4	-.252	-.239	-.244
	5	+.024	+.024	+.024
$M_A(AS) = 0.438$	6	-.157	-.155	-.153
	7	-.269	-.266	-.261
	8	-.257	-.254	-.249
	9	-.244	-.242	-.236
	10	-.281	-.278	-.273
	1	-.083	-.083	-.083
$M_F = 0.499$	2	-.305	-.302	-.296
	3	-.298	-.295	-.289
$M_A(TS) = 0.479$	4	-.272	-.269	-.264
	5	+.025	+.025	+.025
$M_A(AS) = 0.488$	6	-.165	-.163	-.160
	7	-.286	-.283	-.277
	8	-.274	-.271	-.266
	9	-.261	-.258	-.253
	10	-.303	-.300	-.294

TS Transonic similarity
AS Area similarity

TABLE 2 Contd.

	No. Hole	F.12 C_p	Air C_p (TS)	Air C_p (AS)
	1	-.044	-.044	-.044
	2	-.319	-.316	-.309
M_F = 0.555	3	-.306	-.303	-.296
	4	-.283	-.280	-.274
M_A(TS) = 0.535	5	+.023	+.023	+.023
	6	-.204	-.202	-.198
M_A(AS) = 0.543	7	-.297	-.294	-.288
	8	-.285	-.282	-.276
	9	-.264	-.261	-.256
	10	-.323	-.320	-.313
	1	-.048	-.048	-.048
M_F = 0.601	2	-.339	-.334	-.329
	3	-.322	-.316	-.312
M_A(TS) = 0.581	4	-.298	-.294	-.288
	5	+.024	+.024	+.024
M_A(AS) = 0.589	6	-.178	-.174	-.172
	7	-.318	-.312	-.308
	8	-.303	-.297	-.293
	9	-.275	-.270	-.267
	10	-.324	-.318	-.314
	1	-.042	-.042	-.042
M_F = 0.653	2	-.361	-.354	-.348
M_A(TS) = 0.634	3	-.342	-.335	-.330
M_A(AS) = 0.641	4	-.307	-.301	-.297
	5	+.026	+.026	+.026
	6	-.187	-.183	-.180
	7			
	8			
	9	-.287	-.281	-.278
	10	-.365	-.358	-.353
	1	-.050	-.049	-.050
M_F = 0.683	2	-.381	-.374	-.369
M_A(TS) = 0.665	3	-.357	-.350	-.346
	4	-.317	-.311	-.307
M_A(AS) = 0.671	5	+.031	+.031	+.031
	6	-.194	-.190	-.188
	7			
	8			
	9	-.298	-.292	-.288
	10	-.360	-.363	-.348

TABLE 2 Contd.

	No. Hole	F.12 C_p	Air C_p (TS)	Air C_p (AS)
	1	-.056	-.055	-.054
	2	-.395	-.385	-.383
M_F = 0.703	3	-.344	-.335	-.332
M_A(TS) = 0.686	4	-.324	-.316	-.312
	5	+.031	+.031	+.029
M_A(AS) = 0.691	6	-.200	-.195	-.194
	7	-.378	-.369	-.366
	8	-.353	-.344	-.341
	9	-.301	-.293	-.291
	10	-.375	-.366	-.362
	1	-.053	-.052	-.051
M_F = 0.728	2	-.417	-.407	-.403
M_A(TS) = 0.711	3	-.360	-.351	-.348
M_A(AS) = 0.716	4	-.330	-.322	-.320
	5	+.032	+.032	+.031
	6	-.208	-.203	-.200
	7	-.403	-.393	-.390
	8	-.375	-.366	-.362
	9	-.305	-.296	-.295
	10	-.394	-.384	-.380
	1	-.054	-.053	-.052
M_F = 0.762	2	-.457	-.446	-.442
M_A(TS) = 0.746	3	-.387	-.377	-.373
	4	-.338	-.330	-.328
	5	+.038	+.038	+.038
M_A(AS) = 0.751	6	-.217	-.212	-.210
	7	-.458	-.447	-.443
	8	-.416	-.406	-.408
	9	-.430	-.419	-.416
	10	-.433	-.422	-.410

TABLE 2 Contd.

	No. Hole	F.12 C_p	Air C_p (TS)	Air C_p (AS)
	1	-.056	-.054	-.054
	2	-.496	-.481	-.480
M_F = 0.787	3	-.414	-.402	-.400
M_A(TS) = 0.772	4	-.342	-.332	-.330
	5	+.043	+.042	+.045
M_A(AS) = 0.776	6	-.224	-.217	-.217
	7	-.476	-.462	-.460
	8	-.412	-.400	-.400
	9	-.302	-.293	-.292
	10	-.448	-.434	-.432
	1	-.045	-.044	-.043
	2	-.534	-.518	-.507
M_F = 0.806	3	-.426	-.413	-.407
M_A(TS) = 0.793	4	-.334	-.324	-.320
M_A(AS) = 0.796	5	+.049	+.048	+.047
	6	-.216	-.210	-.206
	7	-.570	-.553	-.542
	8	-.451	-.437	-.431
	9	-.289	-.280	-.276
	10	-.452	-.438	-.432
	1	-.144	-.140	-.140
M_F = 0.851	2	-.528	-.512	-.500
	3	-.398	-.386	-.378
M_A(TS) = 0.838	4			
	5	-.035	-.034	-.033
M_A(AS) = 0.842	6	-.473	-.459	-.450
	7	-.621	-.602	-.585
	8	-.749	-.727	-.703
	9	-.219	-.212	-.208
	10	-.404	-.392	-.383

TABLE 3

RAE 104/10% (symmetrical) Drag Measurements

(a) $\alpha = 0^\circ$

	Corrected freestream Mach number	Drag Coefficient	Reynolds number
Freon-12 results Free Transition	M_c	C_{D_c}	Re No.
	0.403	0.0119	
	0.604	0.0093	
	0.775	0.0082	
	0.809	0.0091	
	0.835	0.0198	
Freon-12 results Fixed Transition	0.402	0.0107	
	0.448	0.0106	
	0.500	0.0108	
	0.601	0.0107	
	0.731	0.0111	
	0.818	0.0170	
N.P.L. air results 5in.chord model at atmospheric stagnation pressure	0.607	0.0087	
	0.711	0.0088	
	0.794	0.0092	
	0.823	0.0106	
	0.850	0.0226	
	0.874	0.0415	

(b) $\alpha = 4^\circ$

N.P.L. air results 5in.chord Fixed transition.	0.403	0.0109	
	0.607	0.0114	
	0.712	0.0174	
	0.769	0.0361	
Freon-12 results Fixed transition	0.403	0.0154	
	0.607	0.0172	
	0.712	0.0197	
	0.761	0.0286	
	0.796	0.0565	

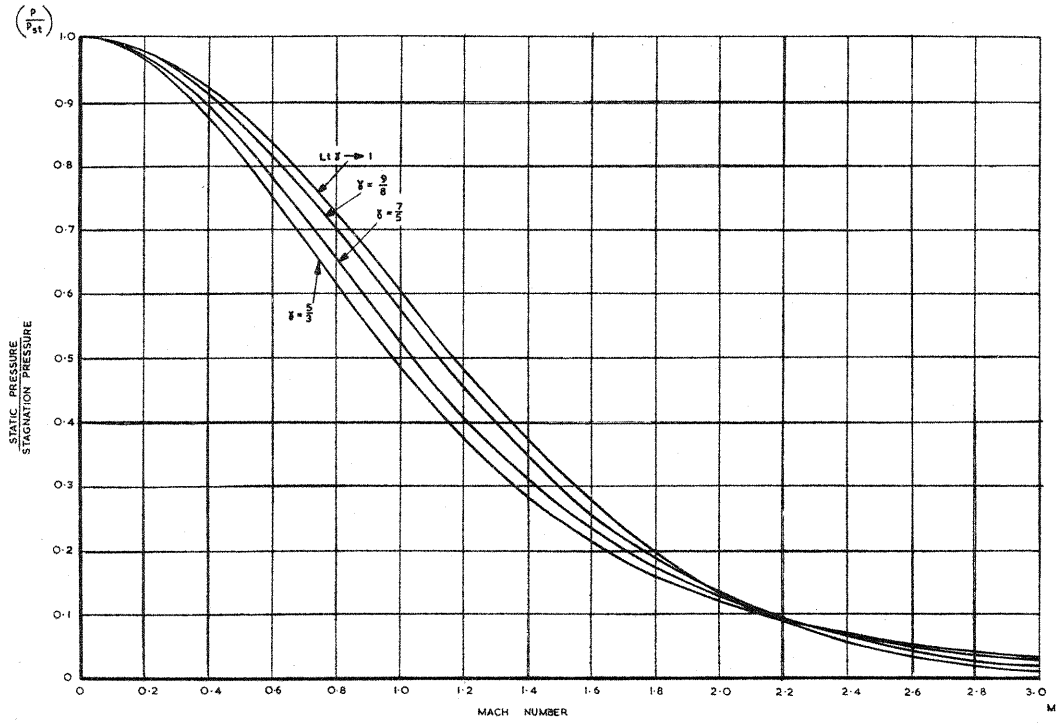

FIG. 1 VARIATION OF PRESSURE WITH MACH NUMBER IN ISENTROPIC FLOW.

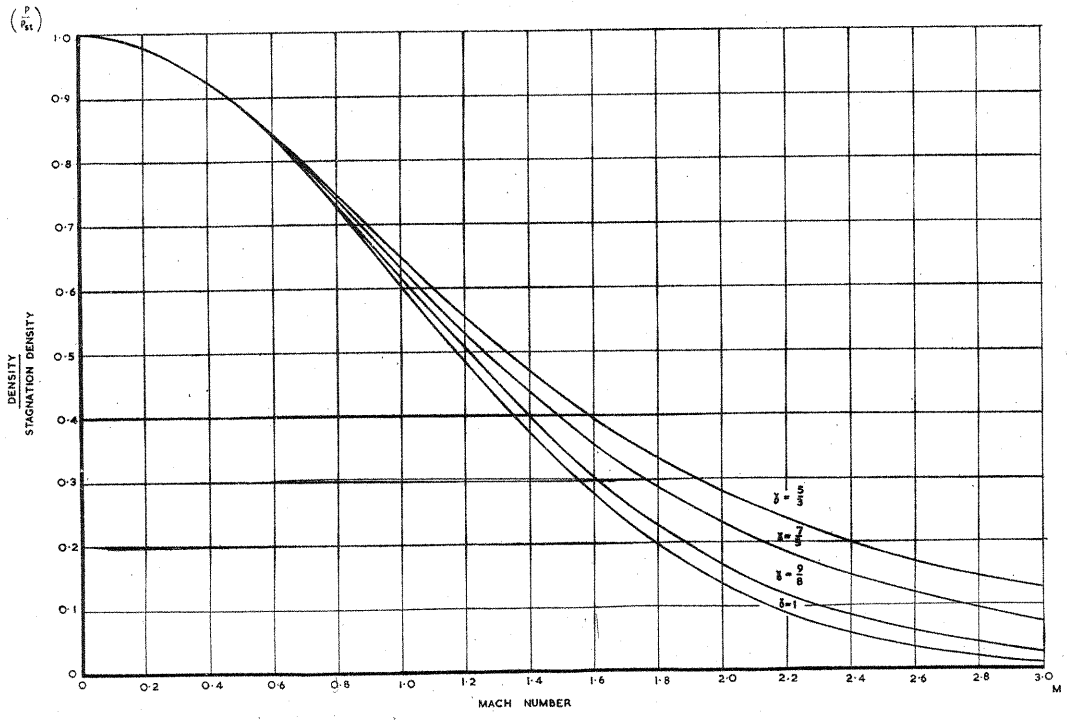

FIG. 2 VARIATION OF DENSITY WITH MACH NUMBER IN ISENTROPIC FLOW.

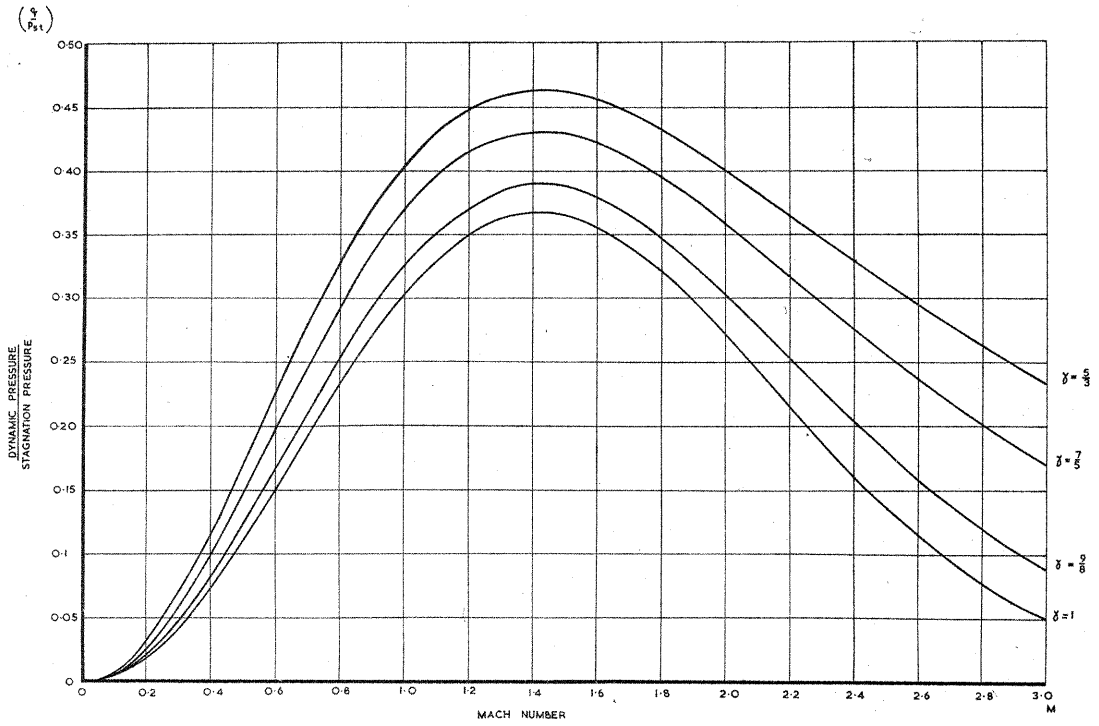

FIG. 3 VARIATION OF DYNAMIC PRESSURE WITH MACH NUMBER IN ISENTROPIC FLOW.

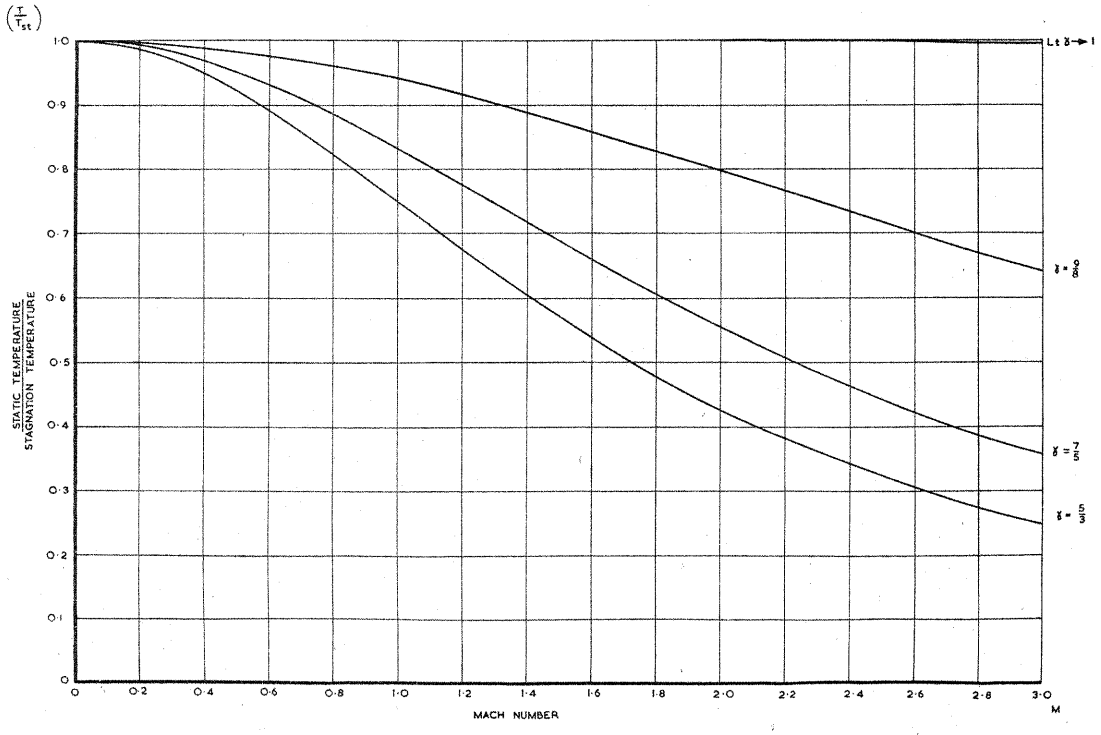

FIG. 4 VARIATION OF TEMPERATURE WITH MACH NUMBER IN ISENTROPIC FLOW.

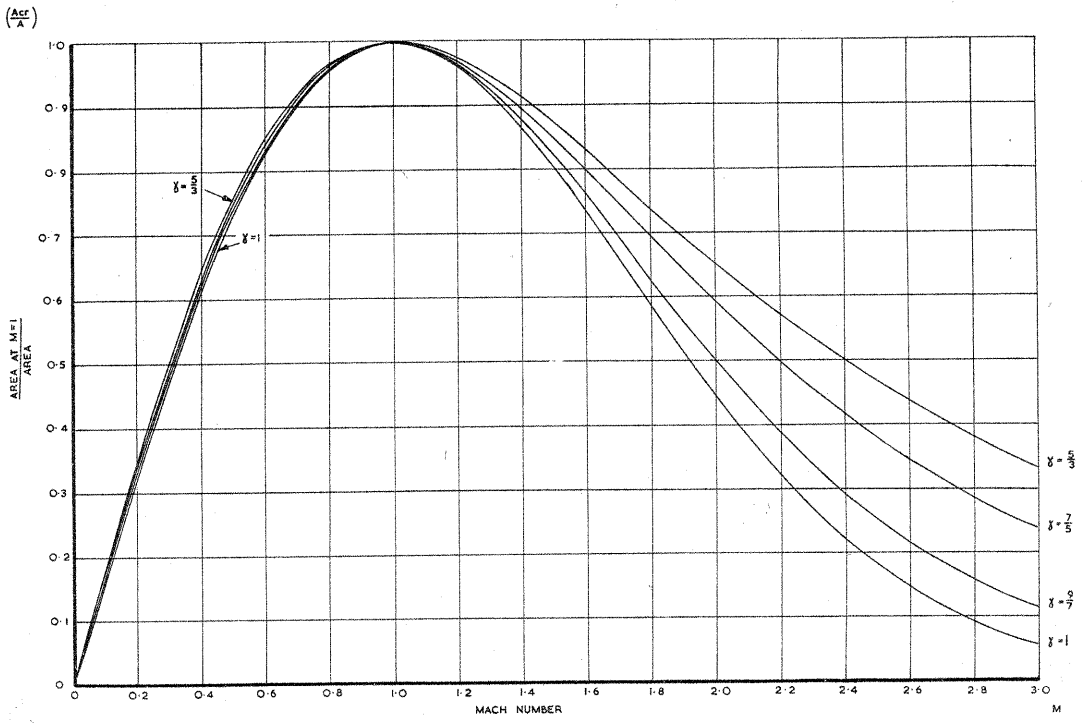

FIG. 5 VARIATION OF AREA RATIO WITH MACH NUMBER IN ISENTROPIC FLOW.

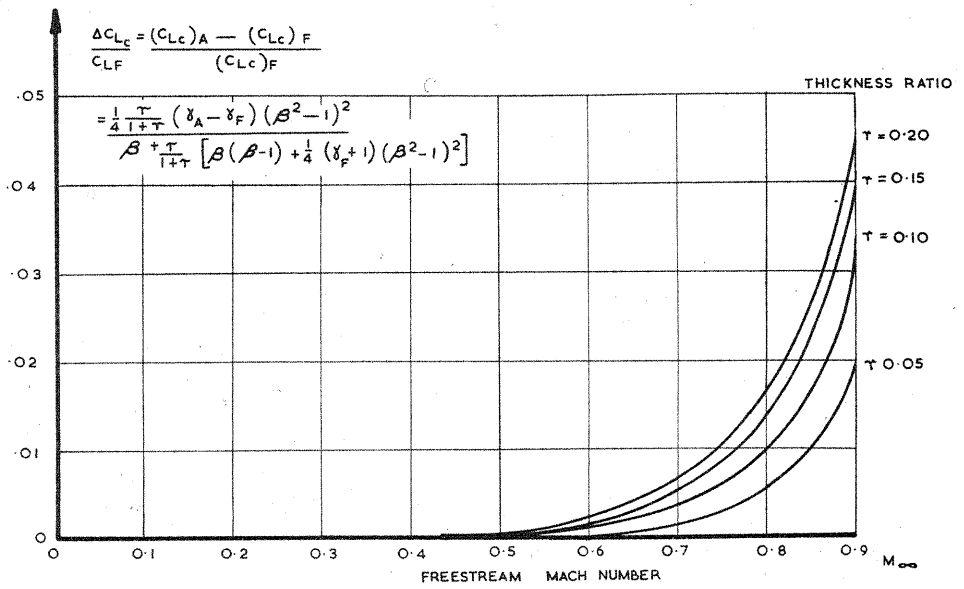

FIG.6 LIFT COEFFICIENT CORRECTIONS ON ELLIPTIC CYLINDERS DERIVED FROM KAPLAN RULES (REF. 25).

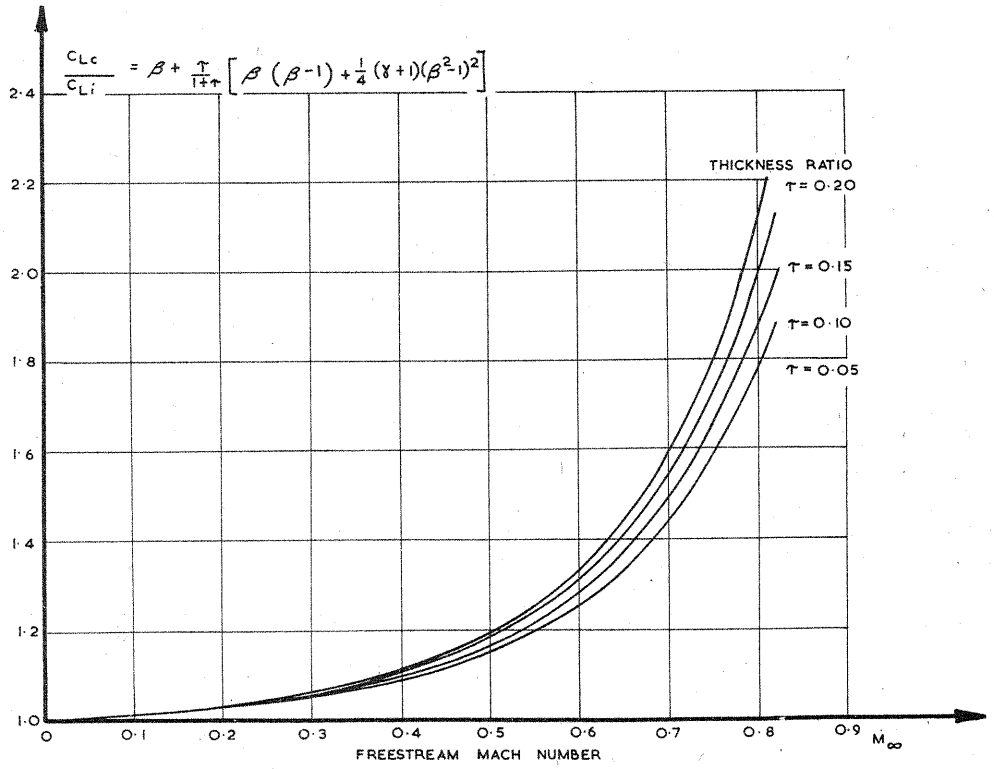

FIG.7 VARIATION OF THE LIFT COEFFICIENT ON AN ELLIPTIC CYLINDER WITH MACH NUMBER.

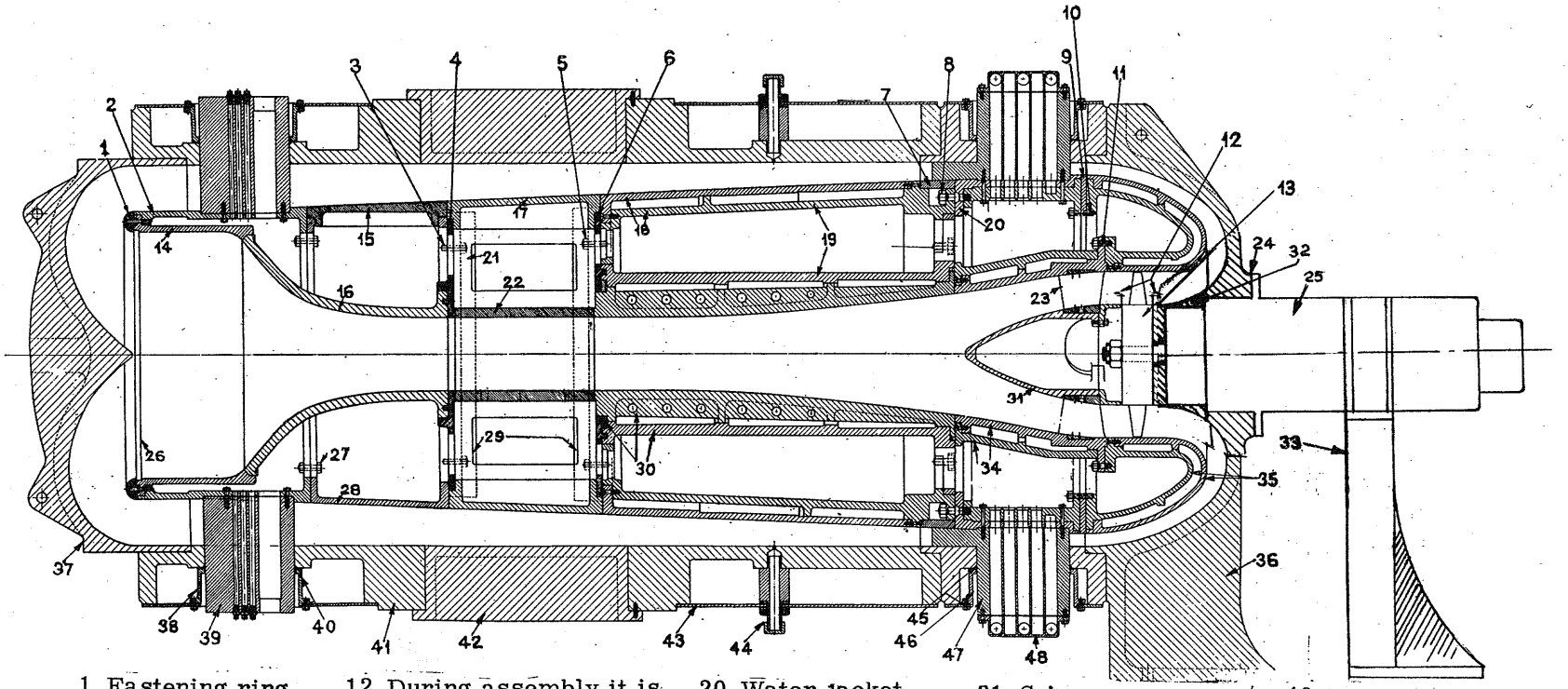

1. Fastening ring
2. Support section
3. Studs
4. End plate
5. Studs
6. End plate
7. Fastening ring
8. Studs
9. Joint plate
10. Studs
11. Studs
12. During assembly it is important that clearances of .03 in. are obtained.
13. Fan
14. Settling chamber
15. Manhole
16. Contraction cone
17. Outer cover
18. Outer casing & water jacket.
19. Casing
20. Water jacket
21. Working section
22. Inner covers
23. Guide vanes.
24. Seal
25. Drive motor
26. Honeycomb
27. Bolts
28. Casing
29. Fastening rings
30. Outer section & water jacket.
31. Spinner
32. Fairing
33. Drive support
34. Inner casing & water jacket.
35. Water jacket
36. Driving end cover
37. Cast iron end cover
38. Outer casing seal
39. Support
40. Rubber joints
41. Outer casing
42. Manhole cover
43. Outer casing water jacket
44. Alternative vacuum connection.
45. Rubber joints
46. Outer casing seal
47. Support
48. Header.

FIG. 8 MODEL HIGH SPEED WIND TUNNEL: DETAIL ARRANGEMENT OF INNER SHELL.

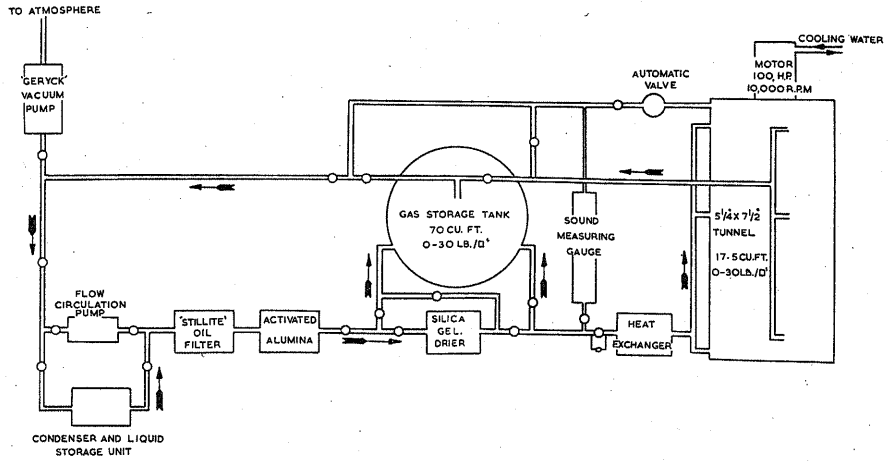

FIG. 9 DIAGRAMMATIC ARRANGEMENT OF FREON-12 TUNNEL AND ANCILLARY EQUIPMENT.

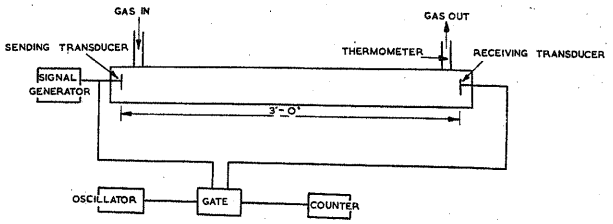

FIG. 10 SOUND MEASURING GAUGE

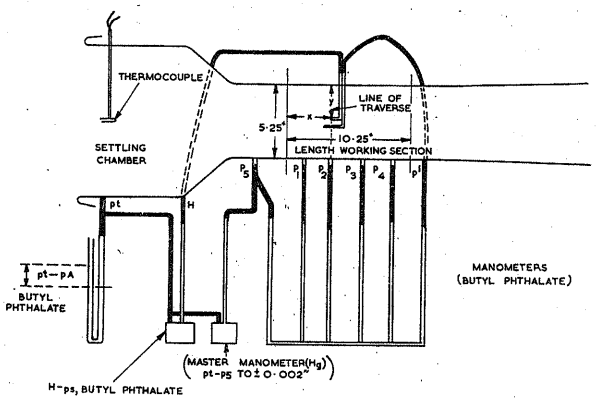

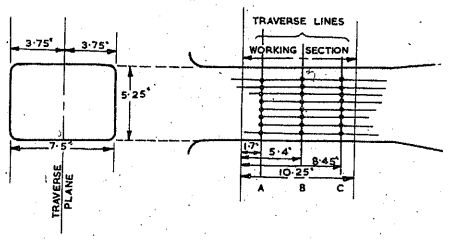

FIG. 11 DIAGRAMMATIC ARRANGEMENT OF MANOMETERS USED FOR THE WIND TUNNEL CALIBRATION.

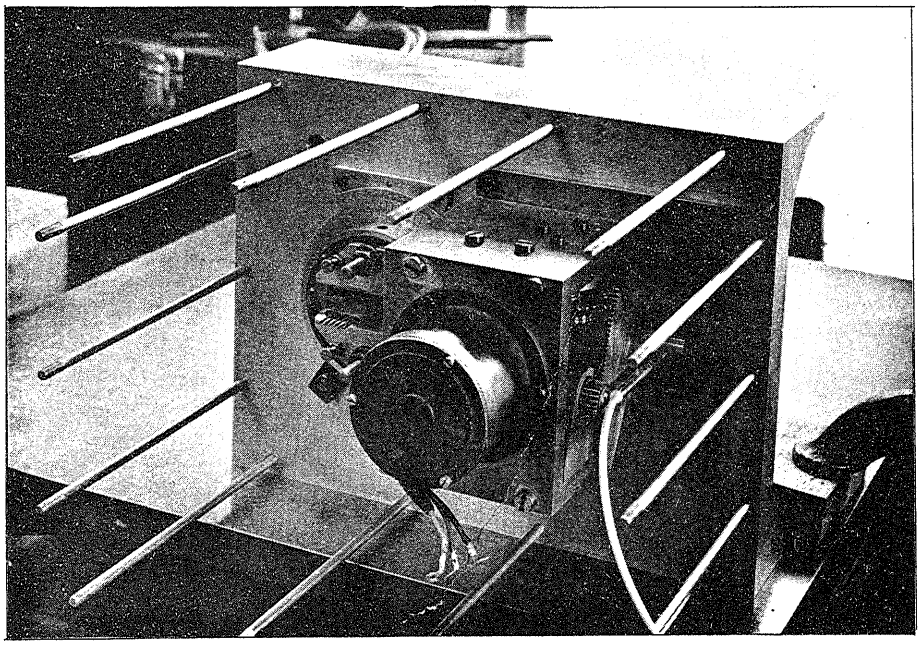

FIG. 12 TUNNEL WALL WITH TRAVERSING GAUGE.

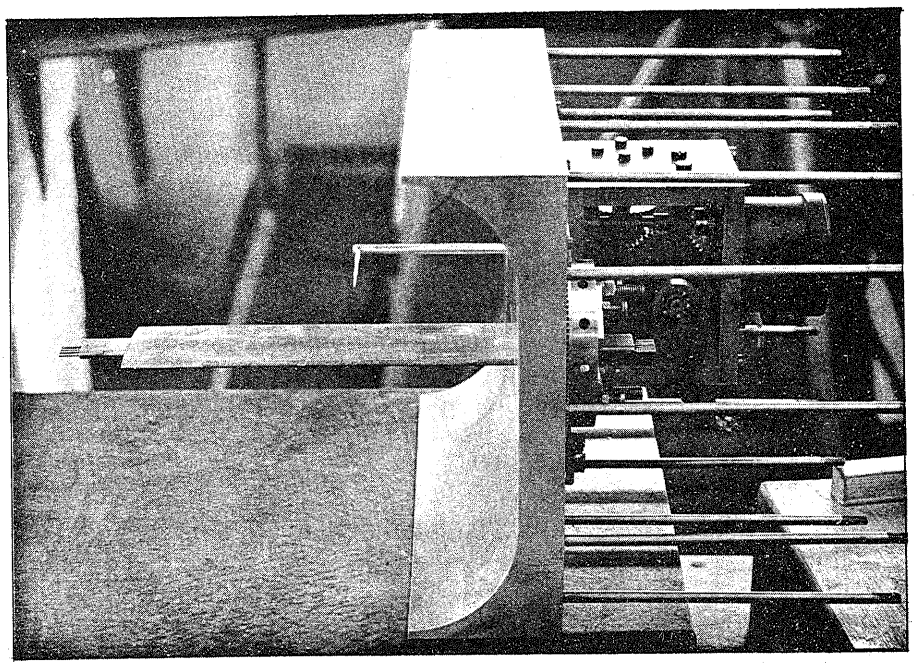

FIG. 13 TUNNEL WALL WITH TRAVERSING GAUGE AND 2-DIMENSIONAL WING MODEL.

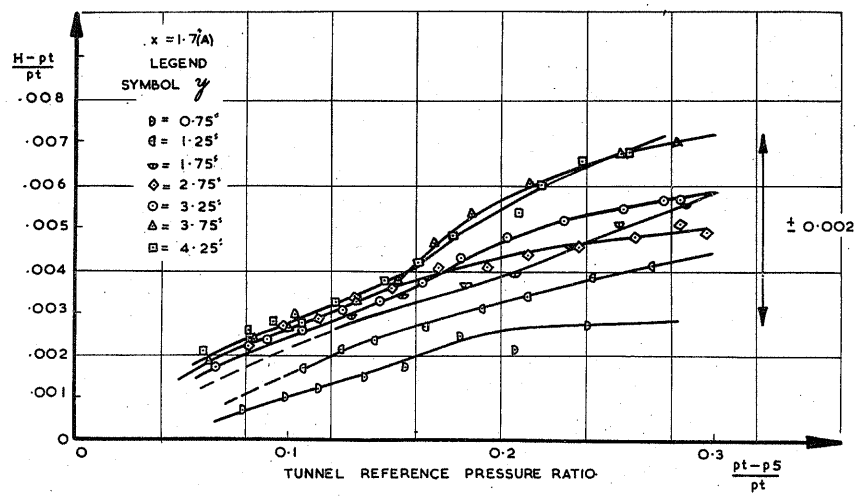

FIG. 14

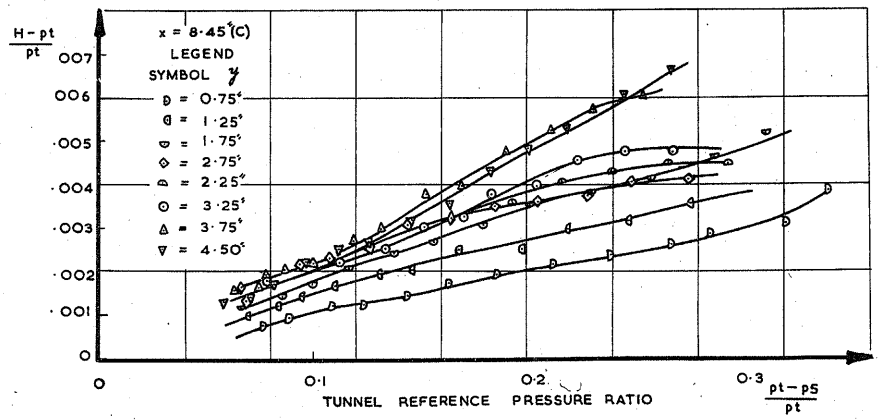

FIG. 15

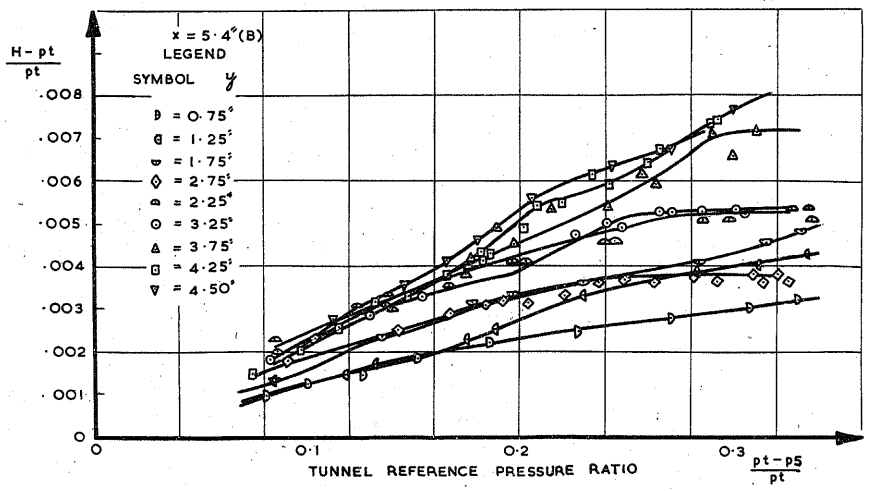

FIG. 16

TUNNEL CALIBRATION: VARIATION OF TOTAL HEAD IN WORKING SECTION WITH VELOCITY.

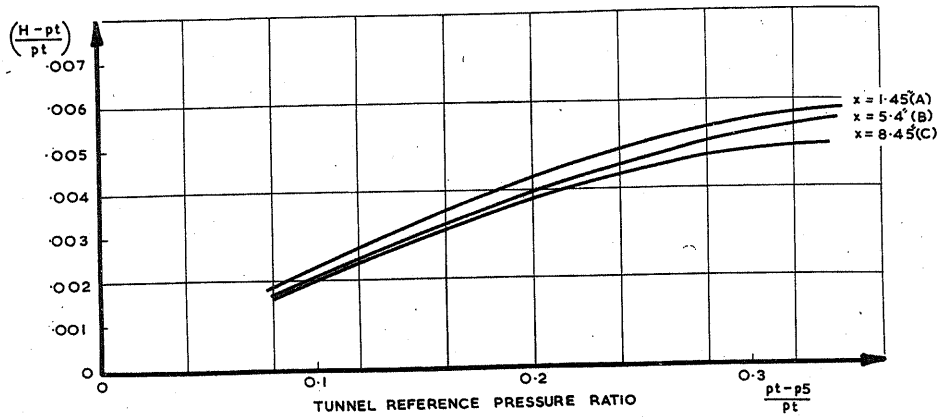

FIG. 17

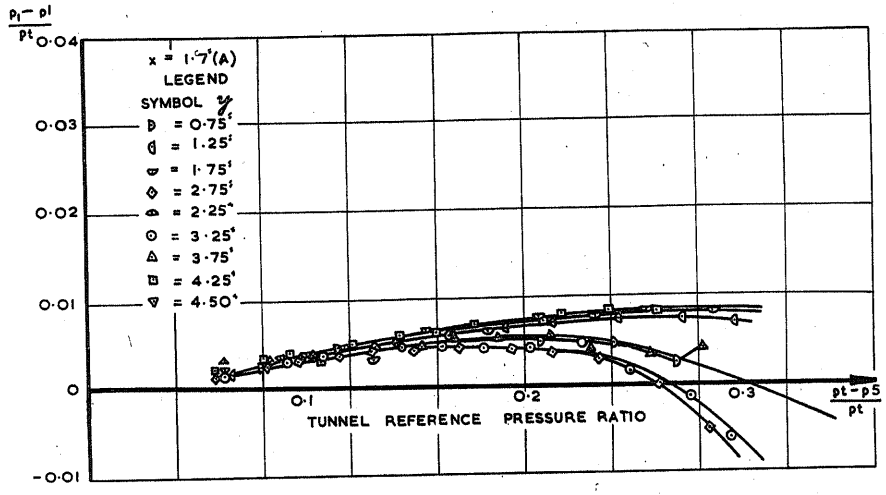

FIG. 18

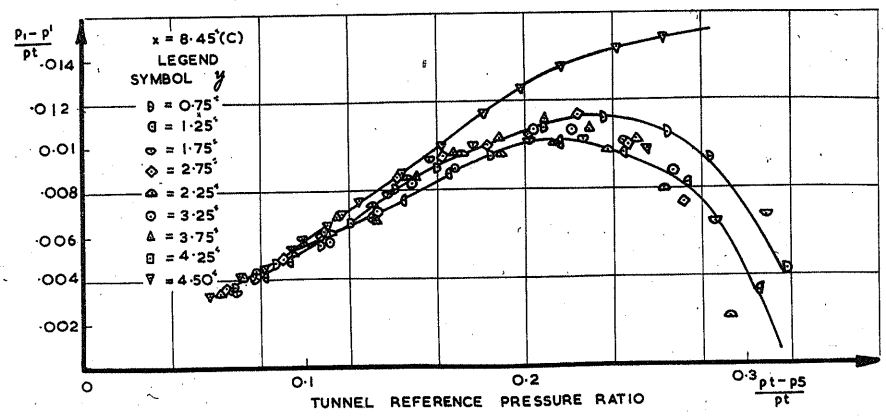

FIG. 19

TUNNEL CALIBRATION: VARIATION OF AVERAGE TOTAL HEAD ACROSS THE WORKING SECTION WITH VELOCITY.

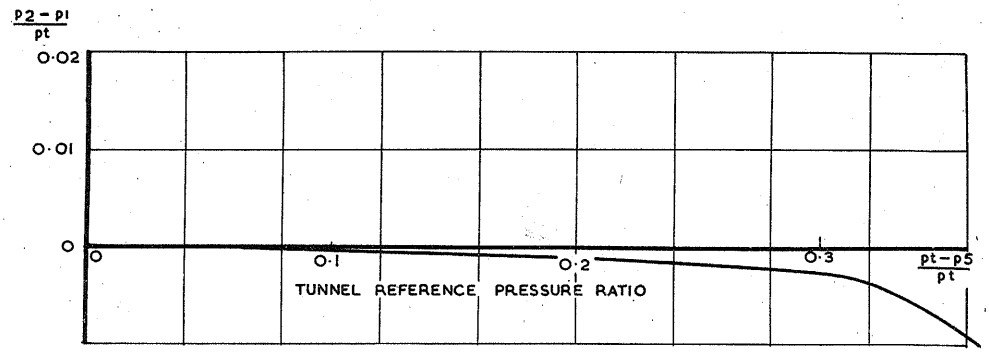

FIG. 20

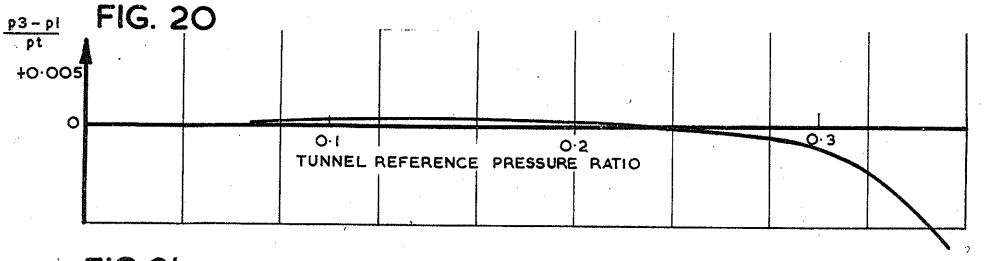

FIG. 21

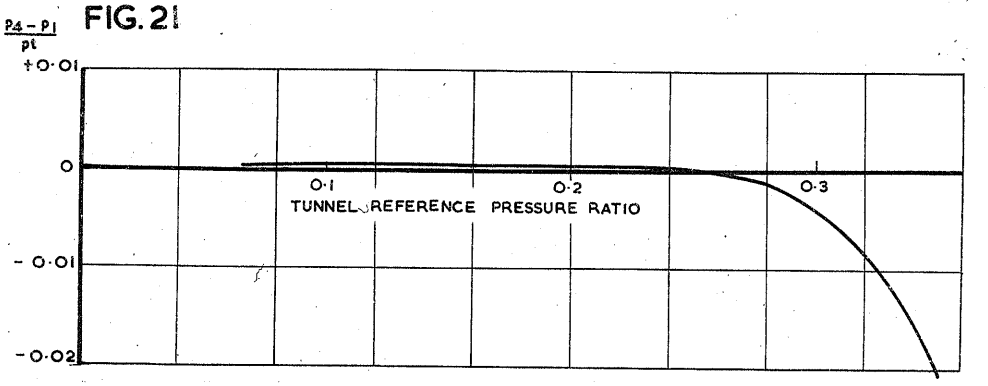

FIG. 22

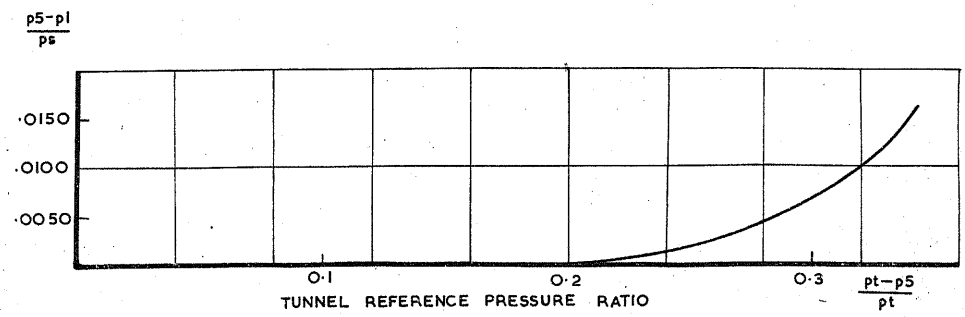

FIG. 23

TUNNEL CALIBRATION: VARIATION OF STATIC PRESSURE ALONG THE WORKING SECTIONS AT DIFFERENT TUNNEL VELOCITIES.

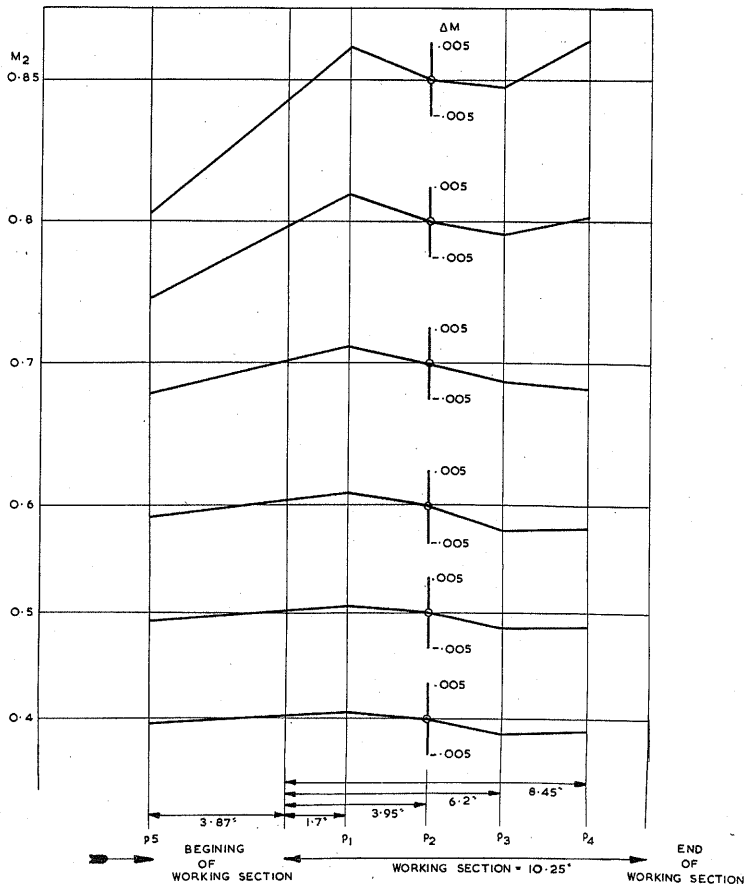

FIG. 24 TUNNEL CALIBRATION: VARIATION OF MACH NUMBER ALONG WORKING SECTION.

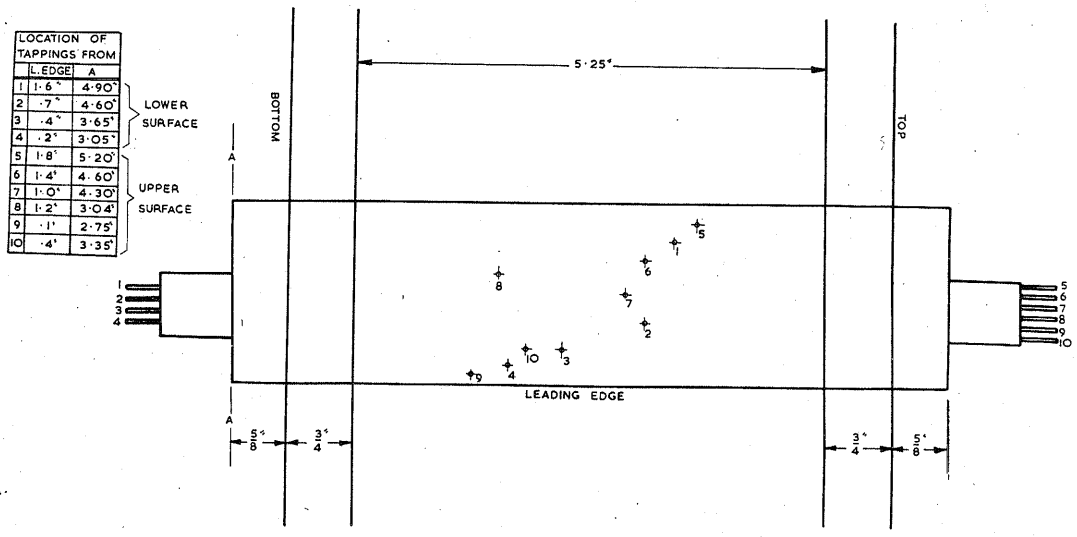

FIG. 25 POSITIONS OF THE PRESSURE HOLES IN THE 2 IN. CHORD AEROFOIL.
(R.A.E. 104 – 10% SYMMETRICAL)

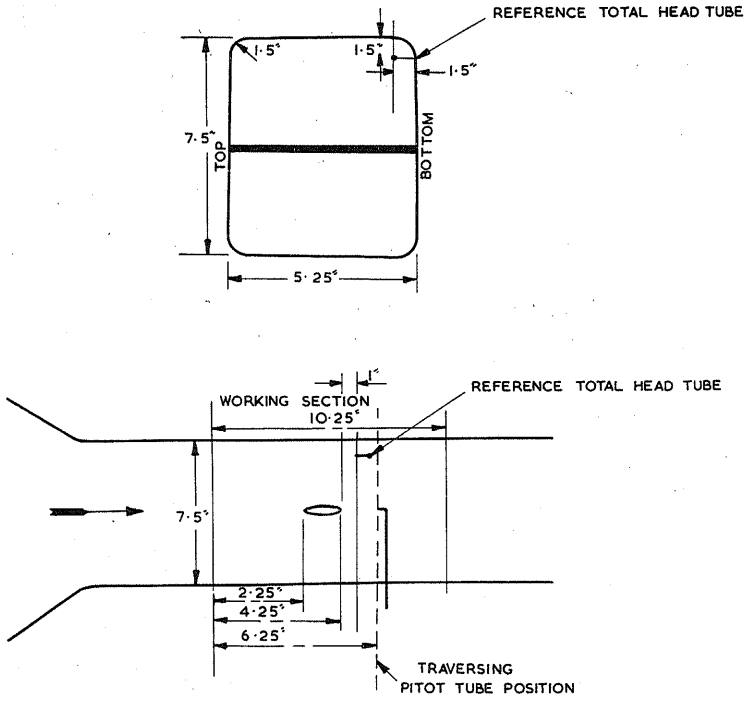

FIG. 26 POSITION OF THE R.A.E. 104 – 10% SYMMETRICAL AEROFOIL IN THE WORKING SECTION.

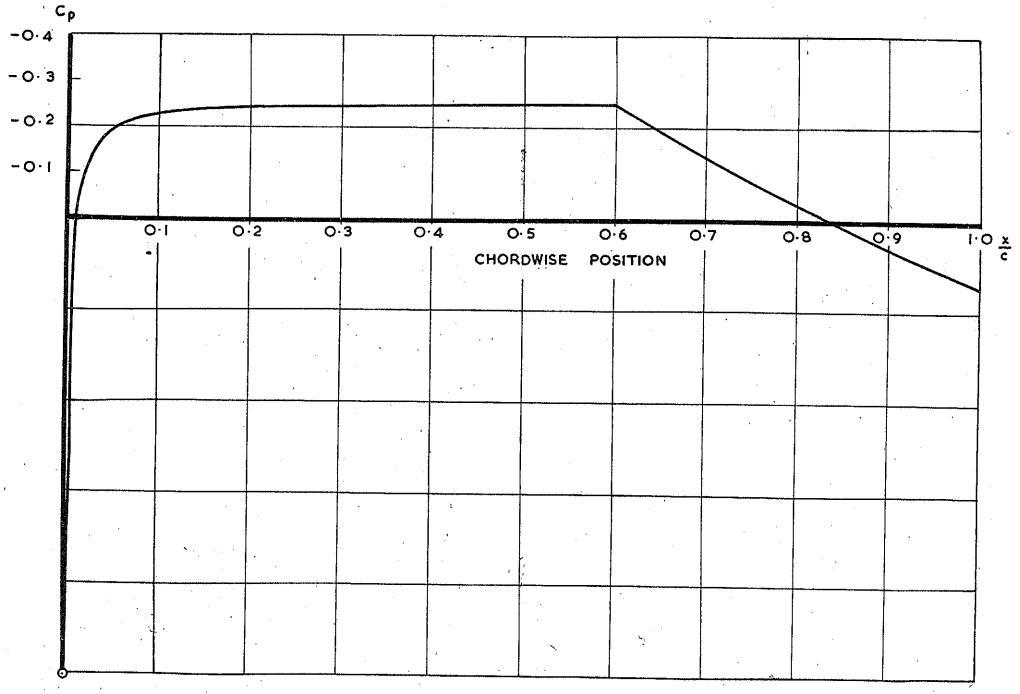

FIG. 27 CALCULATED PRESSURE DISTRIBUTION ON THE R.A.E. 104 – 10% SYMMETRICAL SECTION.

$\alpha = 0°$

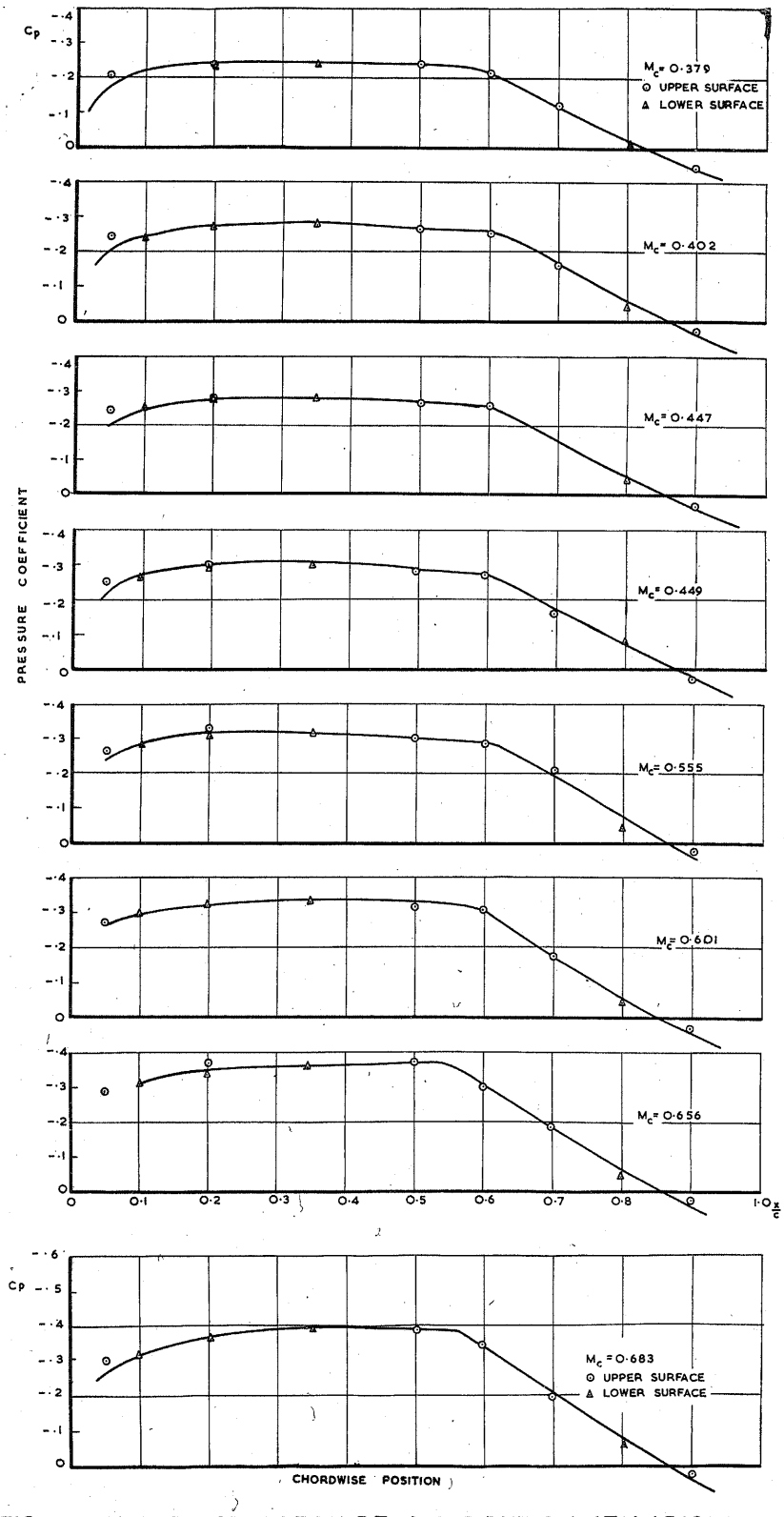

FIG. 28 CHORDWISE PRESSURE DISTRIBUTION AT VARIOUS MACH NUMBERS ON THE R.A.E. 104 - 10% SYMMETRICAL SECTION IN FREON - 12. $\alpha = 0^\circ$

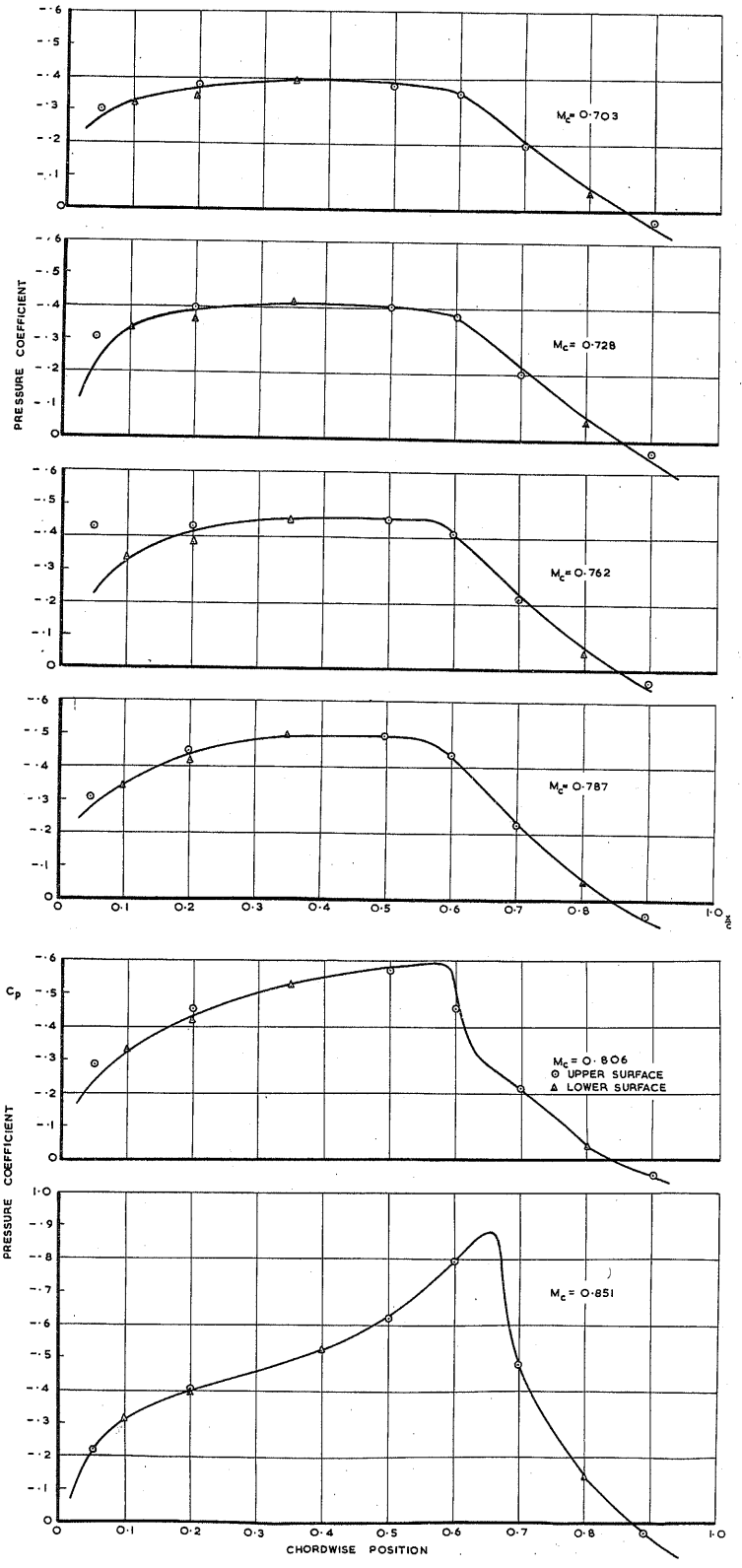

FIG. 28 (CONT.) CHORDWISE PRESSURE DISTRIBUTION AT VARIOUS MACH NUMBERS ON THE R.A.E. 104 - 10% SYMMETRICAL SECTION IN FREON-12. $\alpha = 0°$

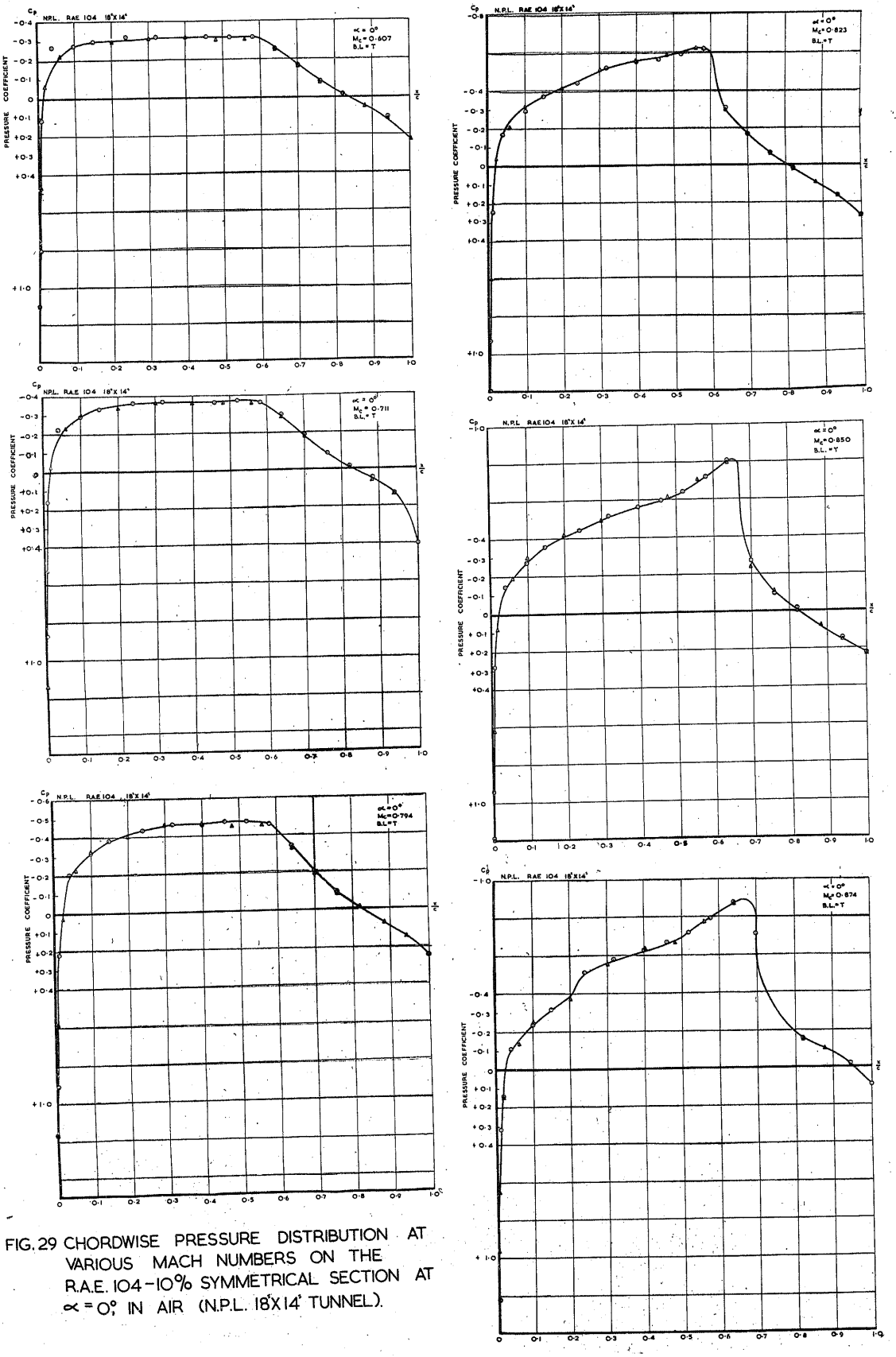

FIG. 29 CHORDWISE PRESSURE DISTRIBUTION AT VARIOUS MACH NUMBERS ON THE R.A.E. 104 – 10% SYMMETRICAL SECTION AT $\alpha = 0°$ IN AIR (N.P.L. 18"X14" TUNNEL).

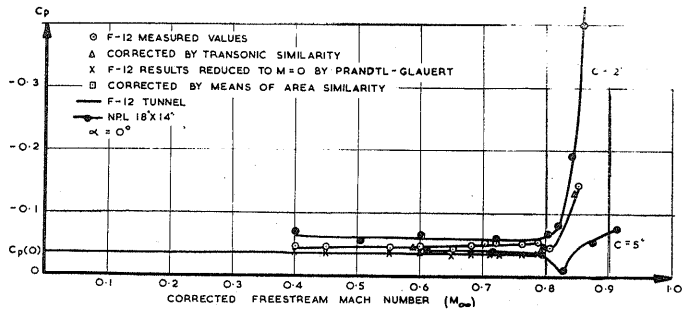

FIG. 30

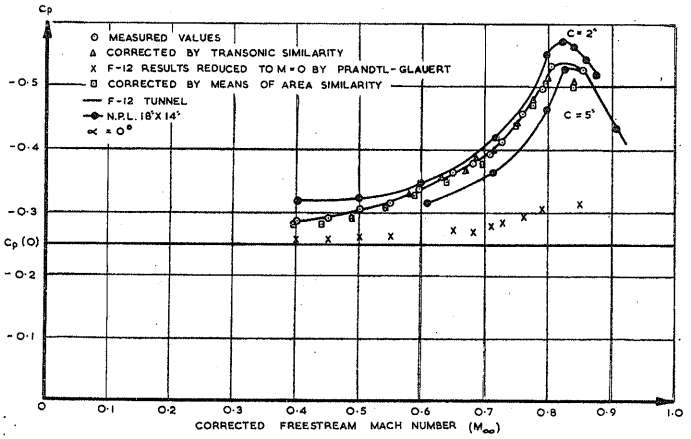

FIG. 31

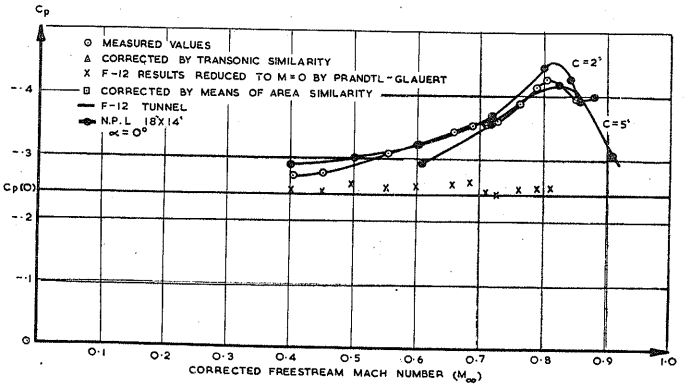

FIG. 32

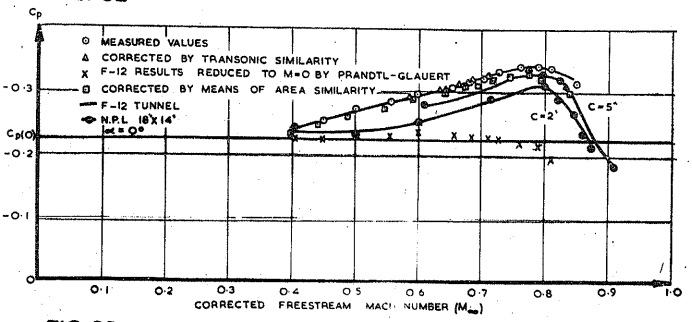

FIG. 33

COMPARISON BETWEEN THE PRESSURE COEFFICIENTS IN AIR AND FREON-12 AT HOLES 1, 2, 3, 4.

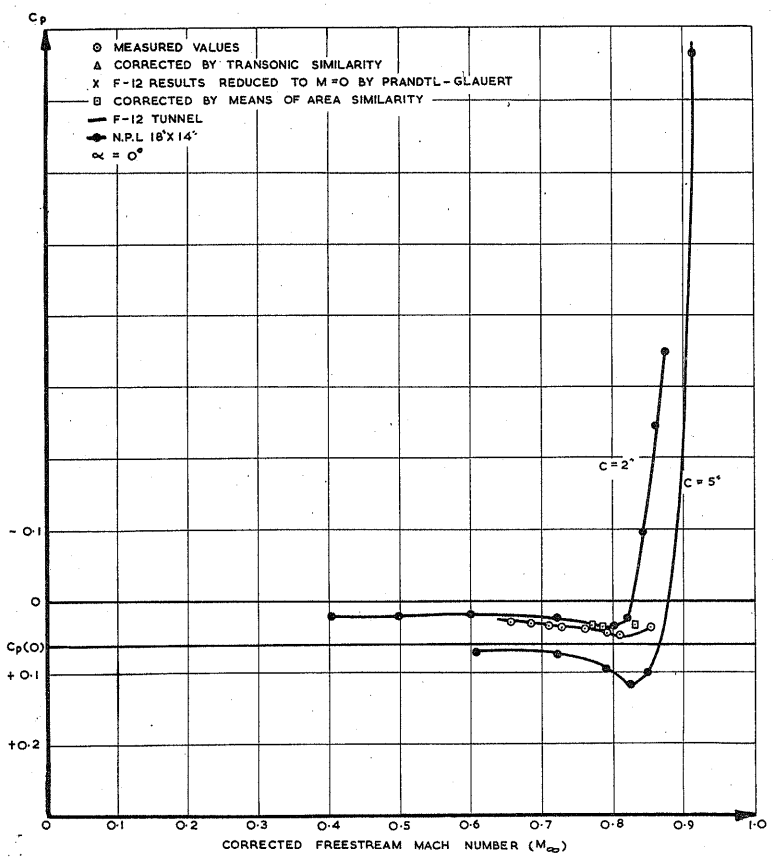

FIG. 34

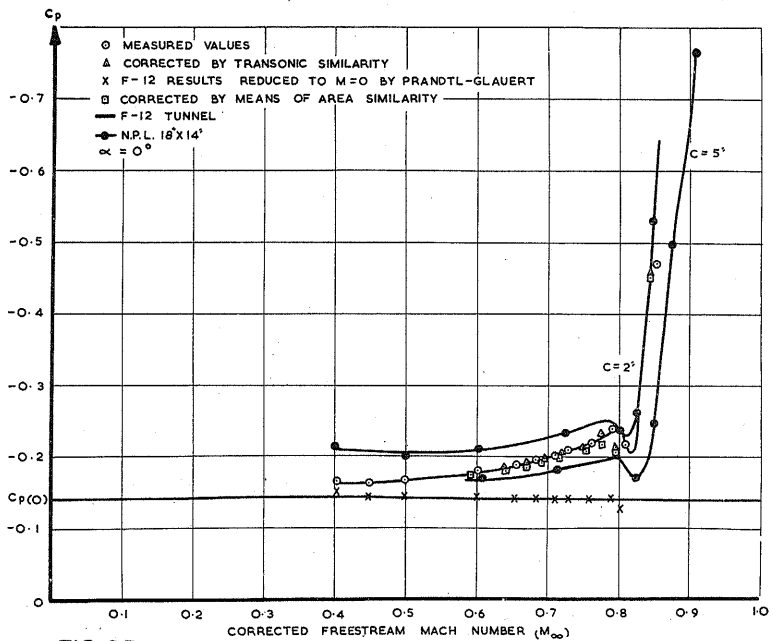

FIG. 35

COMPARISON BETWEEN THE PRESSURE COEFFICIENTS IN AIR AND FREON-12 AT HOLES 5, 6.

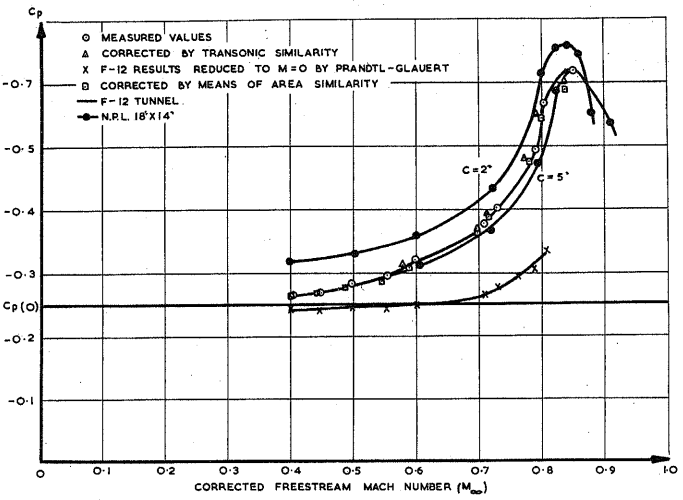

FIG. 36

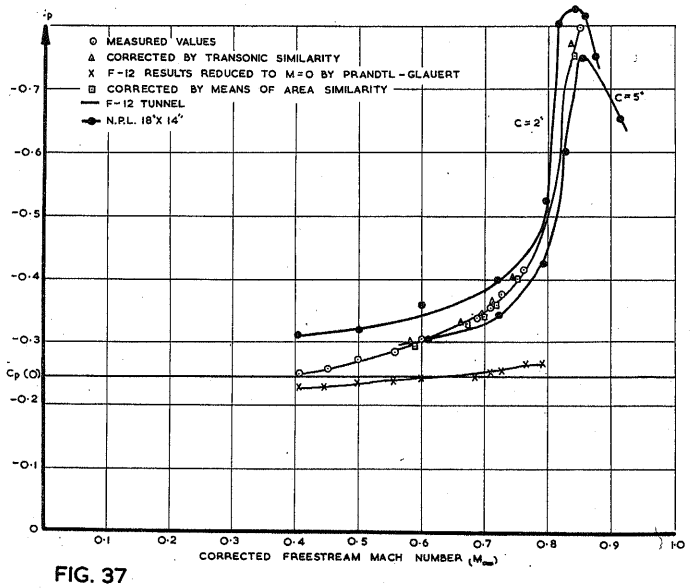

FIG. 37

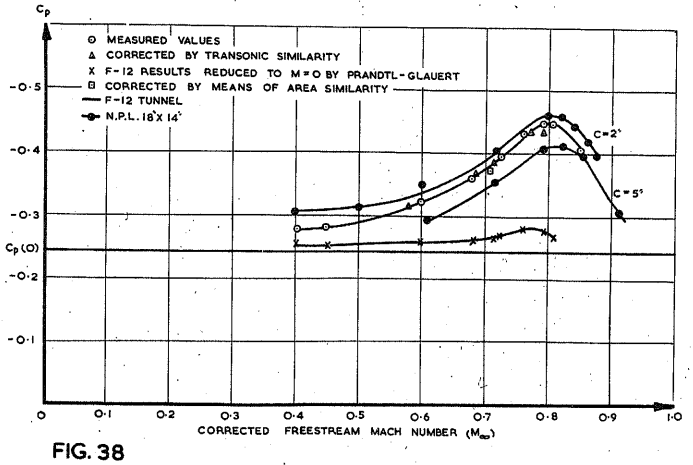

FIG. 38

COMPARISON BETWEEN THE PRESSURE COEFFICIENTS IN AIR AND FREON-12 AT HOLES 7, 8, 10.

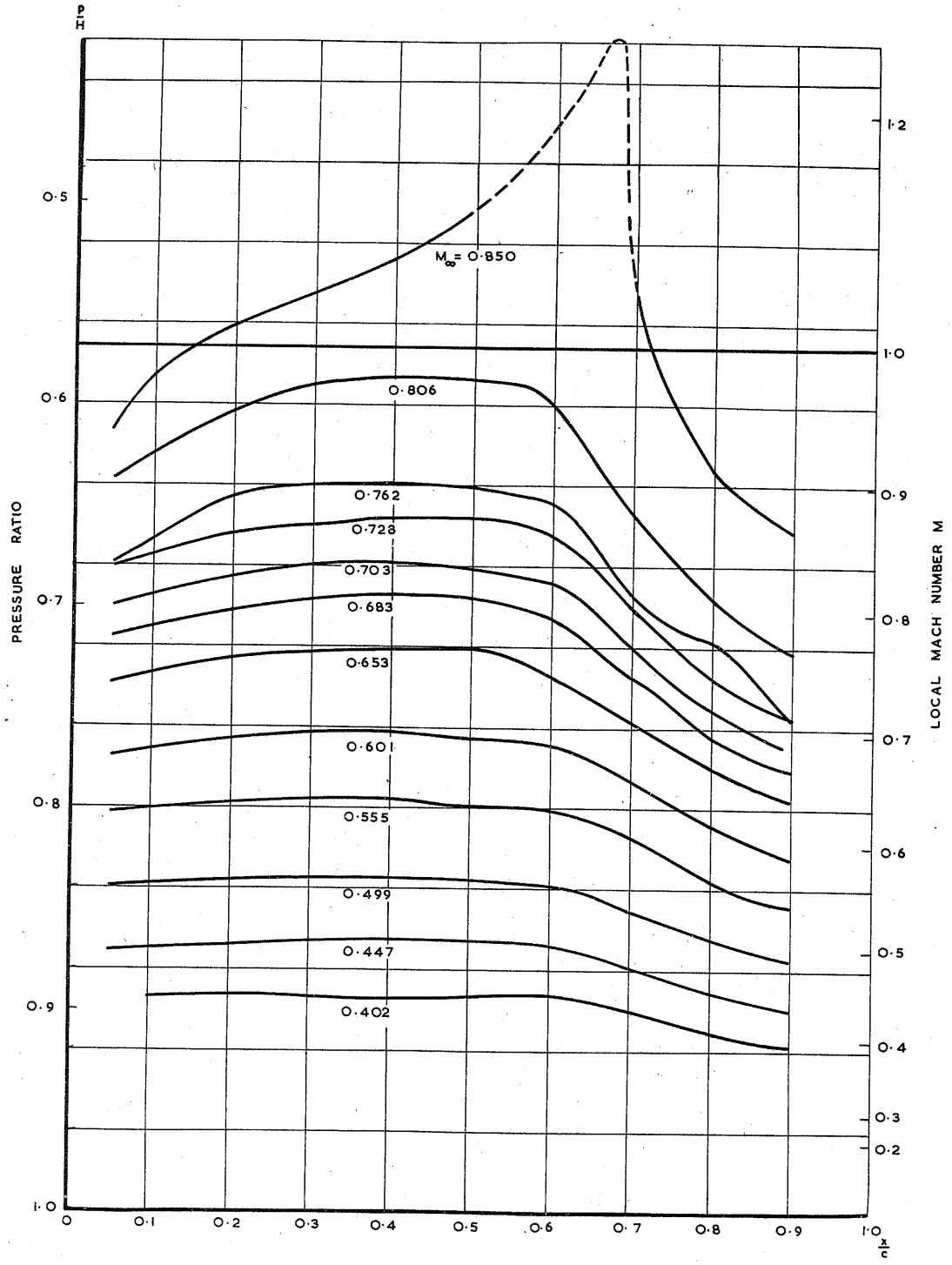

FIG. 39 CHORDWISE PRESSURE DISTRIBUTIONS AT VARIOUS MACH NUMBERS IN FREON-12 ON R.A.E. 104 - 10% SYMMETRICAL AEROFOIL.

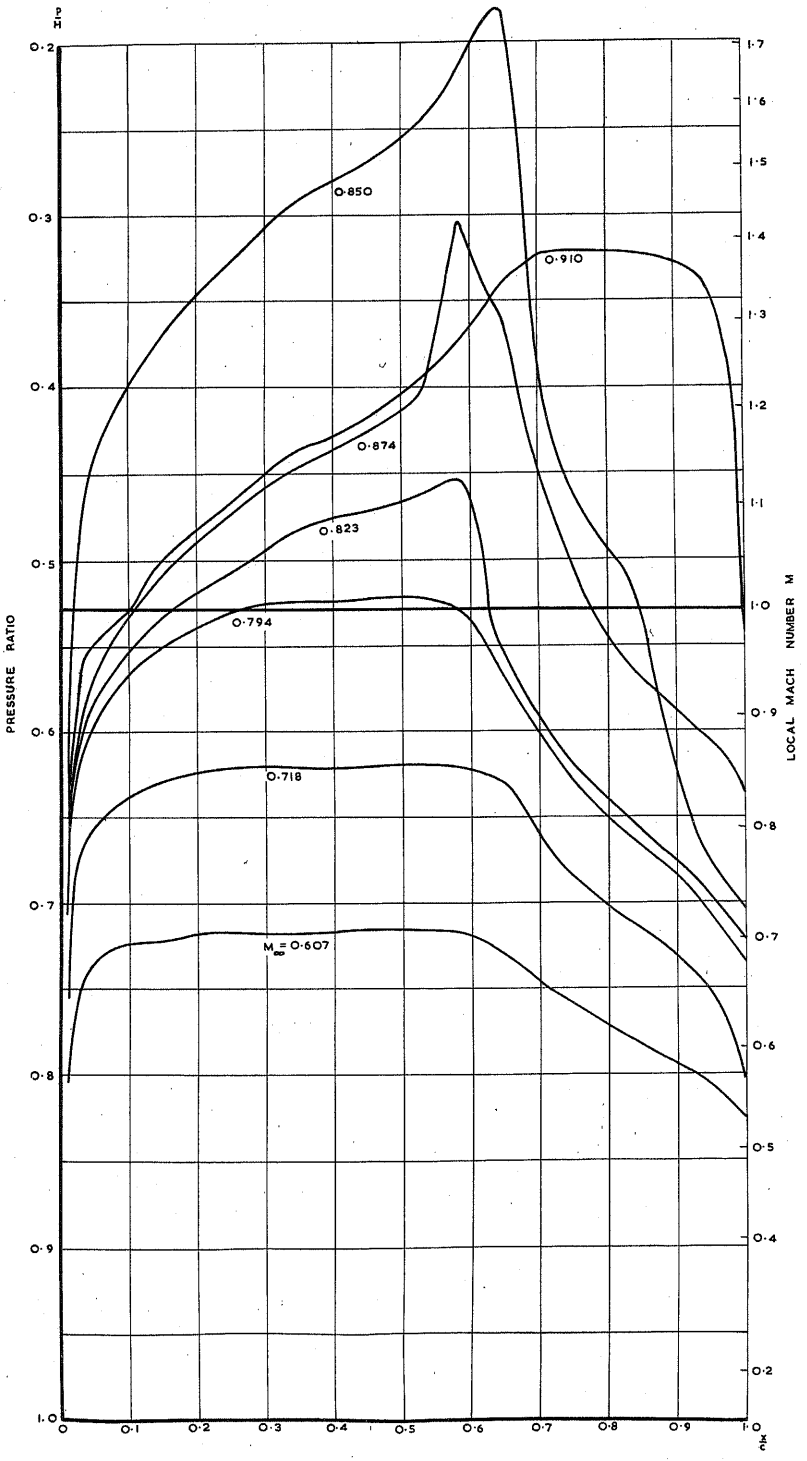

FIG. 40 CHORDWISE PRESSURE DISTRIBUTION AT VARIOUS MACH NUMBERS ON THE R.A.E. 104–10% SYMMETRICAL 5 IN. CHORD MODEL. N.P.L. MEASUREMENTS IN 18" X 14" TUNNEL.

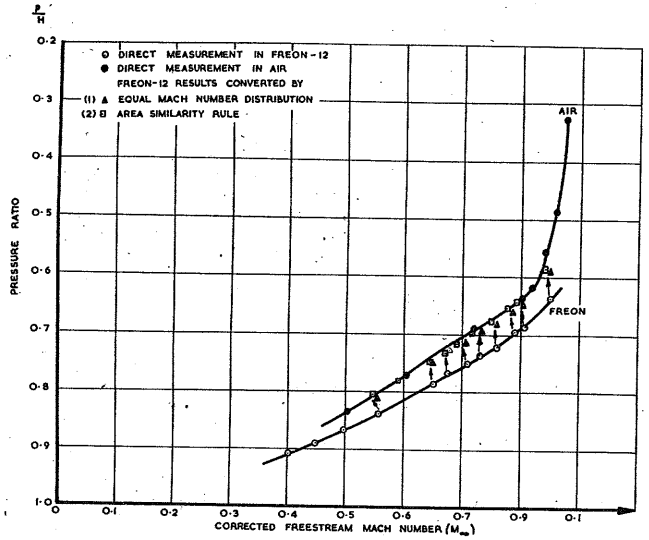

FIG. 41

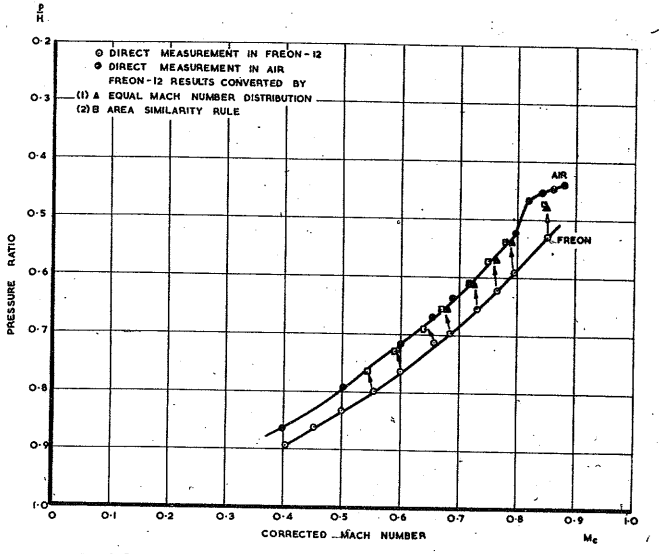

FIG. 42

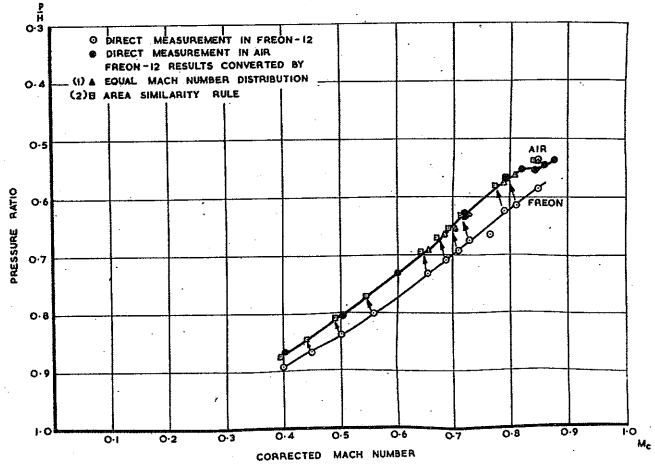

FIG. 43

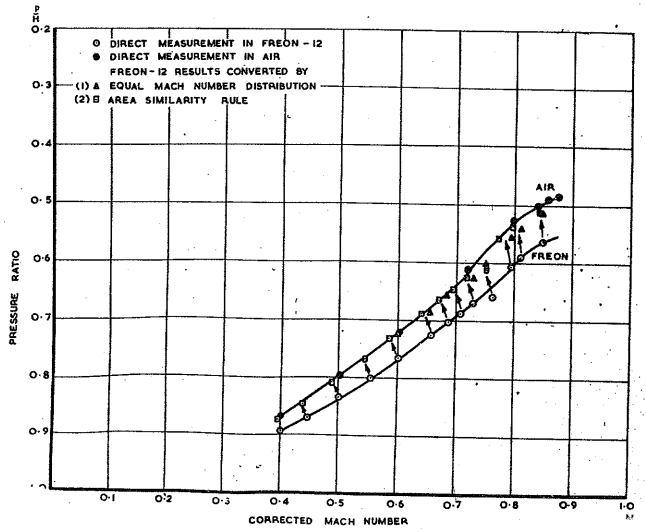

FIG. 44

COMPARISON BETWEEN THE PRESSURE DISTRIBUTION IN AIR AND FREON-12 AT HOLES 1, 2, 3, 4.

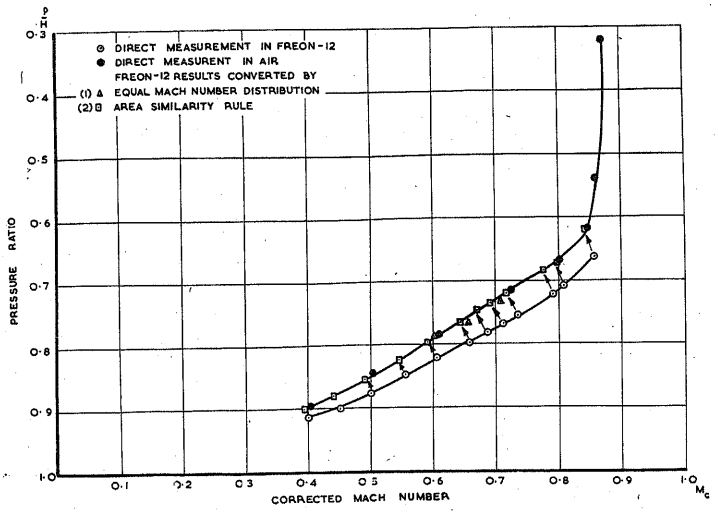

FIG. 45

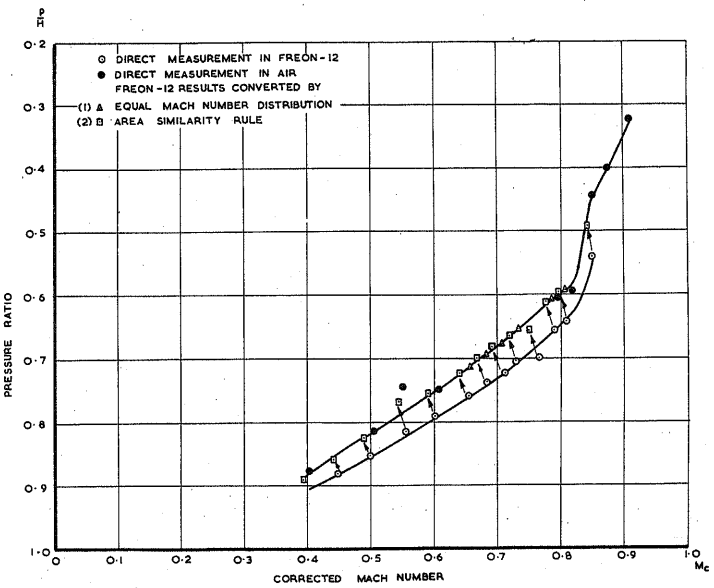

FIG. 46

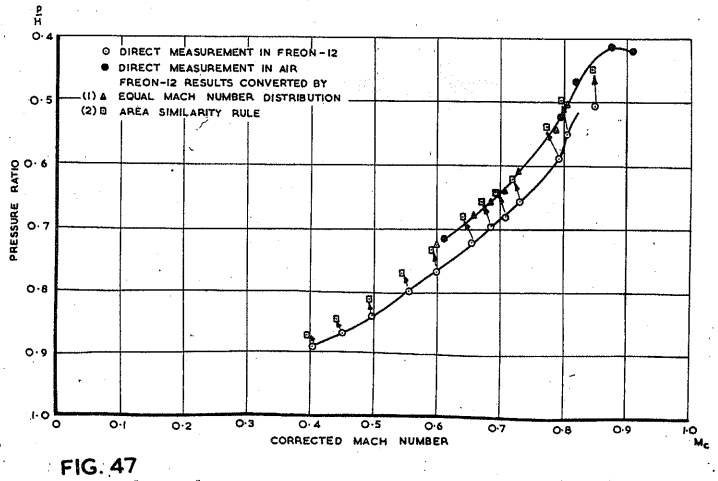

FIG. 47

COMPARISON BETWEEN THE PRESSURE DISTRIBUTION IN AIR AND FREON-12 AT HOLES 5, 6, 7.

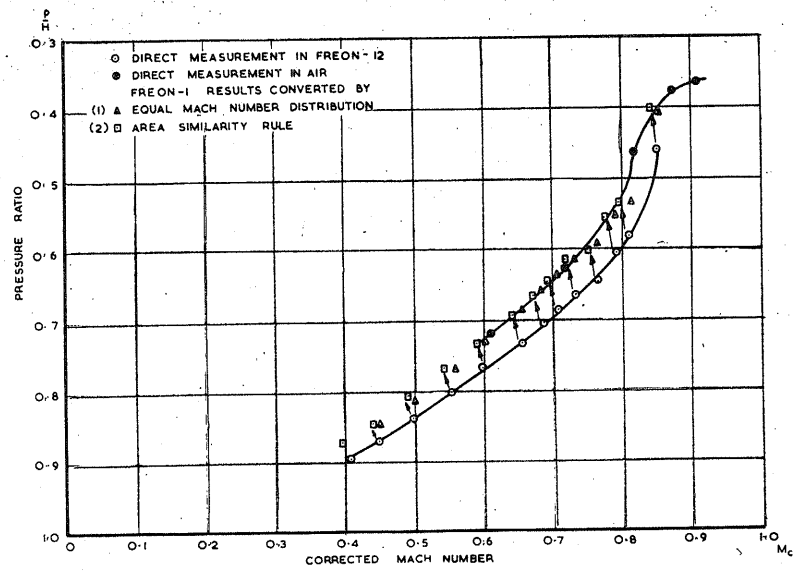

FIG. 48

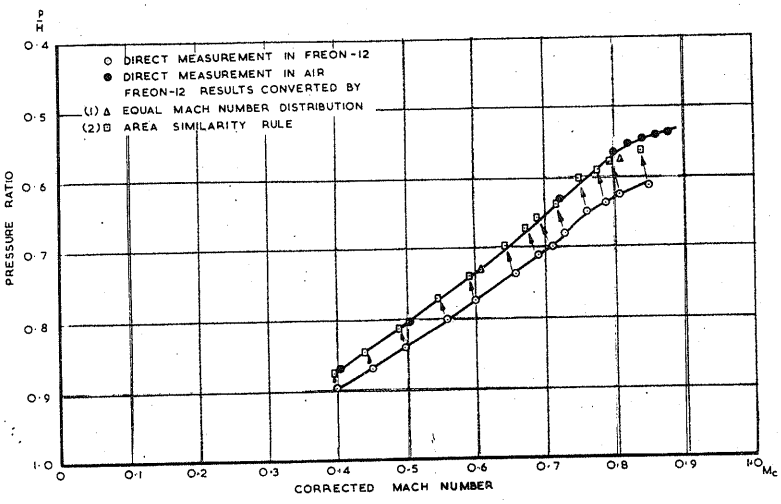

FIG. 49

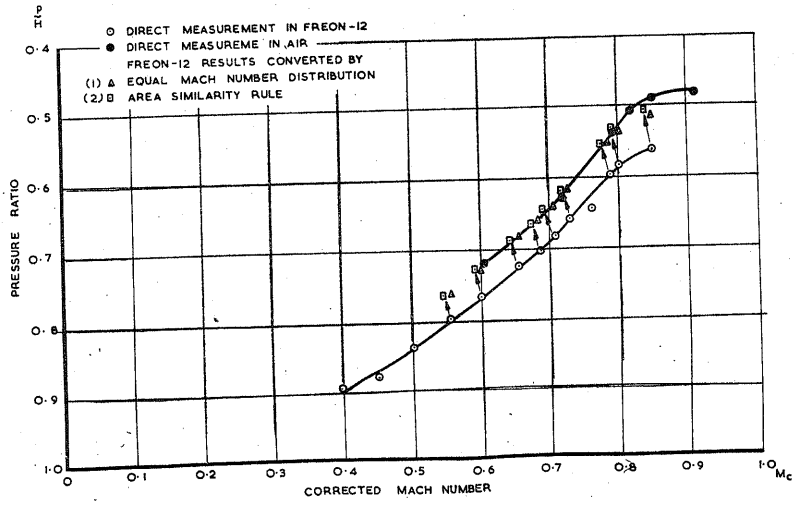

FIG.50
COMPARISON BETWEEN THE PRESSURE DISTRIBUTION IN AIR AND FREON-12 AT HOLES 8, 9, 10.

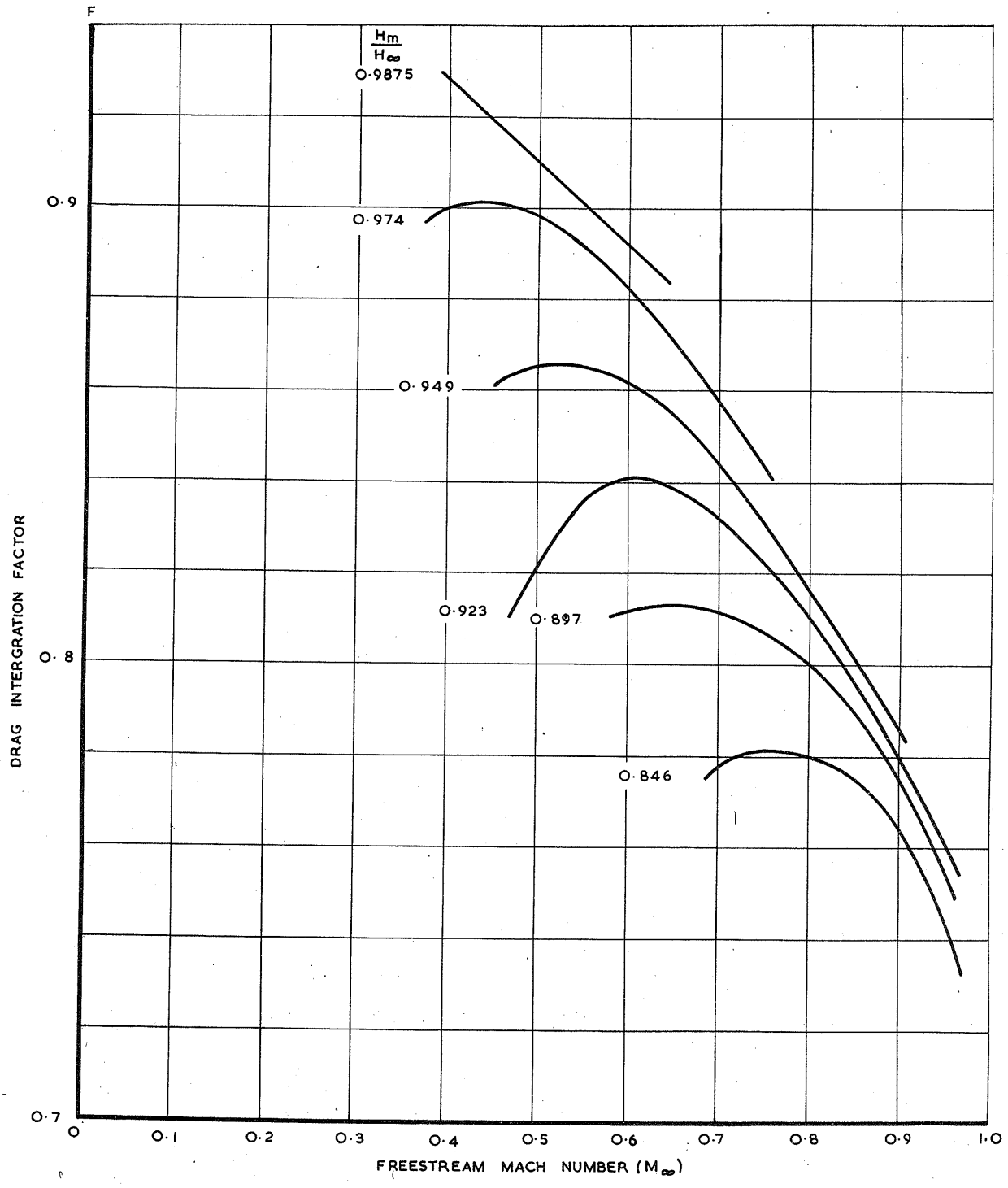

FIG. 51 VARIATION OF THE DRAG INTEGRATION FACTOR F WITH M_∞ AND THE MINIMUM TOTAL HEAD RATIO.

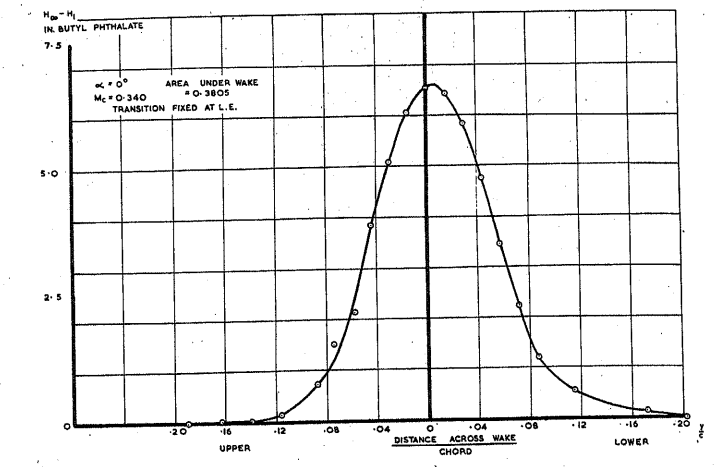

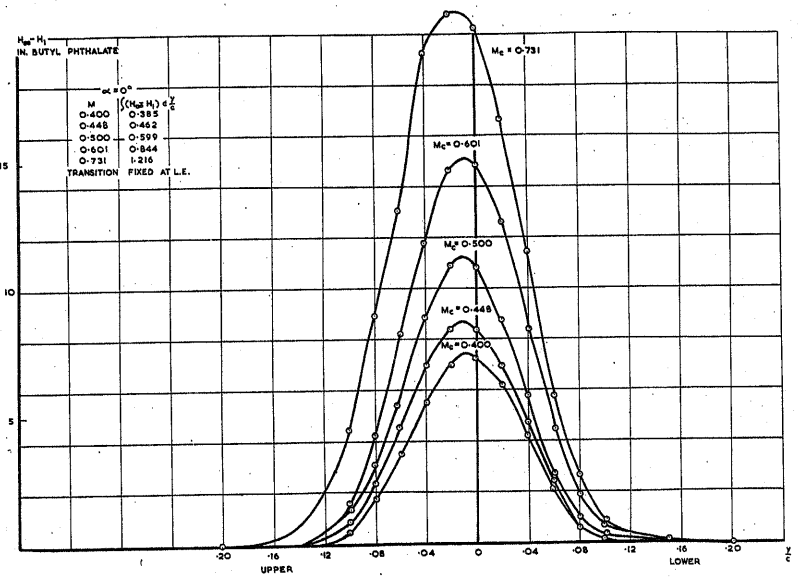

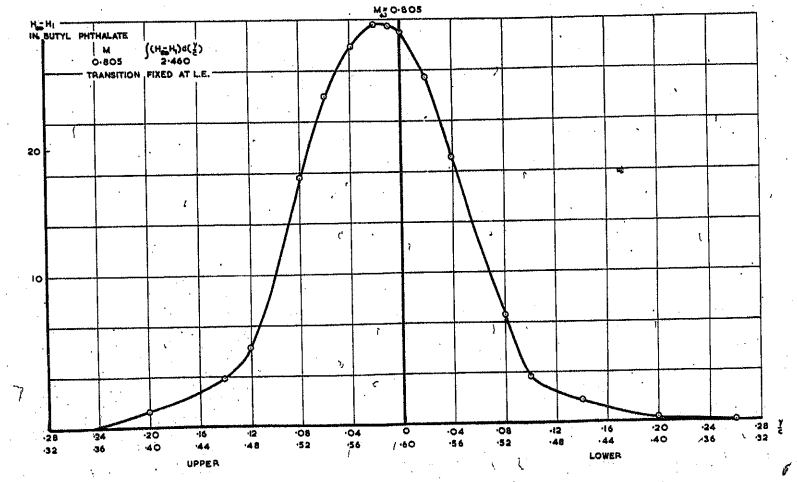

FIG. 52 VARIATION OF TOTAL HEAD IN WAKE OF R.A.E. 104–10% AEROFOIL AT VARIOUS FREE-STREAM MACH NUMBERS WITH TRANSITION FIXED. $\alpha = 0°$

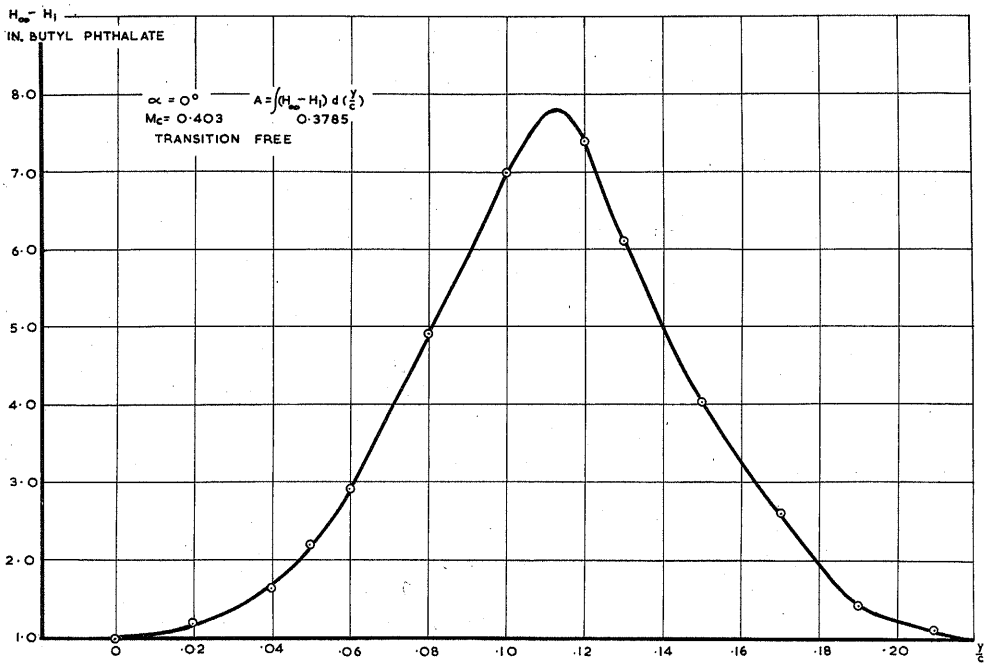

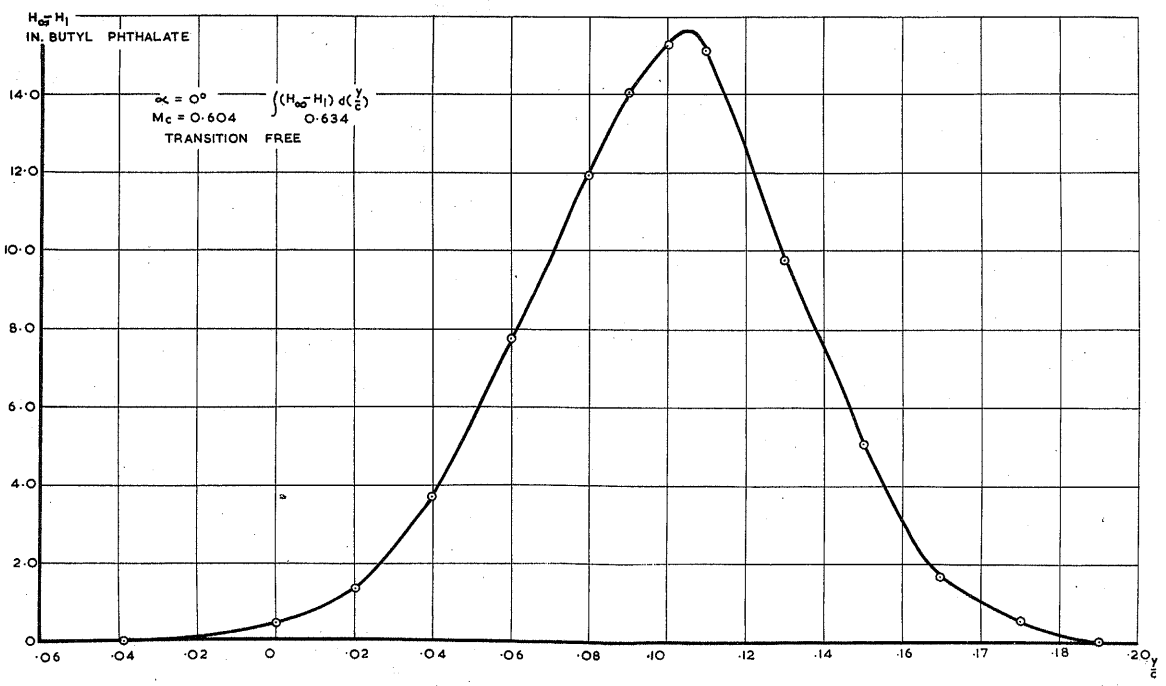

FIG. 53 VARIATION OF TOTAL HEAD IN WAKE OF R.A.E. 104 – 10% AEROFOIL AT VARIOUS MACH NUMBERS WITH FREE TRANSITION, $\alpha = 0°$

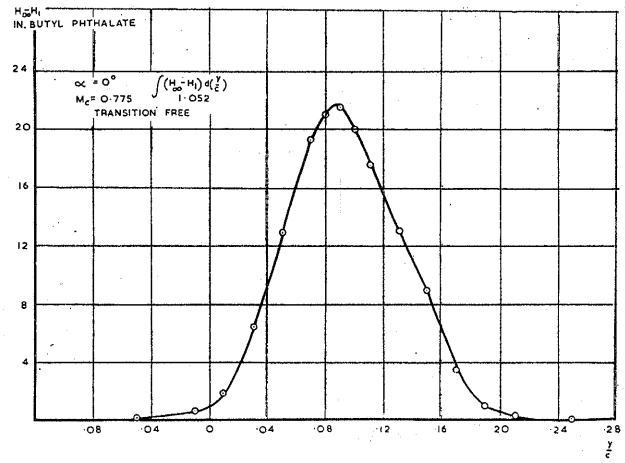

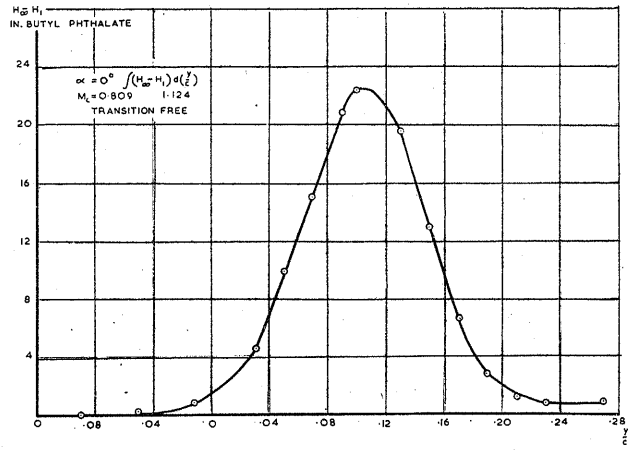

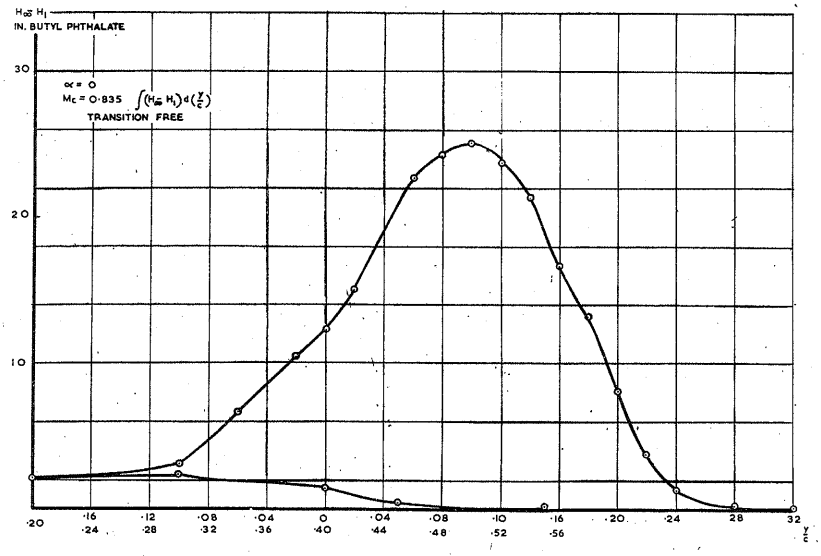

FIG. 53(CONT.) VARIATION OF TOTAL HEAD IN WAKE OF R.A.E. 104 – 10% AEROFOIL AT VARIOUS MACH NUMBERS WITH FREE TRANSITION, $\alpha = 0$.

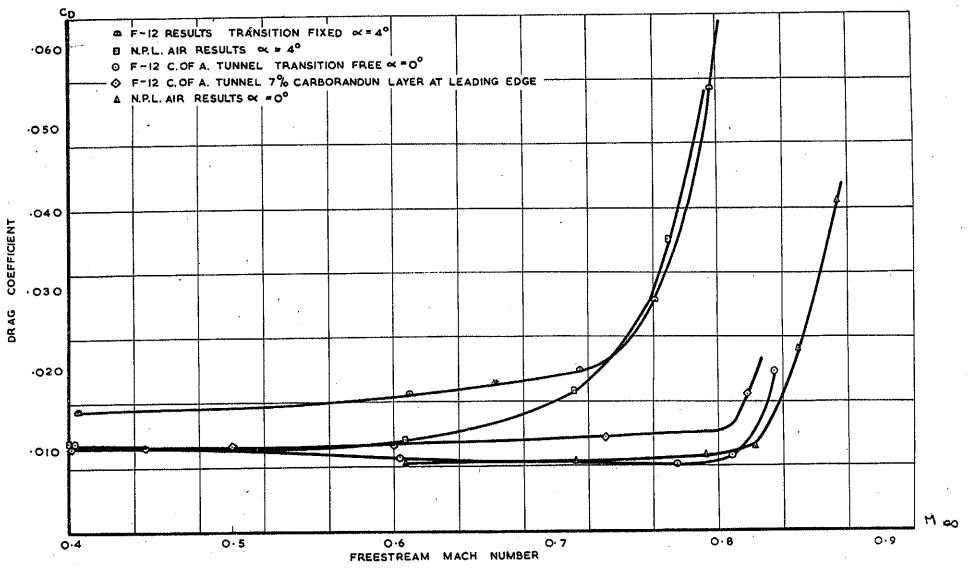

FIG. 54 VARIATION OF DRAG COEFFICIENT WITH MACH NUMBER FROM WAKE DRAG MEASUREMENTS IN AIR AND FREON-12, $\alpha = 0$ AND $4°$.

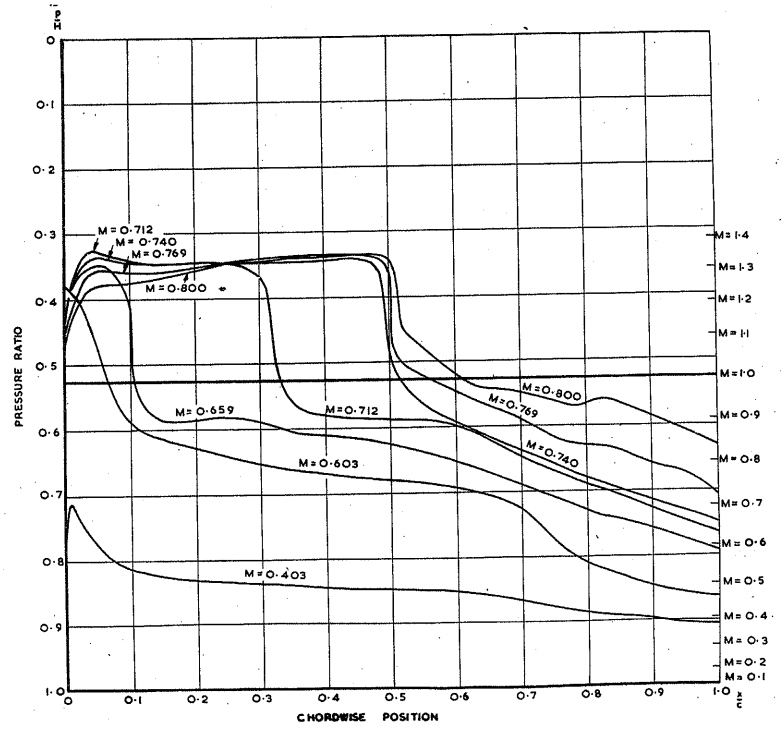

FIG. 55 VARIATION OF CHORDWISE PRESSURE DISTRIBUTION AT VARIOUS MACH NUMBERS, $\alpha = 4°$ IN AIR (5 IN. CHORD MODEL IN 18" X 14" TUNNEL). UPPER SURFACE, TRANSITION FIXED.

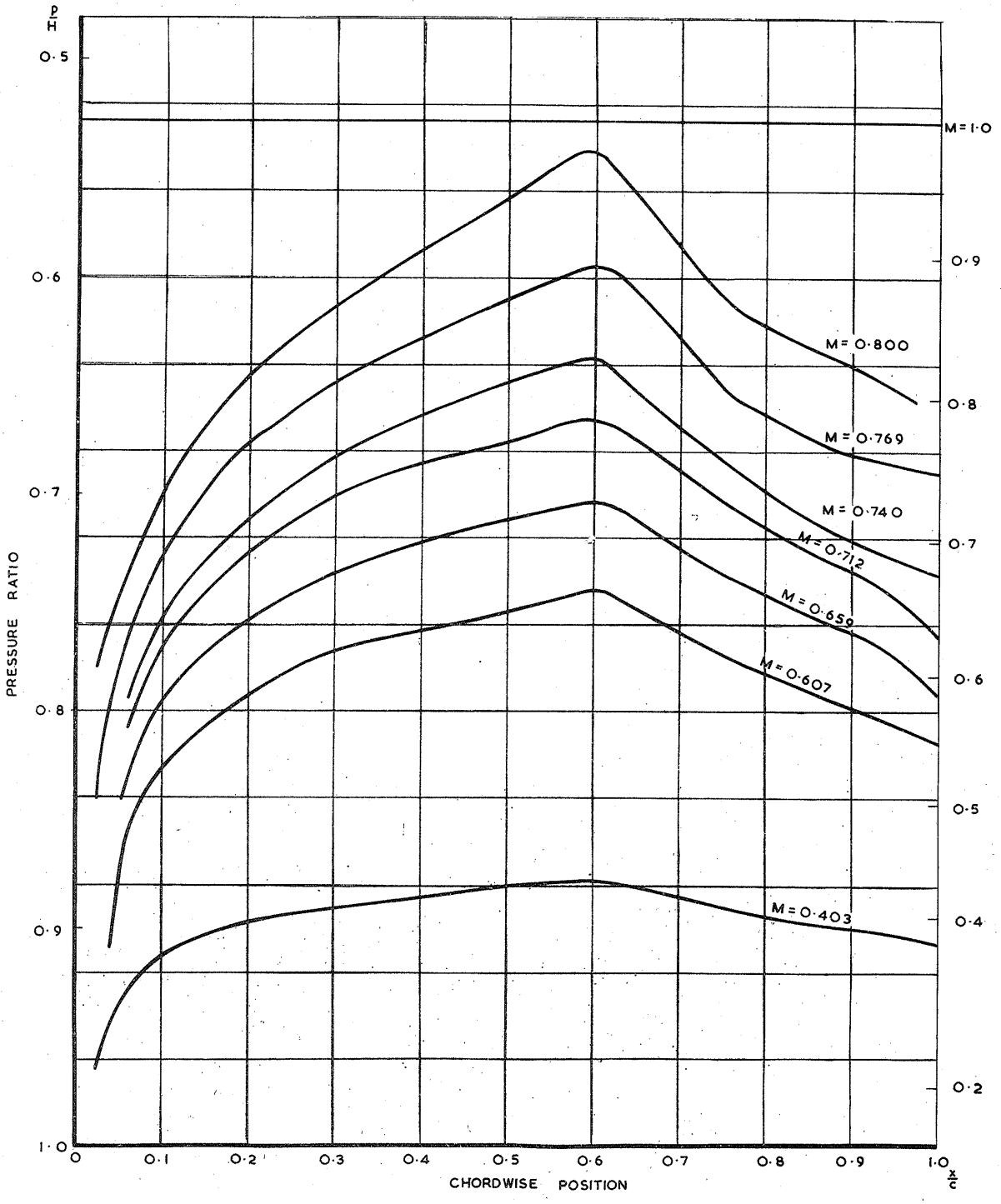

FIG. 56 VARIATION OF CHORDWISE PRESSURE DISTRIBUTION WITH MACH NUMBER $\alpha = 4^{\circ}$ IN AIR (5 IN. CHORD MODEL 18" X 14" TUNNEL.) LOWER SURFACE, TRANSITION FIXED.

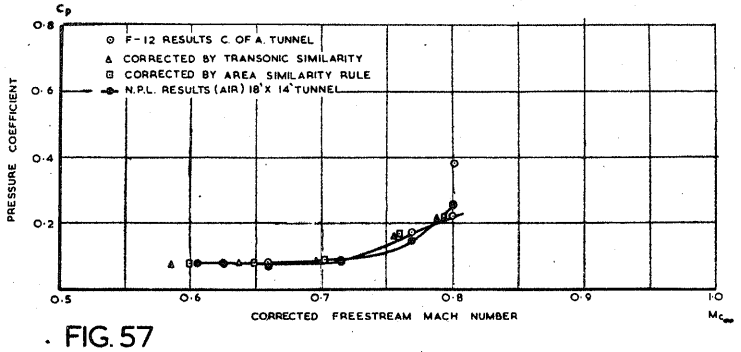

FIG. 57

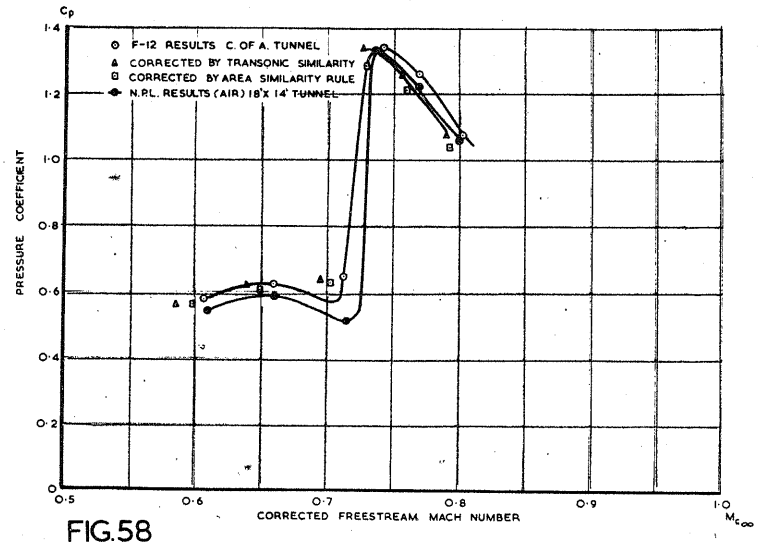

FIG.58

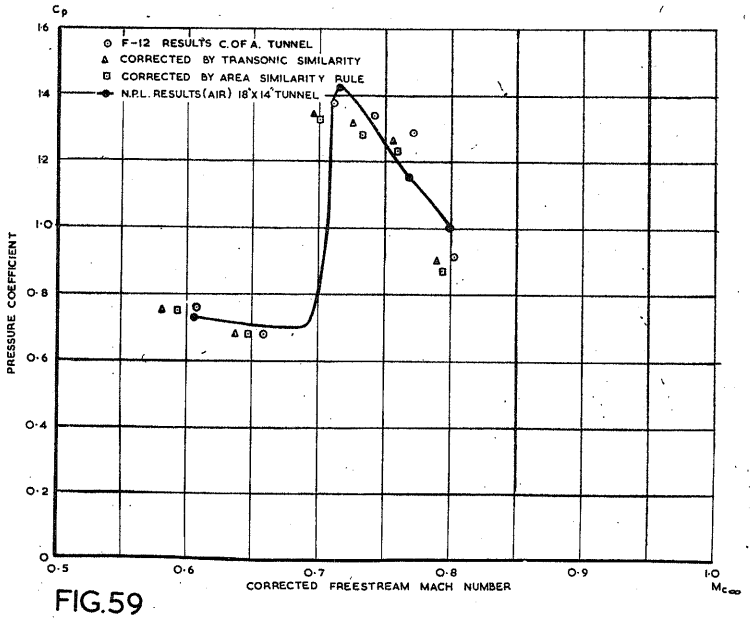

FIG.59

COMPARISON OF PRESSURE COEFFICIENT IN AIR AND FREON-12 AT HOLES 1, 2, 3, AT $\alpha = 4^\circ$ WITH TRANSITION FIXED.

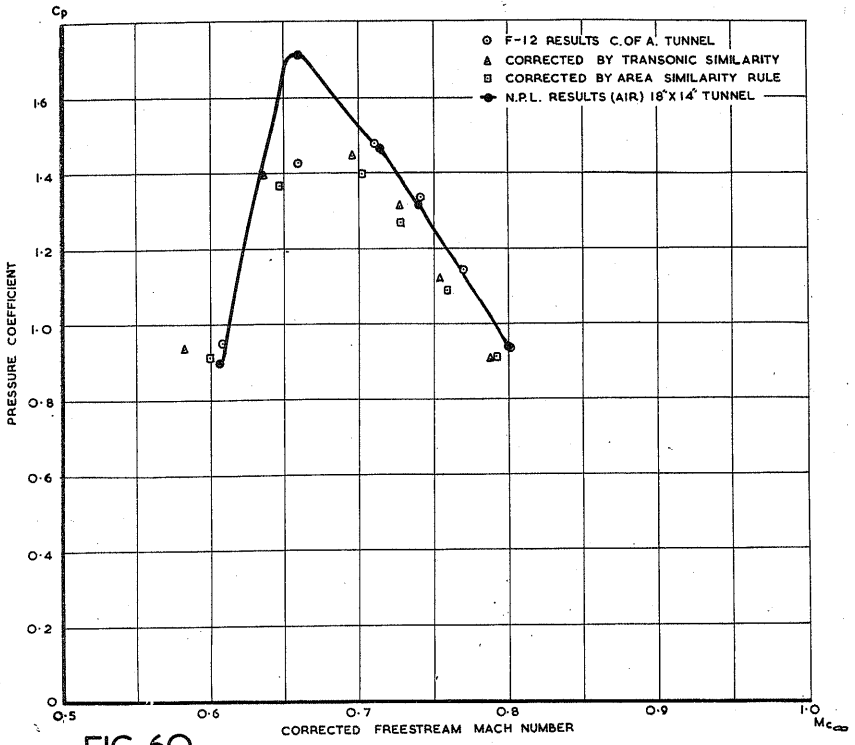

FIG. 60

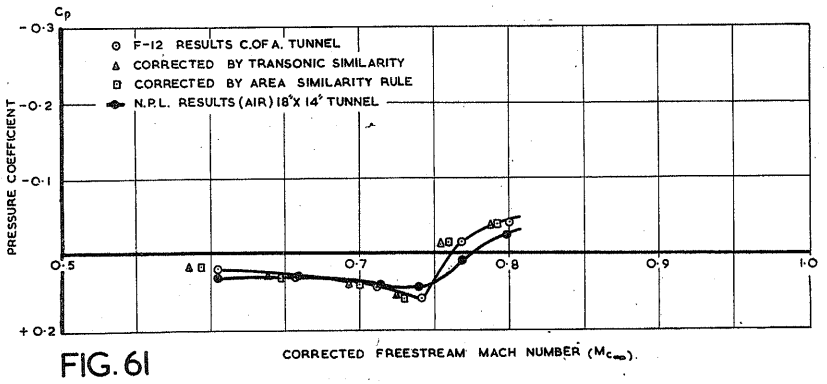

FIG. 61

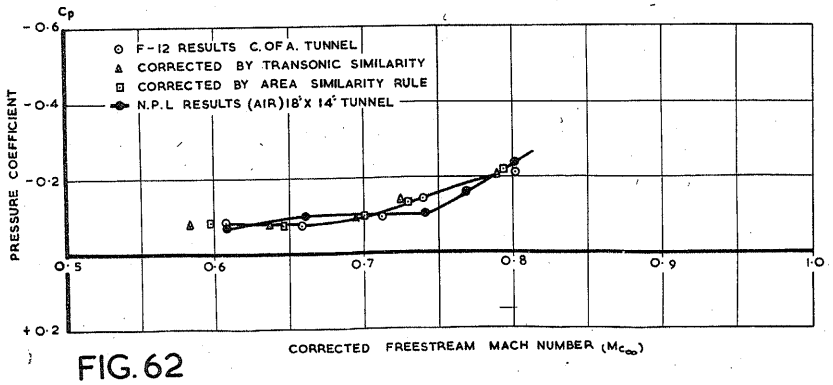

FIG. 62

COMPARISON OF PRESSURE COEFFICIENT IN AIR AND FREON-12 AT HOLES 4, 5, 6. AT $\alpha = 4^\circ$ WITH TRANSITION FIXED.

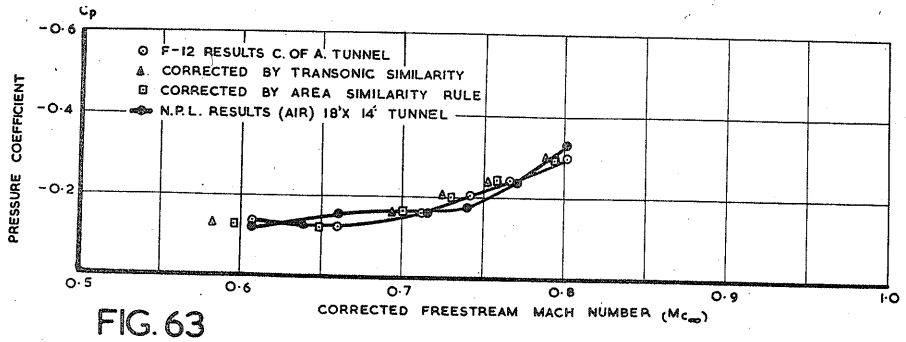

FIG. 63

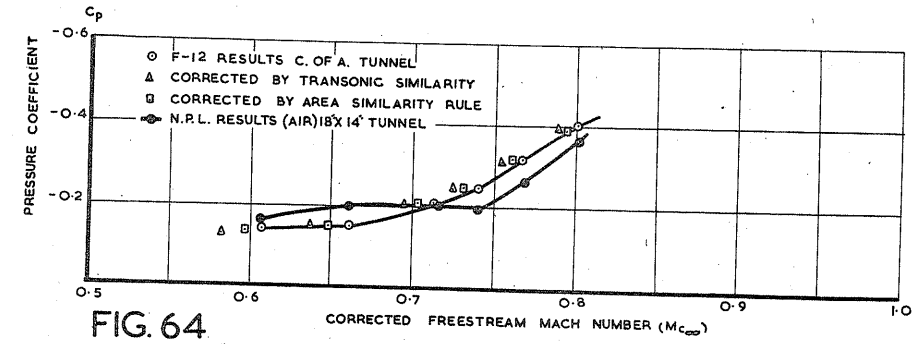

FIG. 64

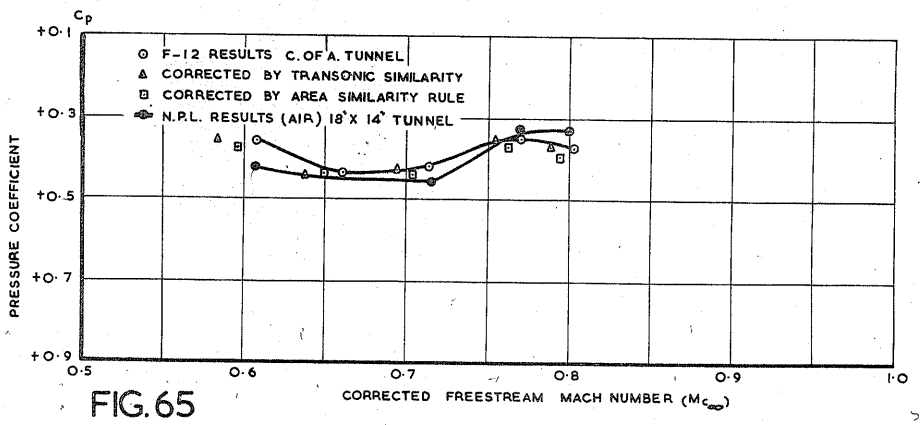

FIG. 65

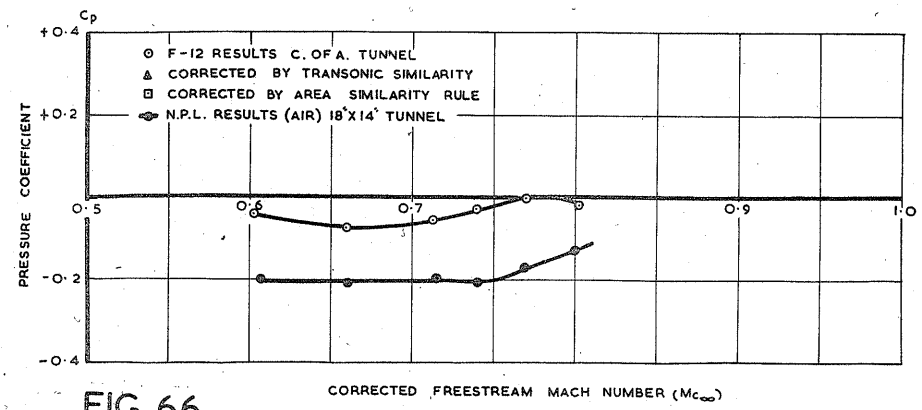

FIG. 66

COMPARISON OF PRESSURE COEFFICIENT IN AIR AND FREON-12 AT HOLES 7, 8, 9, 10, AT $\alpha = 4^{\circ}$ WITH TRANSITION FIXED.

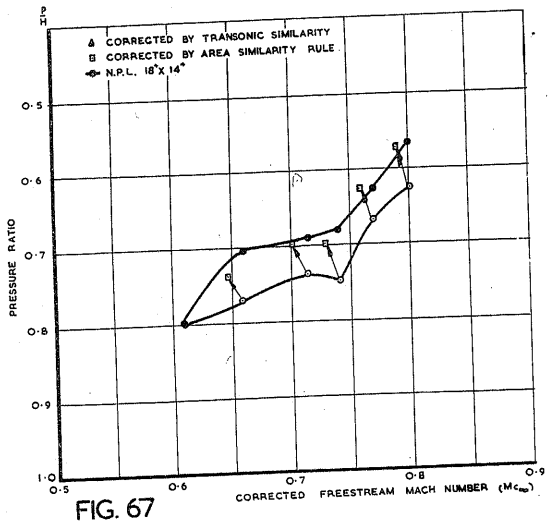

FIG. 67

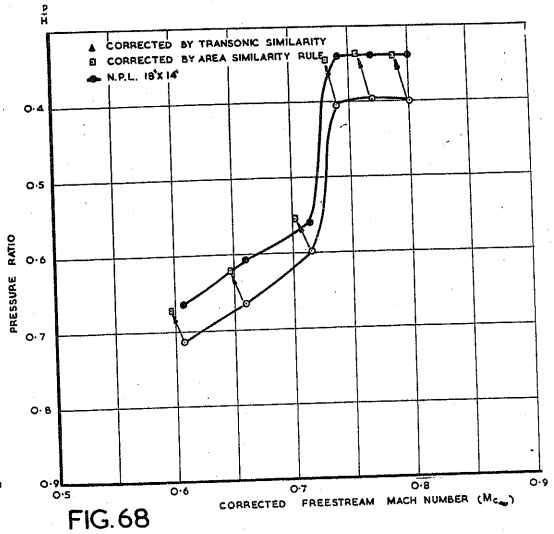

FIG. 68

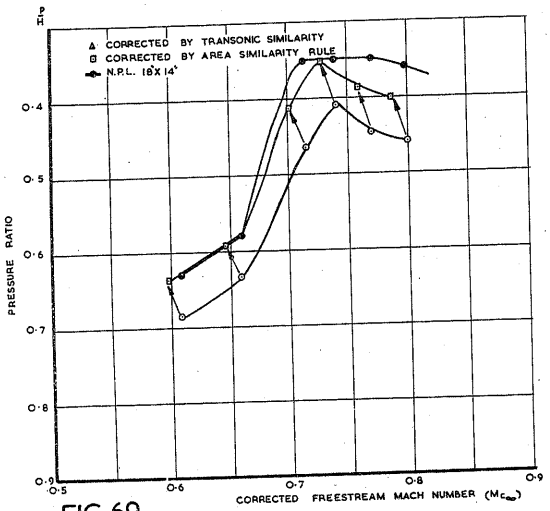

FIG. 69

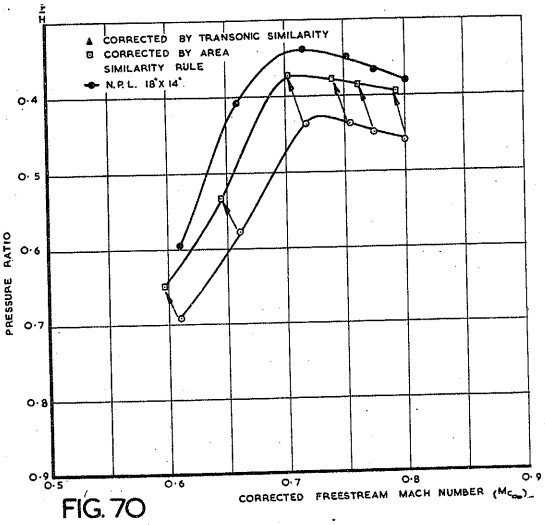

FIG. 70

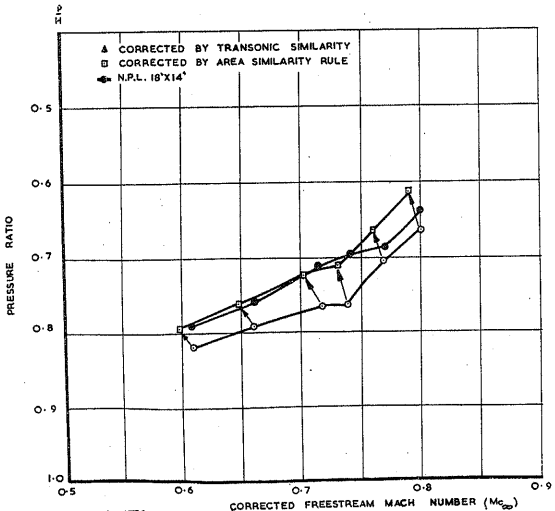

FIG. 71

COMPARISON OF PRESSURE DISTRIBUTIONS IN AIR AND FREON-12 AT HOLES 1,2,3,4,5. WITH TRANSITION FIXED AT $\alpha = 4^\circ$.

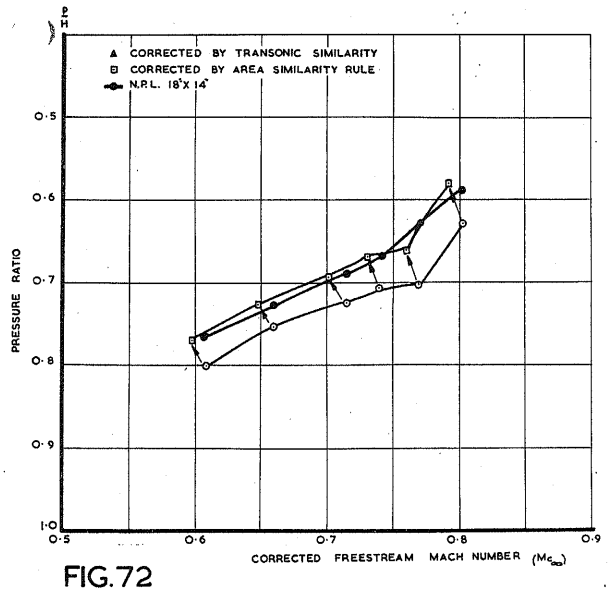

FIG. 72

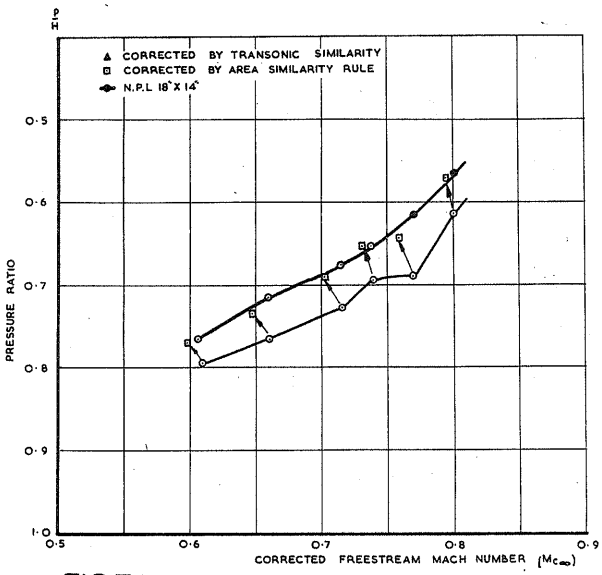

FIG. 73

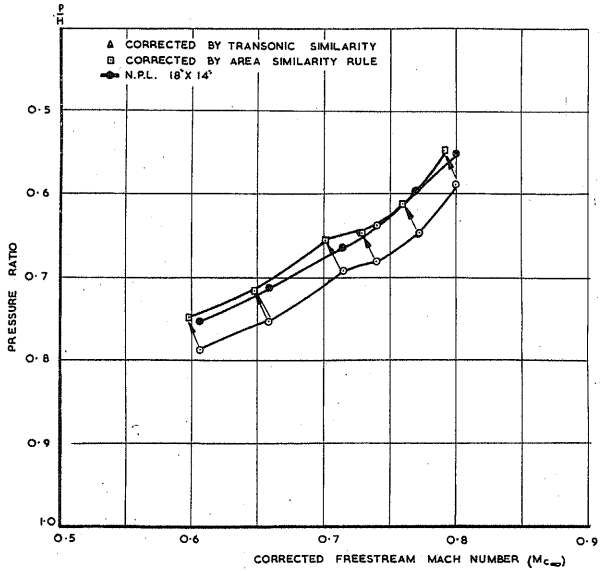

FIG. 74

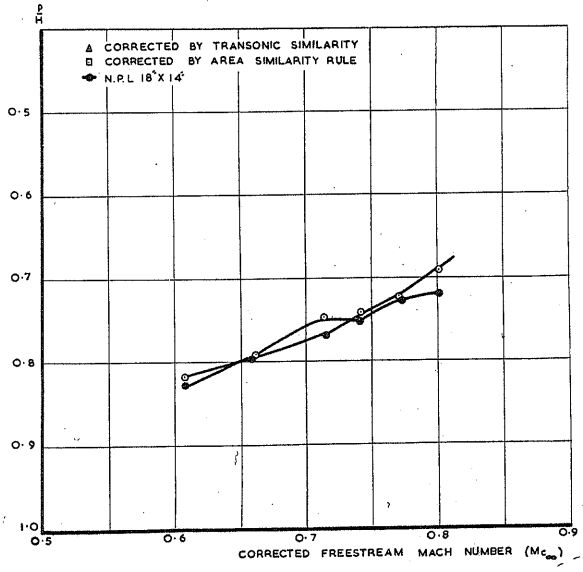

FIG. 75

COMPARISON OF PRESSURE DISTRIBUTIONS IN AIR AND FREON-12 AT HOLES 6, 7, 8, 10, WITH TRANSITION FIXED AT $\alpha = 4°$.

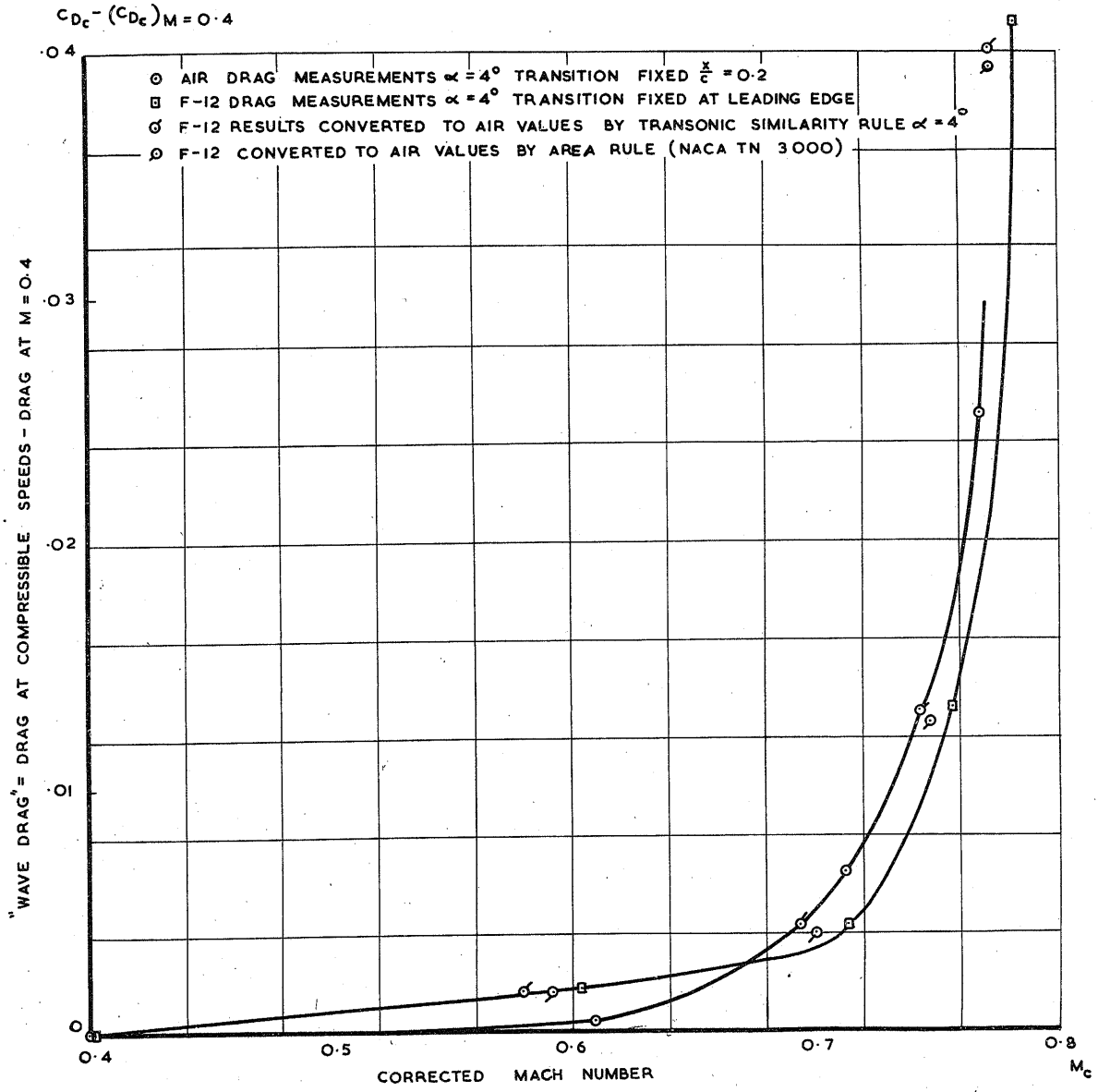

FIG. 76 VARIATION OF WAVE DRAG WITH CORRECTED MACH NUMBER.

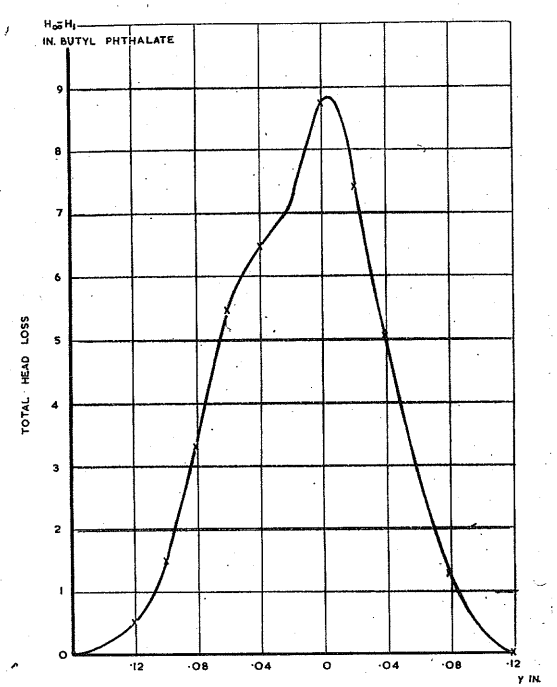

FIG. 77

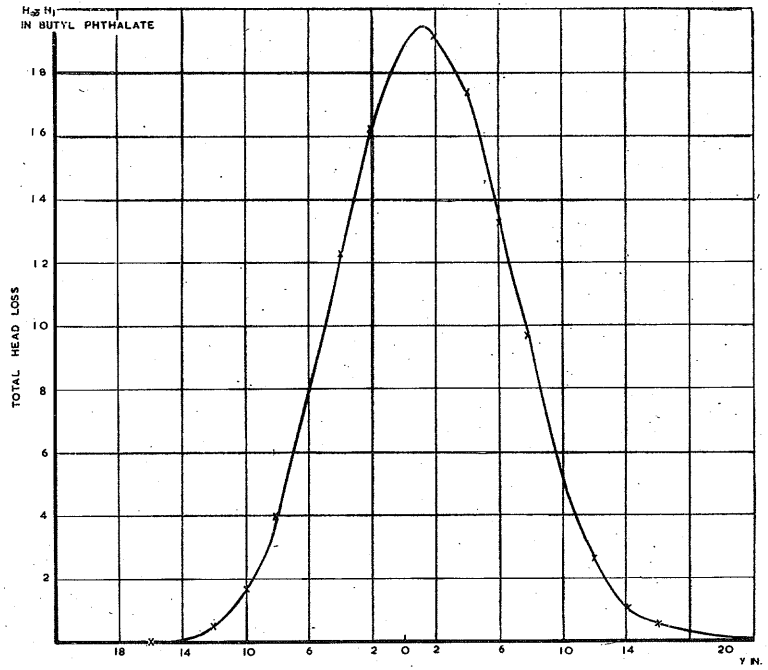

FIG. 78

VARIATION OF TOTAL HEAD IN WAKE OF AEROFOIL 1 CHORD DOWNSTREAM OF TRAILING EDGE AT FREE-STREAM MACH NUMBERS, Mc = 0·403, 0·607, 0·712, AND $\alpha = 4°$.

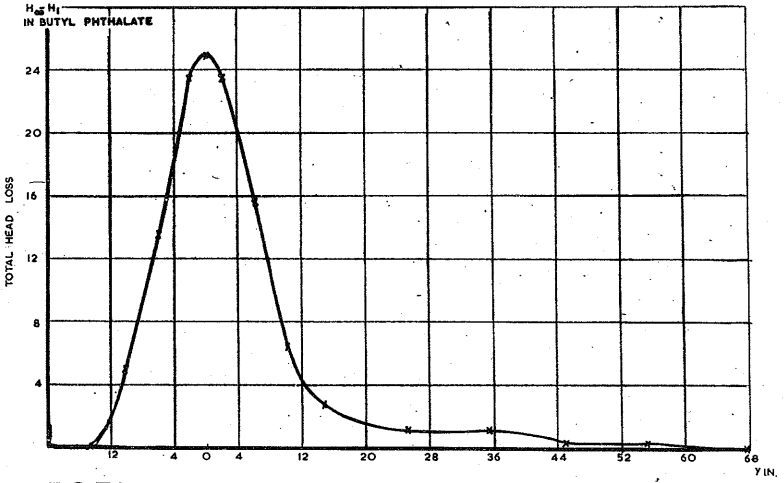

FIG. 79

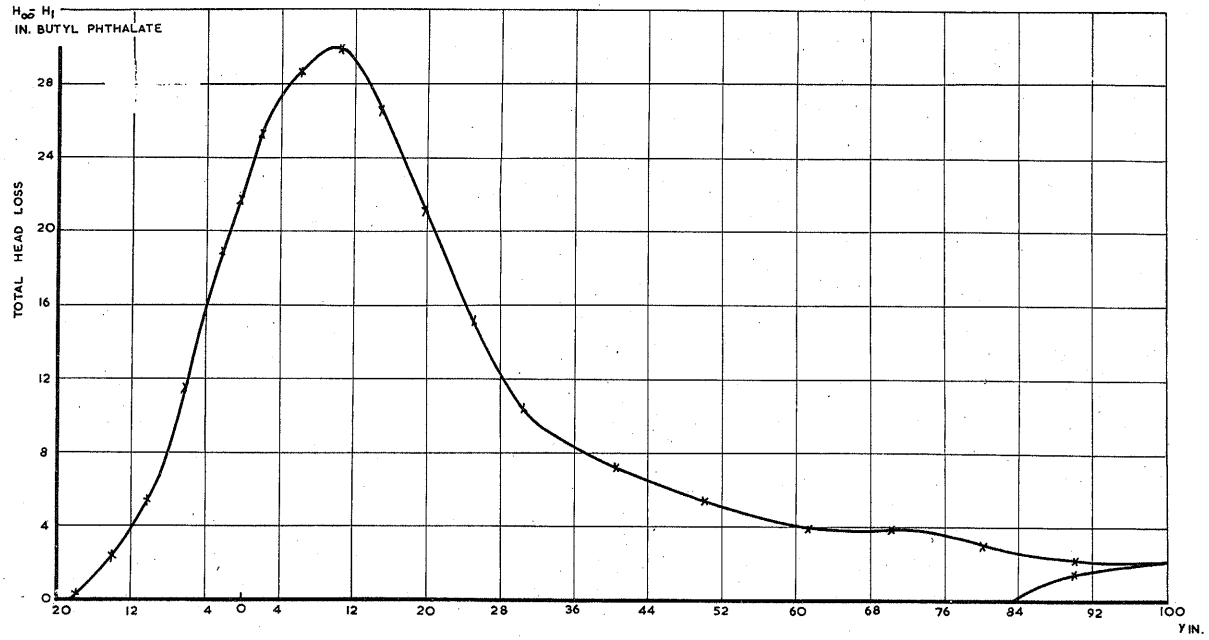

FIG. 80

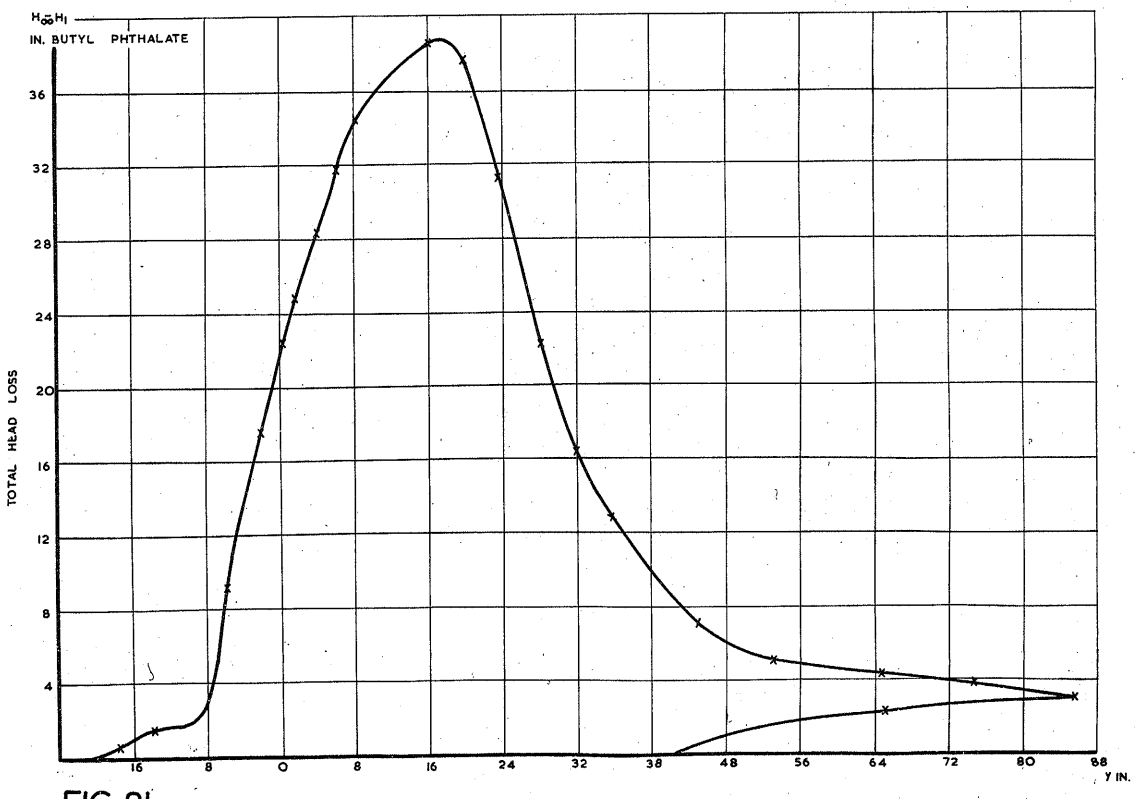

FIG. 81

VARIATION OF TOTAL HEAD IN WAKE OF AEROFOIL 1 CHORD DOWNSTREAM OF TRAILING EDGE AT FREE-STREAM MACH NUMBERS, Mc = 0·761, 0·796 AND $\alpha = 4°$

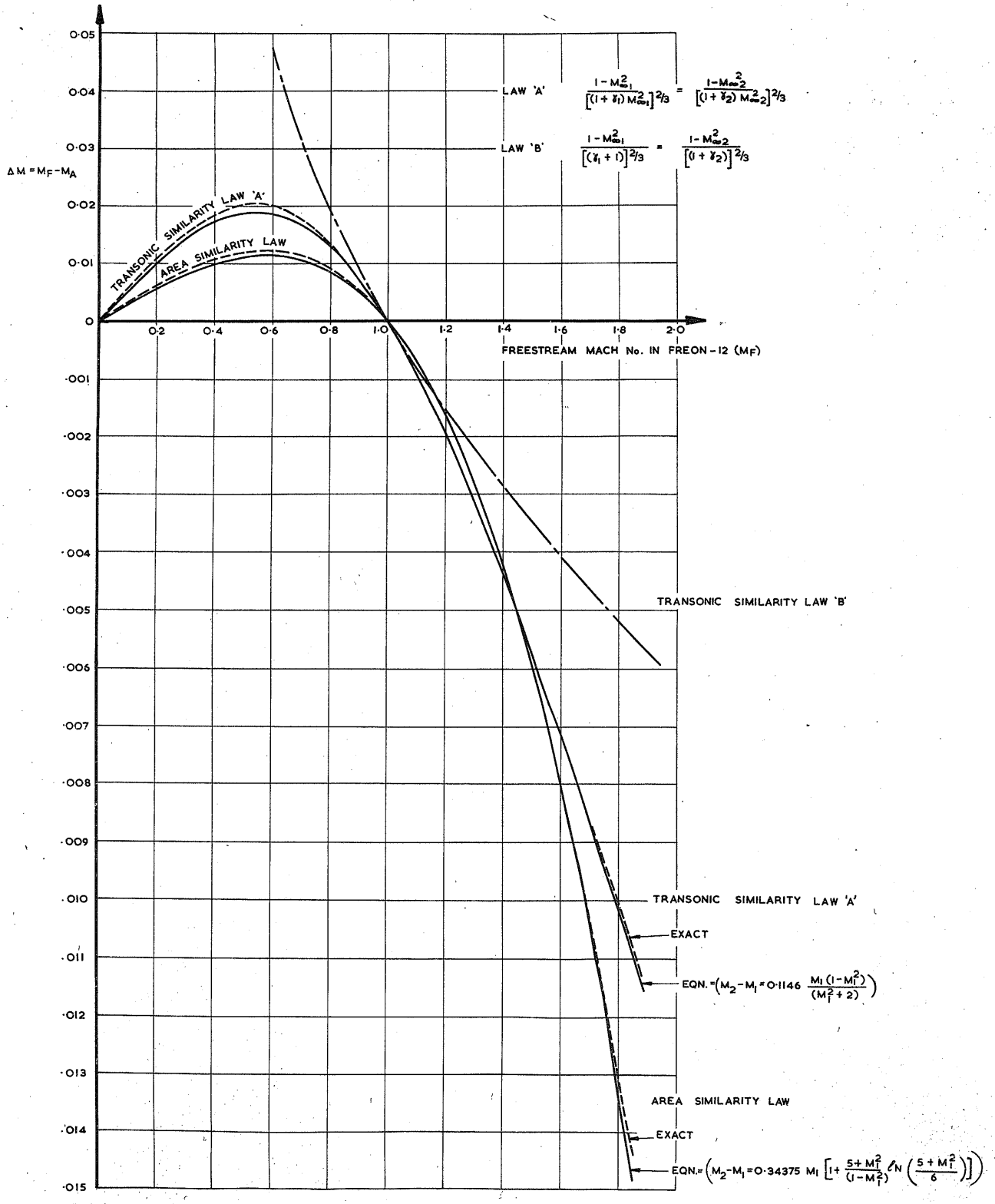

FIG. 82 MACH NUMBER INCREMENTS BETWEEN TESTS IN FREON-12 AND AIR ACCORDING TO VARIOUS TRANSONIC LAWS.

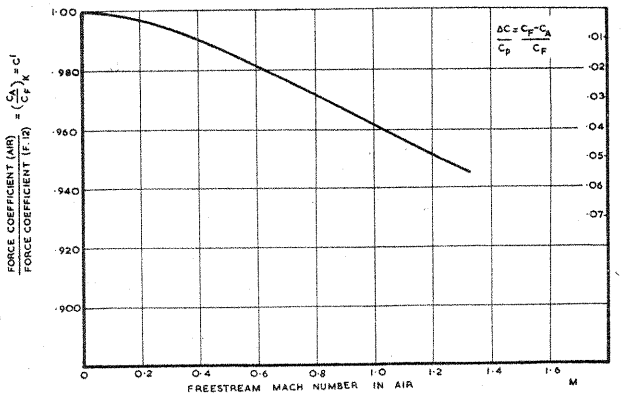

FIG.83 RATIO OF FORCE COEFFICIENTS BETWEEN TESTS IN AIR AND FREON-12 ON A 2-D AEROFOIL ACCORDING TO TRANSONIC SIMILARITY LAW.

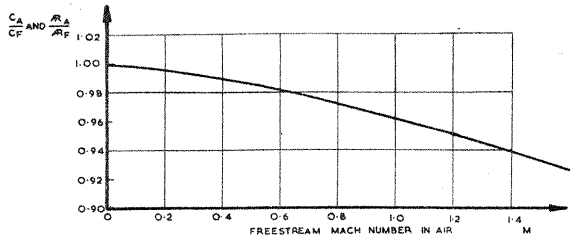

FIG.84 RATIO OF FORCE COEFFICIENTS BETWEEN TESTS IN AIR AND FREON-12 ON WINGS OF FINITE ASPECT RATIO ACCORDING TO THE TRANSONIC SIMILARITY LAW.

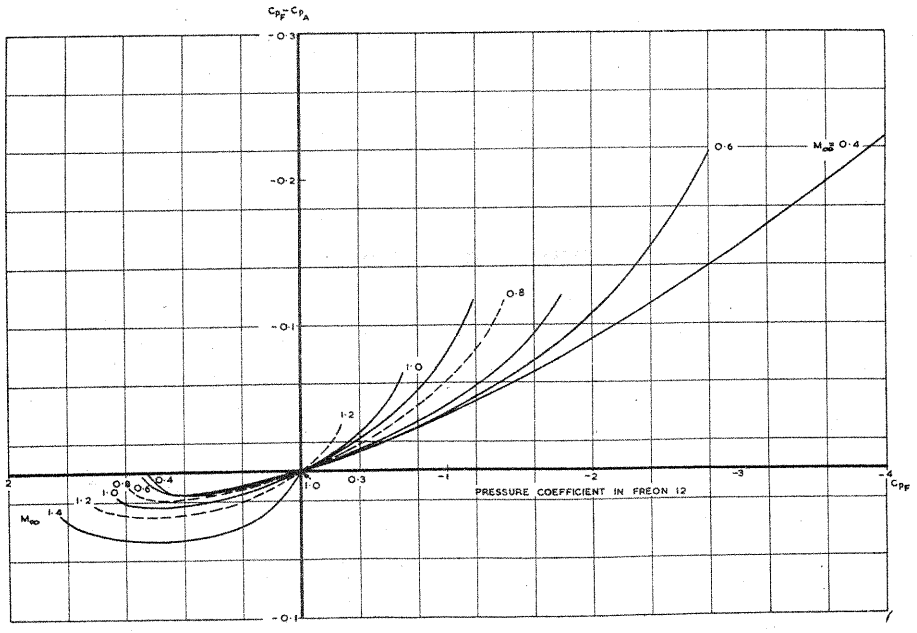

FIG.85 PRESSURE COEFFICIENT INCREMENT BETWEEN TESTS IN AIR AND FREON-12 ACCORDING TO AREA SIMILARITY LAW.

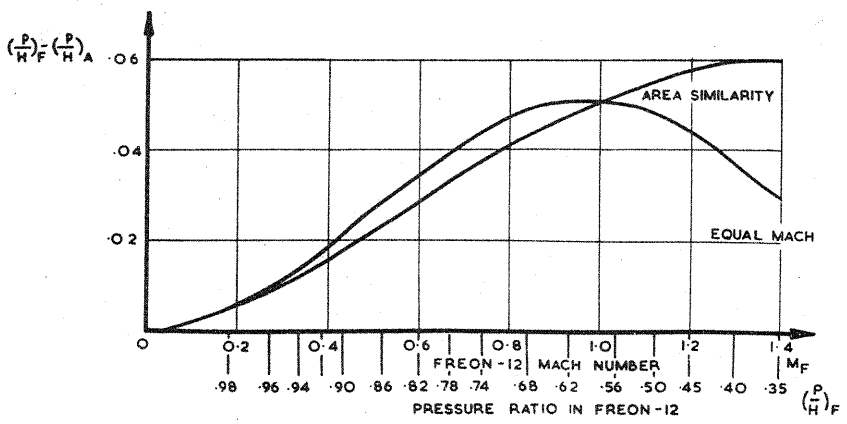

FIG. 86 PRESSURE RATIO INCREMENT BETWEEN TESTS IN AIR AND FREON-12 ACCORDING TO THE AREA SIMILARITY RULE AND EQUAL MACH NUMBER DISTRIBUTION.

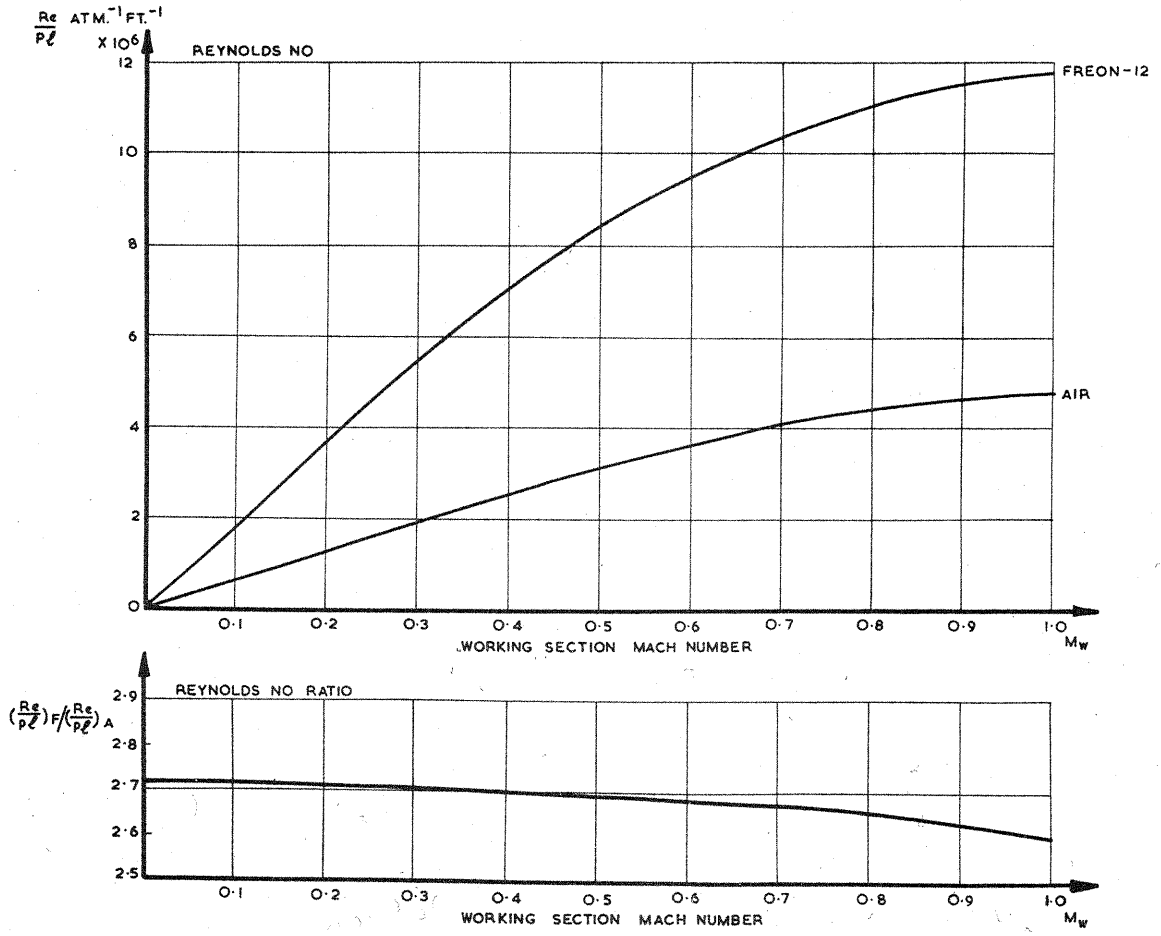

FIG. 87 VARIATION OF REYNOLDS NUMBER WITH MACH NUMBER IN AIR AND FREON-12.

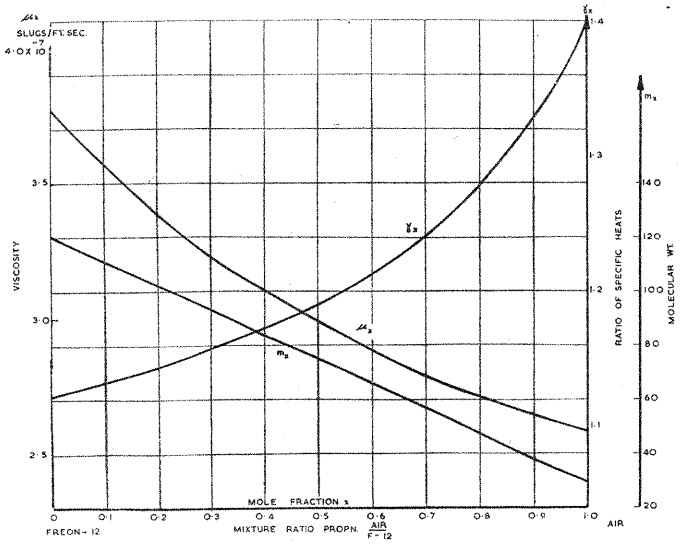

FIG. 88 RATIO OF SPECIFIC HEAT, VISCOSITY AND MOLECULAR WEIGHT OF MIXTURE.

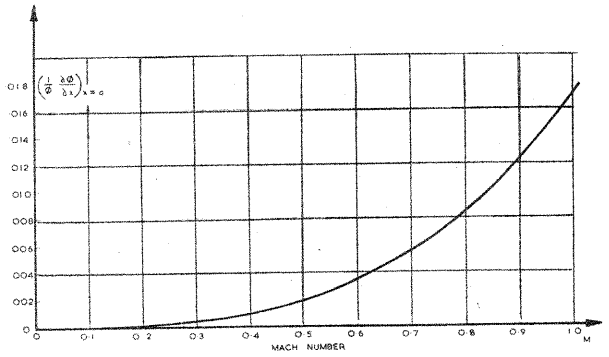

FIG. 89 THE VARIATION OF $(\frac{1}{\phi}\frac{\partial \phi}{\partial x})_{x=0}$ WITH MACH NUMBER.

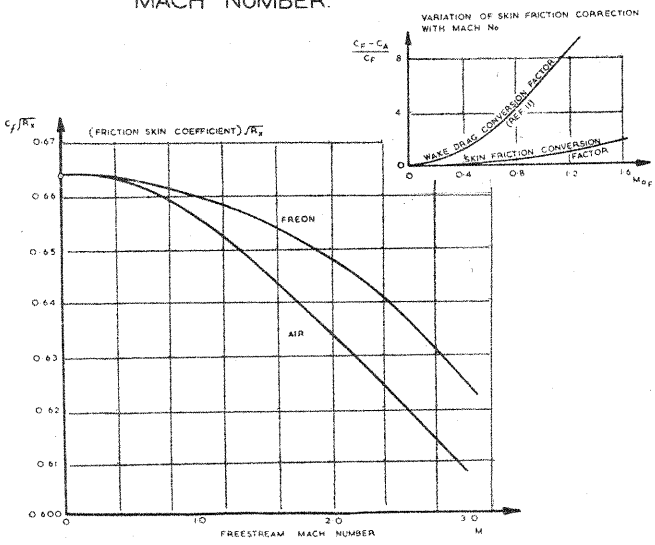

FIG. 90 VARIATION OF FRICTIONAL COEFFICIENT WITH MACH NUMBER IN FREON-12 AND AIR.

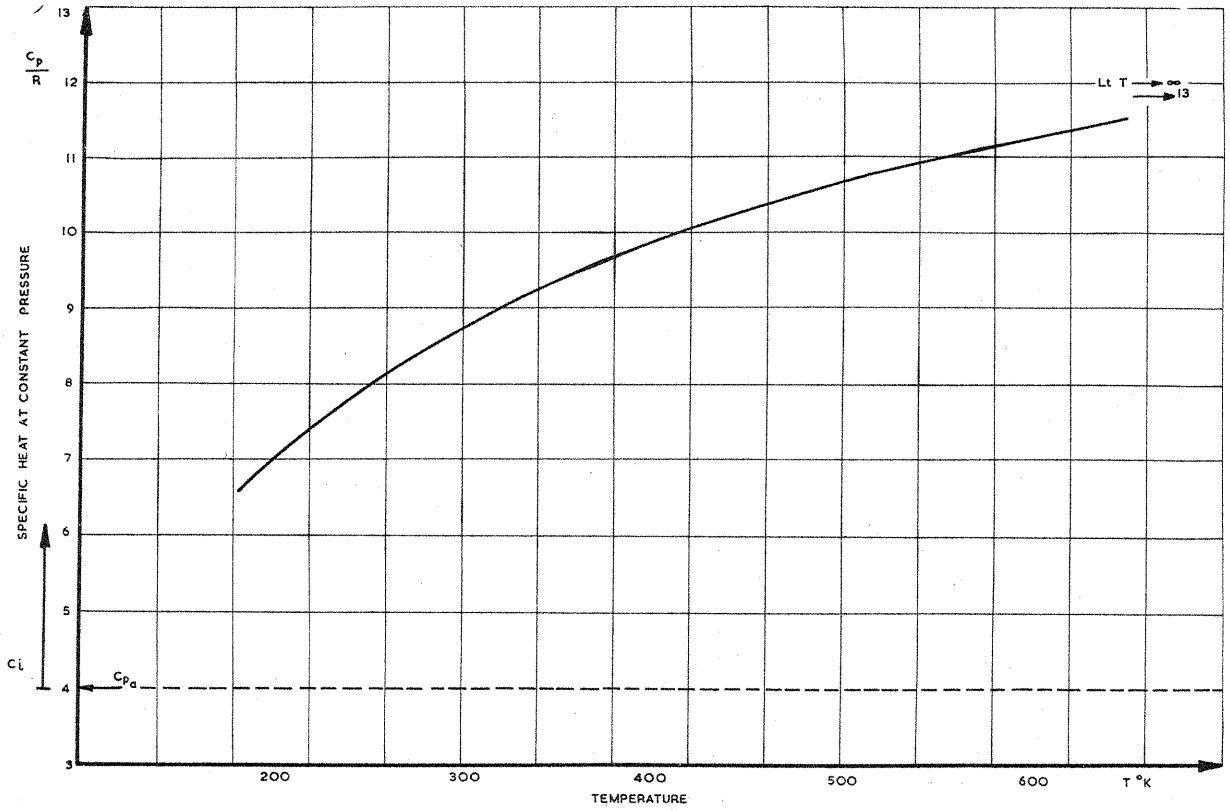

FIG. 91 TEMPERATURE VARIATION OF THE SPECIFIC HEAT OF FREON-12.

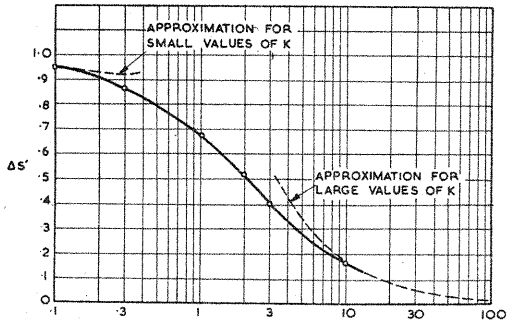

FIG. 92 THE NON-DIMENSIONAL ENTROPY INCREASE IN THE FLOW APPROACHING A SOURCE-SHAPED IMPACT TUBE

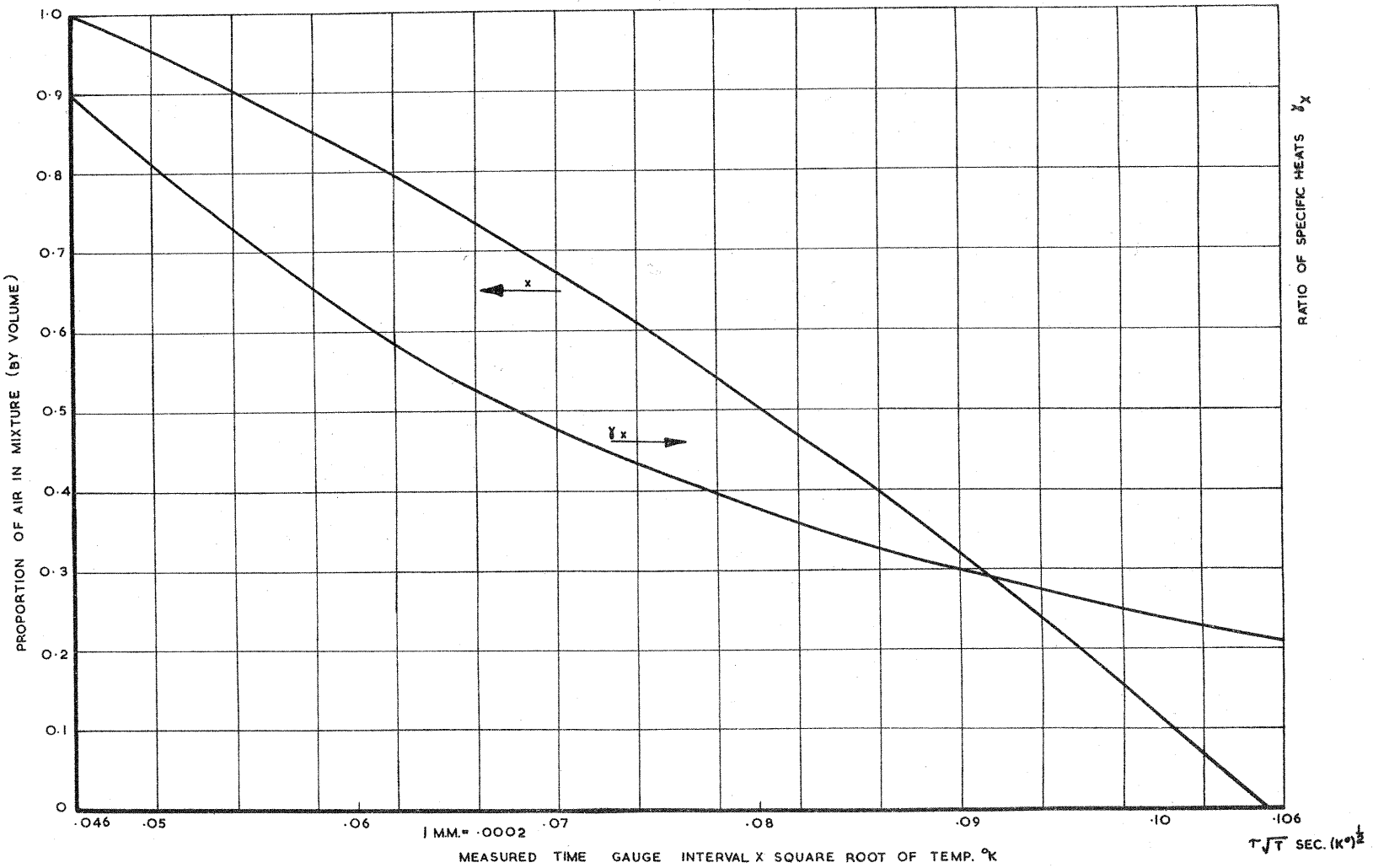

FIG.93 PROPORTION OF AIR (BY VOLUME) AND RATIO OF SPECIFIC HEATS IN FREON-12 AND AIR MIXTURES FROM SOUND MEASURING GAUGE.